Photodynamics of
BLUF Domain Proteins
a New Class of the Biological Blue-Light Photoreceptors

Dissertation

Zur Erlangung des Doktorgrades

der Naturwissenschaften

(Dr. rer. nat.)

der Fakultät Physik

der Universität Regensburg

vorgelegt von

Peyman Zirak Yousefabadi

aus Tabriz, Iran

Regensburg 2007

Photodynamics of
BLUF Domain Proteins
a New Class of the Biological Blue-Light Photoreceptors

Dissertation

Zur Erlangung des Doktorgrades

der Naturwissenschaften

(Dr. rer. nat.)

der Fakultät Physik

der Universität Regensburg

vorgelegt von

Peyman Zirak Yousefabadi

aus Tabriz, Iran

Regensburg 2007

Diese Arbeit wurde angeleitet von Prof. Dr. A. Penzkofer

Prüfungsausschuss:

Vorsitzender: Prof. Dr. I. Morgenstern
Erster Gutachter: Prof. Dr. A. Penzkofer
Zweiter Gutachter: Prof. Dr. C. Schüller
Prüfer: Prof. Dr. D. Weiss

Regensburg, 16 Mai 2007

Table of Contents

1 Introduction

1.1 Photoreceptors

For centuries, poets, philosophers, artists and scientists have noted and studied the phototrophic movement of plants. In one of the earliest depictions of plant phototropism, Venus the ancient goddess of love, transforms Clytie, a water nymph, into a plant because of her infatuation with Apollo, the sun god. Associated with her metamorphosis into a green plant, Clytie turns and follows the movement of Apollo [Ovi98]. This tale of unrequited love is based on believes of early classical philosophers (mostly Aristotelians) that plants exhibit passive responses to the environment. Accordingly the phototrophic (and solar tracking) tendencies of plant is attributed to the sun activity in removing fluid from the illuminated side of the plant [Whi06].

This simple explanation of phototropism persisted until 17th century, where experimental observations (which were downplayed due to Aristotelians) began to recognize plant sensitivity [Web66b].

As due to these observations it became more and more accepted that phototropism is stimulated by light, the focus returned to the property of light response where it was revealed that blue light is more effective at orienting the plants [Whi06].

For many years the only proof for the existence of blue light photoreceptors was this sensitivity to blue light. These photoreceptors are called cryptochrome due to the difficulty for isolating them (crypto is taken from the Greek word Kryptos that means “hidden”) [Hor03]. However nowadays the name cryptochrome is only used for the first identified protein of blue light photoreceptors family. Eventually a 120-kD membrane bound flavin based protein called “Phot”, was identified as the key element necessary for phototropism [Gal88,Rey92] although the role of other red and blue light photoreceptors could not be completely excluded [Bri63, Ahm98].

To date the many different identified photoreceptor proteins could be classified into a limited number of families. The most rational approach is to base this classification on the absorption maxima and chemical structure of the light-absorbing chromophores involved, as well as arguments from chromophore-protein interaction. Accordingly, the six classified families are the rhodopsins, phytochromes, xanthopsins, cryptochromes, phototropins and BLUF proteins.

In contrast to rhodopsins, phytochromes and xanthopsins which undergo cis/trans isomerization cryptochromes, phototropins and BLUF proteins all have a different flavin-based photochemistry.

Rhodopsins are green light photoreceptors which employ retinal as their light sensor [Spu00]. Despite controversy in the primary photochemistry of rhodopsins, recent transient (UV-Vis and vibrational) spectroscopy evidences indicate that the change of configuration from all-trans to 13-cis is the primary event [Xia00]. The photo-cycle of rhodopsins is completed within 100ms-1μs in which intermediate states are named alphabetically from K to O [Xia00].

Besides visual rhodopsins from Eukarya and archaea, they are also found to be phototaxis receptors in *chlamydomonas* [Sak02].

Phytochrome photoreceptor family was discovered as the receptor responsible for red/far -red-light, reversible plant responses. A linear tetrapyrrole is their light-sensitive chromophore [Yeh98]. Red light triggers an isomerization of all-cis red-absorbing "Pr" to far-red-absorbing "Pfr" conformation. Subsequently it recovers back slowly to the dark within hour time scale or almost instantaneously upon absorption of far-red-light. During these transitions, structural changes take place in the protein as well as proton uptake and release reactions [Sak96]. Phytochromes can function in light-regulated gene expression, light induced tactic movement or setting circadian rhythm [Sch00].

Xanthopsins are the photoreceptor family carrying trans-p-coumaric acid as their blue-light-sensitive chromophore. Photoactive yellow protein (PYP) from *Ectothiorhodospira halophila* is archetype for this family in which blue light absorption leads to chromophore isomerization and formation of the signaling state [Ihe05]. The signaling state "pB" which is formed through several picosecond and nanosecond intermediates can then decay in the dark to the "pG" state (dark state) [Gen98]. The current consensus on the function of PYP is light induced behavioral response which allows the bacterium to avoid regions with high intensities of blue light [Spr93].

Phototropins get their name after verification of their enrollment in several light responses in plants, like phototropism, chloroplast movement and stomatal opening [Chr02]. The light sensitive domain that generates signaling[1] upon blue light absorption is referred to as LOV (Light-Oxygen-Voltage) domain in which non-covalently bound oxidized flavin mononucleotide (FMN) is used as light sensitive chromophore [Sal00]. Although the flavin-C(4a)-cysteinyl is accepted as the photo-adduct, more reaction pathways are suggested for photo-adduct formation

[1] The protein state after excitation

[Swa01,Cro01]. In dark and at room temperature the photo-adduct decays to the initial dark state [Mil90].

Cryptochromes are the oldest family of flavin-containing photoreceptors. These blue-light photoreceptors are present in lower and higher eukaryotes and prokaryotes. Cryptochromes are involved in different processes ranging form synchronization of the circadian clock in animals to flowering in plants [Chr01]. These proteins contain two non-covalently bounded chromophores in their binding pocket, FAD (flavin-adenine dinucleotide) as the key cofactor, and pterin in the form of methenyltetrahydrofolate (MTHF) as the second photo-sensor and more probably an antenna [San00,Pok05]. In addition, several lines of evidence support the hypothesis that activation of cryptochrome is based on changes of the FAD redox state [Gal03,Son06]. However the accurate light response mechanism is yet to be determined.

BLUF proteins are another family of photoreceptors using flavin as their light-sensitive module. The proteins are named BLUF for "sensor for blue light using FAD" [Gom02]. Members of this family are known to be involved in photophobic responses in *Euglena gracilis* (PAC protein [Ise02]) and *synechocystis* (Slr1694 protein [Oka05]) and also transcriptional regulation in *Rhodobacter sphaeroides* (AppA protein) [Mas02]. It is believed that electron transfer upon blue light absorption triggers conformational changes in protein structure leading to signaling state formation, which is distinguished by $\approx 10 \pm 5nm$ red shift in the absorption spectrum. The red shifted spectrum recovers back to the dark state at room temperature in a second or minute time scale.

1.2 Aims

Due to resolvable spectral changes during the signaling process of photoreceptors, the absorption and emission spectroscopy is a convenient tool to follow these changes starting with absorption of a photon and recovering in dark at room temperature (photo-cycle).

In this work the absorption and emission spectroscopy is employed to investigate photo-cycle behavior of some BLUF proteins: AppA and BlrB from R. Sphaeroides, Slr1694 from Synechocystis sp. PCC6803 and AppA-H44R a mutant of AppA protein in which His44[2] is replaced with Arg. Moreover prolonged high-intensity blue-light illumination is used to study processes that could occur via signaling state excitation.

[2] Amino acid histidine at position 44 (see appendix for structural formulae of 20 standard amino acids).

Since the primary event in the photo-cycle is absorption of a photon by the flavin chromophore, it is reasonable to have an overview of physical and chemical properties of free flavins in aqueous solution. These properties are briefly reviewed in chapter 2.

Although spectroscopic studies provide insights into the light-response mechanism of the photoreceptor proteins, physiological and crystal structural data are essential for understanding the overall photo-cycle mechanism. These data for investigated proteins are presented in chapter 3. Chapter 4 contains the basic principles necessary to analyze and understand the experimental results. Experimental methods used in the studies are explained in chapter 5. Chapter 6 contains the experimental results for each of the investigated samples together with the methods which are used to analyze them. In chapter 7 the suggested photo-cycles for AppA, BlrB and Slr1694 together with that of AppA-H44R are compared and explained according to their crystal structures and other reported spectroscopic, biochemical and biological evidences. The obtained results and their explanations are summarized in chapter 8.

2 An overview of the physical and chemical properties of free flavins

Flavins are redox-active chromophores (i.e. they participate in oxidation and reduction reactions) found in enzymes and photoreceptors [Mül91,Bri99]. Riboflavin can be found in milk, meat, yeast, peas and beans [Mas00]. Lack of Riboflavin in humans causes disturbances of growth, skin diseases and hair loss [Fri88].

FMN (flavin mononucleotide) is the cofactor in the phototropins (phot) of plants [Bri99]. FAD (Flavin adenine dinucleotide) is the chromophore in cryptochrome [Lin95] and BLUF proteins [Gom02].

2.1 Physics and chemistry of flavins in oxidized form

The structural formula of FAD, FMN, Riboflavin, Lumichrome and Lumiflavin together with internationally accepted numbering system of isoalloxazine moiety are shown in Fig. 2-1 [Mül91]. In aqueous solution the flavins are in their oxidized redox form (Fig. 2-1) which depending on the pH of the solution, they can be found in cationic, neutral or anionic oxidized forms [Mül91]. The structures of the cationic, anionic and neutral oxidized forms of the flavin are depicted in Fig. 2-2 [Isl03]. Accordingly due to the pH range which is used in this work (pH 7-8), only the neutral oxidized form is considered.

The absorption spectrum of flavins in the visible wavelength region is caused by the isoalloxazine ring [Whi53]. As a result the absorption spectrum of FAD, FMN and Riboflavin are practically the same. Fig. 2-3 shows the absorption spectra of FMN, Lumiflavin and Lumichrome [Hol05]. The same explanation is used to describe the similar fluorescence spectral shapes of FAD, FMN and Riboflavin in aqueous solution [Bar73].

However depending on the solvent conditions the fluorescence characteristics of FAD are different from Riboflavin and FMN. This is due to the intramolecular complex formation between the adenine and isoalloxazine moieties of FAD (i.e. adenine moiety bends over the isoalloxazine ring) [Mil68,Ber02].

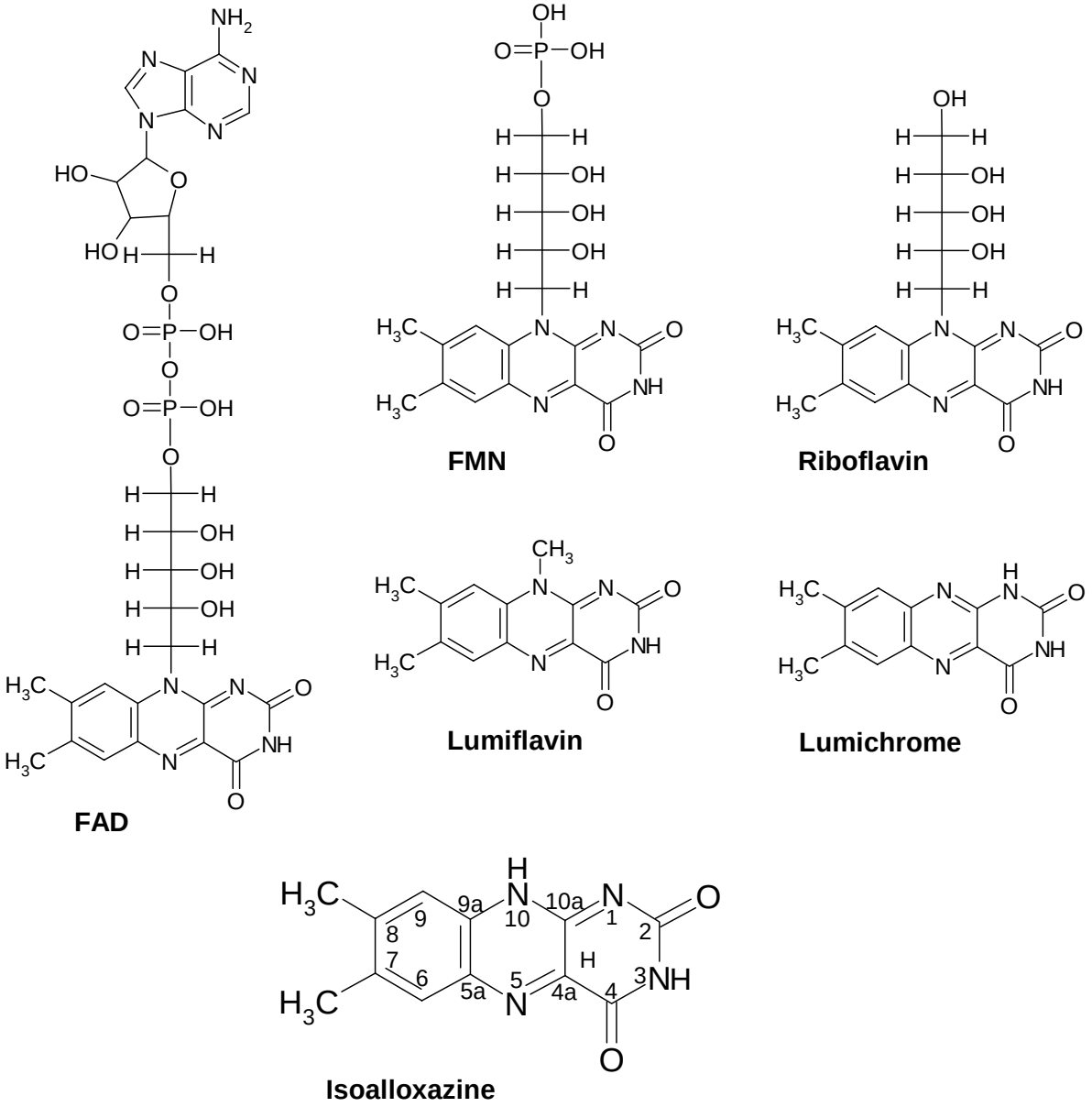

Figure 2-1: The structural formula of FAD, FMN, Riboflavin, Lumichrome and Lumiflavin together with internationally accepted numbering system of isoalloxazine moiety [Mül91].

In addition it is found that FAD has a somewhat shorter fluorescence lifetime compared to the other flavins (riboflavin and FMN). This is because of the photoisomerization of excited FAD from a fluorescent un-stacked form to a nearly non-fluorescent stacked form. Photoisomerization eases photo-induced electron transfer from the adenine part in FAD to the isoalloxazine ring during excited state lifetime of the initially unstacked form [Isl03].

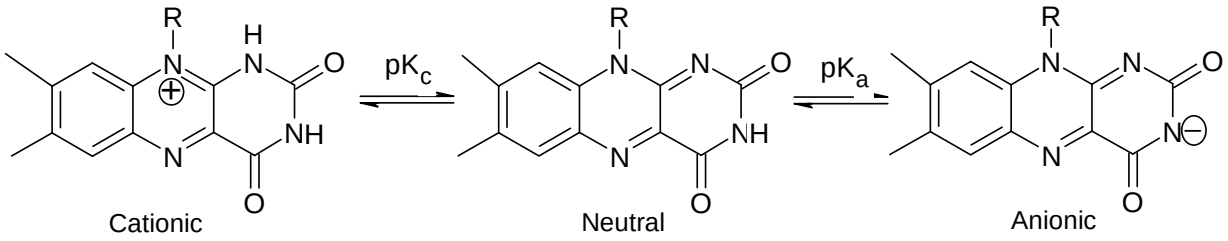

Figure 2-2: The structures of the cationic, anionic and neutral forms of the oxidized flavin [Isl03].

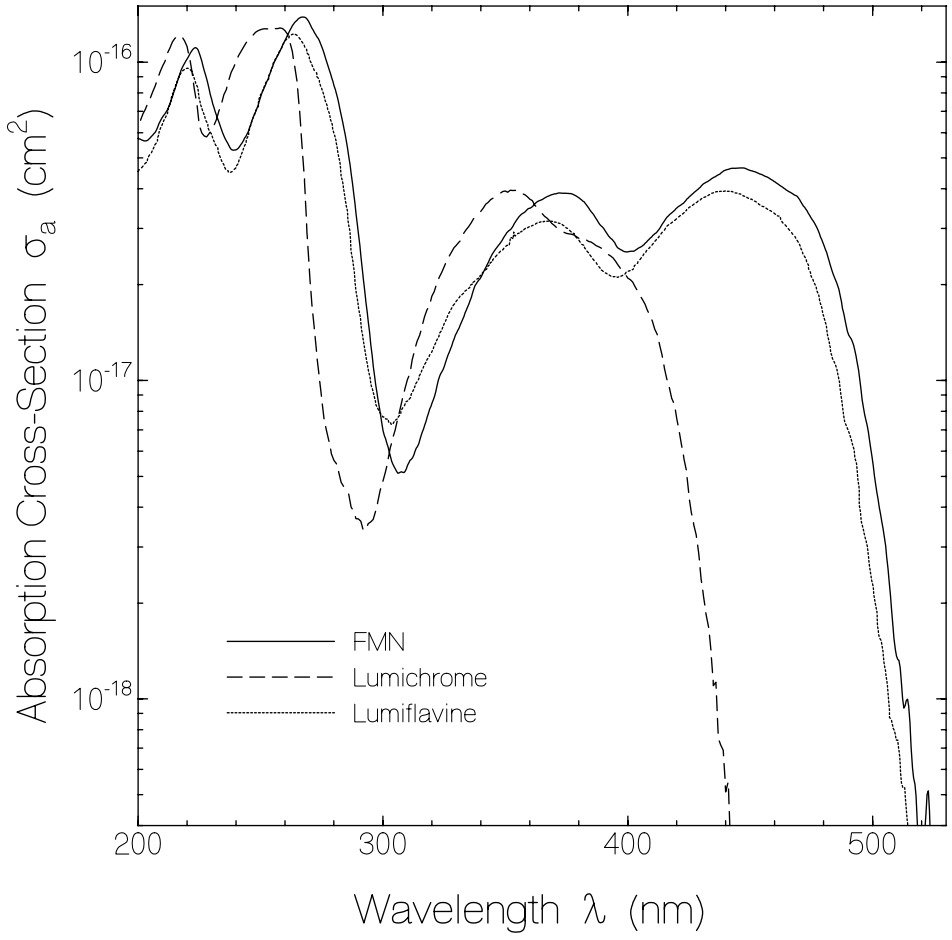

Figure 2-3: Absorption cross-section spectra for FMN (flavin mononucleotide) in aqueous solution at pH 7, lumiflavin in aqueous solution at pH 7 and lumichrome in bi-distilled water [Hol05].

The fluorescence spectra for FMN, Lumiflavin and Lumichrome are shown in Fig. 2-4 [Hol05].

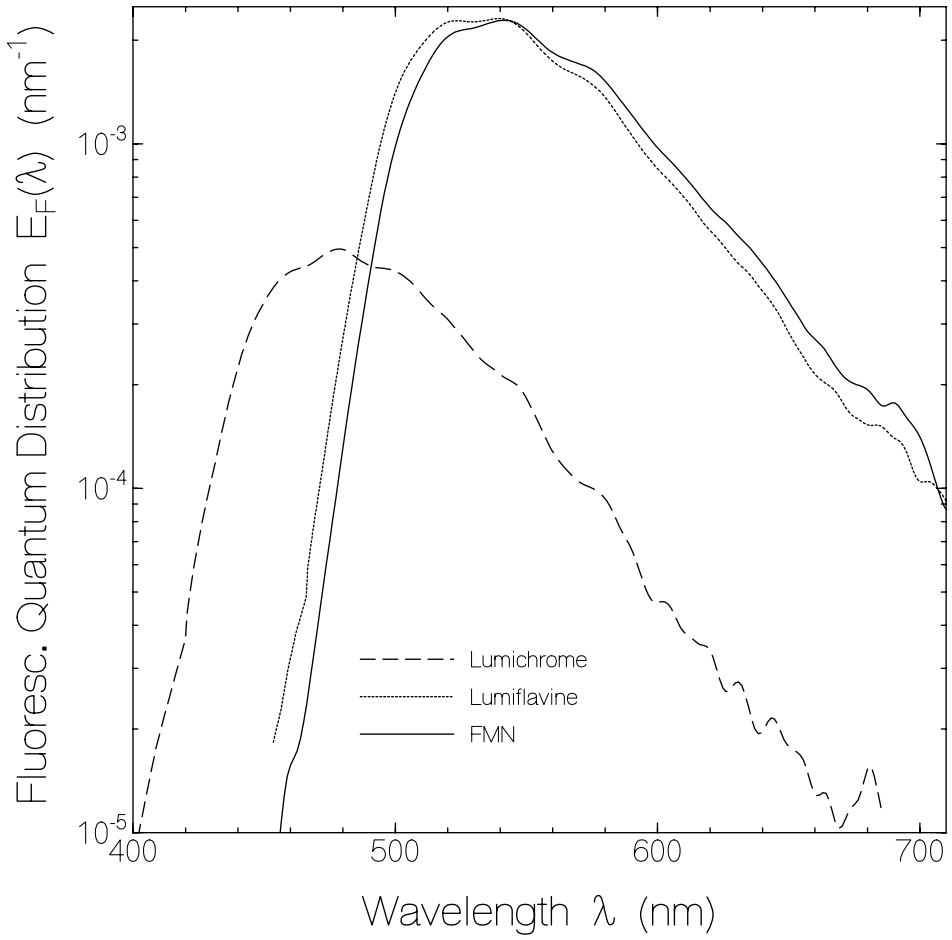

Figure 2-4: Fluorescence quantum distribution of FMN, lumiflavin and lumichrome in aqueous solution at pH 8 [Hol05].

2.2 Physics and chemistry of flavins in different redox states

Flavins are generally found in three different redox states. Under normal conditions[3] they are in oxidized form (flavoquinones). Flavins are also present in semi-reduced form as flavosemiquinones and in fully reduced form as flavohydroquinones. The structural formulae for these forms are shown in Fig. 2-5 [Mül91]. Similar to flavoquinones, flavosemiquinones and flavohydroquinones exist in cationic, anionic and neutral forms [Mül91]. The absorption spectra for neutral flavoquinone, neutral flavosemiauinone and neutral flavohydroquinone are shown in Fig.2-6.

[3] In biological environment and in the absence of species known to donate/accept electron(s) to/from flavin.

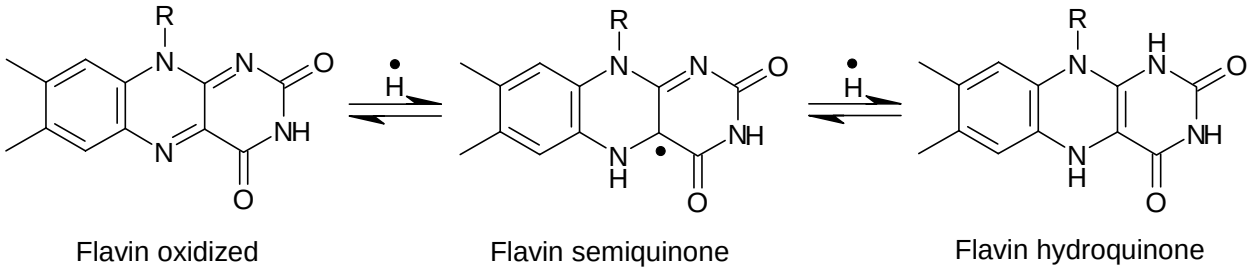

Figure 2-5: Structural formulae for three flavin forms: quinone (oxidized), semiquinone (semi-reduced) and hydro-quinone (fully reduced) flavins.

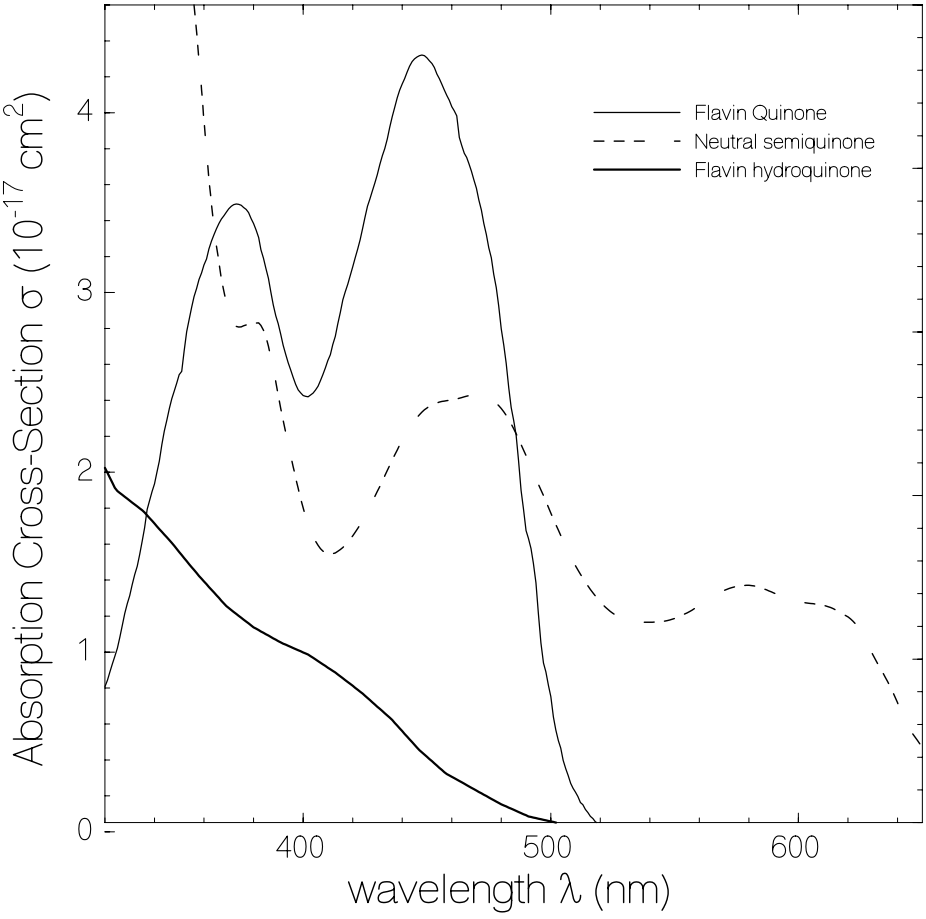

Figure 2-6: Absorption cross-section spectra for: normal oxidized (quinone) [Mas00], neutral semiquinone [Pal97] and neutral hydroquinone [Mül88] flavins.

Upon one and two electron transfer followed by proton transfer (or by hydrogen atom transfer), flavoquinone changes to the flavosemiquinone and flvohydroquinone forms respectively. If these

reactions are triggered by light, they are called photoreduction [Pal97]. The photoreduction affects particularly the chemistry of positions N(1), C(4a) and N(5) [Ghi86].

Excitation of the flavins causes the photodegradation of the molecules (i.e. excitation causes the fragmentation of the photoexcited molecules with a certain probability) [Moo69]. Lumichrome formation by photo-excitation of flavin in aqueous solution under anaerobic conditions is a known example for such a reaction [Moo63]. It is found that lumichrome is also formed under aerobic conditions upon photo-excitation of FMN [Hol05]. The relatively higher photostability of FAD with respect to FMN and riboflavin is thought to be due to the photo-induced electron transfer from adenosine moiety to isoalloxazine ring and subsequent non-radiative recombination resulting in a shorter lifetime in the excited state (singlet and especially triplet state) [Hol05].

3 BLUF proteins

Since the first identification of the BLUF domain as a novel blue light photoreceptor approximately ten years ago [Gom02], more than 50 members of the family have been found, where the physiological functions and/or spectroscopic properties are determined for some of these proteins [Jun06]. Those that have been characterized include complex proteins: AppA from phototrophic proteobacterium *Rhodobacter sphaeroides* (anti-repressor of photosynthetic gene expression, [Gom95]), YcgF from *Escherichia coli* (functions as blue light regulated phosphodiesterase [Has06]), PAC from *Euglena gracilis* (blue light receptor for photophobic response [Ise02]) and short proteins: BlrB from R*hodobacter sphaeroides* [Jun05], Slr1694 from cyanobacterium *Synechocystis* sp. PCC6803 (negative phototaxis, [Oka05]) and Tll0078 from thermophilic unicellular cyanobacterium *Thermosynechococcus elongates* BP-1 [Kit05].

A common feature of BLUF proteins is a very similar reversible red-shift of the UV-Vis absorption spectrum of FAD upon illumination which already indicates that the change in the local environment of the FAD binding site upon illumination maybe very similar for these proteins.

Apart from spectroscopic properties, the structural data and physiological function are the other pieces of puzzle essential for understanding the overall signaling mechanism of photoreceptor proteins. Therefore this chapter is assigned to introduce structural data and briefly describe the physiological function (when available) of the investigated BLUF proteins in this dessertation.

3.1 AppA protein from *Rhodobacter sphaeroides*

3.1.1 Physiological function

Rhodobacter sphaeroides is a photosynthetic (PS) bacterium [Coh57]. In the presence of oxygen it derives energy from aerobic respiration. However, when the oxygen tension drops below a certain threshold, the bacterium develops a PS apparatus which allows the use of light as an energy source [Coh57]. Oxygen and light are therefore the major environmental stimulus regulating the development of the PS apparatus [Kil88]. In 1991 PpsR, an oxygen-responsive transcriptional regulator (for *R. Sphaeroides*), has been isolated and identified [Pen91]. It was

found that PpsR acts as a repressor under aerobic conditions (i.e. it shuts down photosynthetic gene expression when the oxygen tension is above a certain level) [Pen94,Pon95].

Soon after, a second protein participating in oxygen-responsive gene expression regulation (from *R. sphaeroides*) was reported [Gom95,Gom97]. The protein nominated AppA according to its gene appA (activation of photopigment and ***puc*** expression) [Gom95].

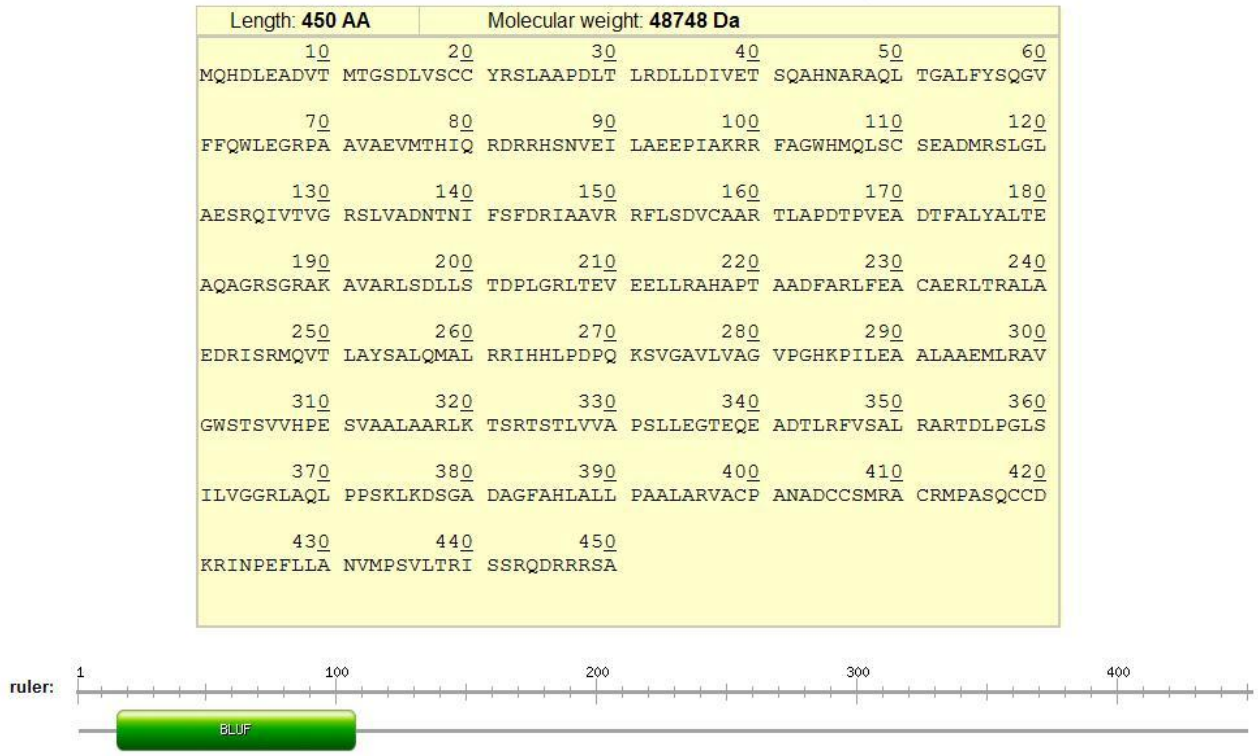

Figure 3-1: Amino acid sequence of AppA protein (top) and graphical view of domain structure (bottom) [1].

AppA contains non-covalently bound FAD in its N-terminal region (~120 amino acids) which exhibits a photo-cycle evidenced by spectral red shift upon excitation with blue light, and back recovery to the start spectrum in dark. The amino acid sequence of AppA protein is shown in Fig. 3-1 [1].

Finally, the results of genetic and biological studies suggest that, *R. sphaeroides* controls its photosynthetic gene expression in three stages [Mas02]. Under aerobic conditions (Fig. 3-2, up), an intramolecular disulfide bond forms between Cys 251 and Cys424 of PpsR protein, that stimulates DNA binding and attenuation of photosynthesis gene expression. Under these conditions, AppA is presumably oxidized (the Cys residues in C-terminal region of AppA make

sulfur bonds) and is therefore functionally inactive as an anti-repressor. As oxygen tension decreases (Fig. 3-2, down), AppA becomes reduced (the sulfur bridges between Cys residues break), which allows it to effectively disrupt the PpsR tetramer by forming a stable AppA-$PpsR_2$ complex.

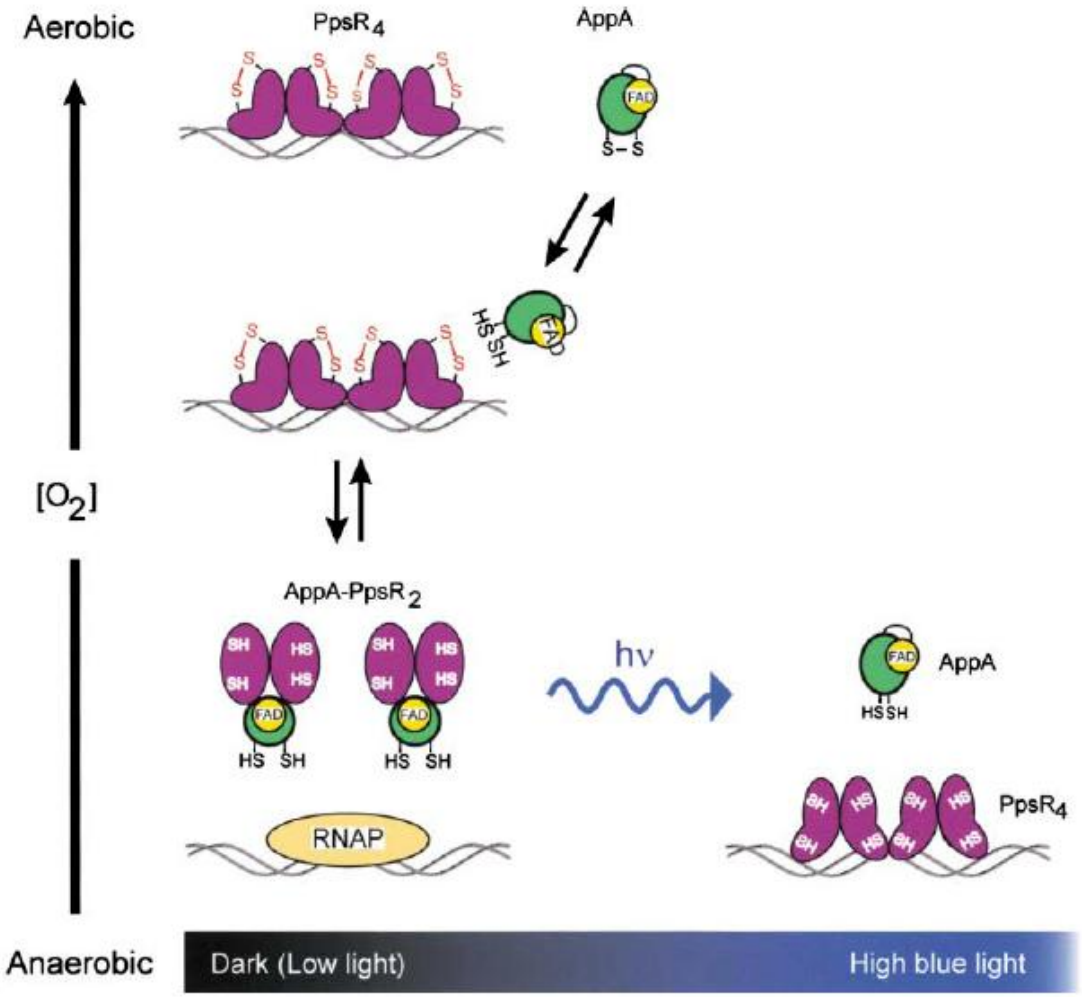

Figure 3-2: Model for AppA-PpsR reaction under aerobic (top) and unaerobic (bottom) conditions. Under aerobic conditions due to the di-sulfide bridge formation (S-S) in the C-terminal of AppA, it is unable to interact with PpsR. As oxygen tension decreases, di-sulfide bond breaks (SH-SH), AppA bonds to PpsR and activates gene expression (RNAP is an enzyme involved in the gene expression and when seated on special loci in the gene initiates gene expression). Under un-aerobic high-light conditions AppA is unable to interact with PpsR. PpsR then represses gene expression [Mas02].

Under strictly anaerobic conditions the ability of AppA to form the AppA-$PpsR_2$ complex is impeded by a blue-light absorption of flavin (under strong blue light exposure the action of the

PS apparatus is slowed down) [Mas02,Shi92]. However unlike oxygen control of the photosynthesis for which molecular mechanism are mostly understood, little is known about light response mechanism and signal transduction pathway between C-terminal and N-terminal of AppA protein.

3.1.2 AppA Crystal structure

Although spectroscopic and genetic studies provide insights into light-response mechanisms of the photoreceptor proteins, crystal structures in exposed and dark state of protein are always essential to understand the atomistic signaling pathway.

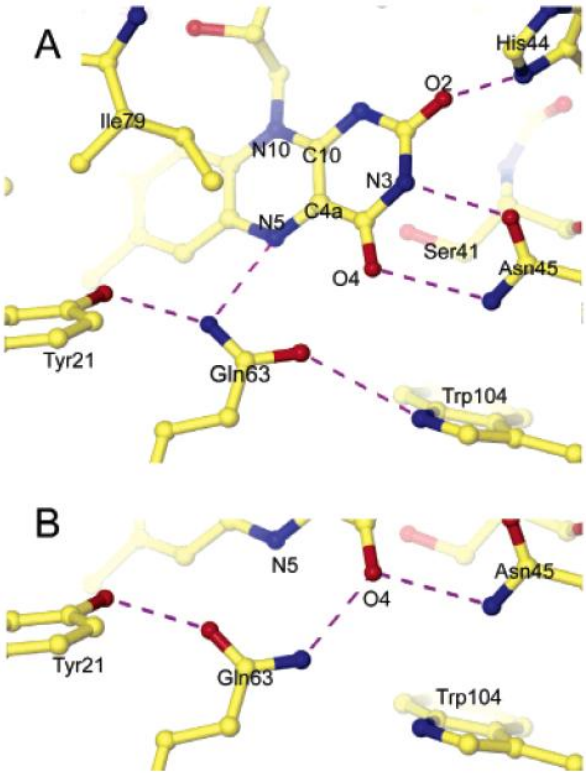

Figure 3-3: (A) Amino acid residues around flavin cofactor in AppA binding pocket according to AppA crystal structure together with suggested H-bound network in dark. (B) suggested H-Bound rearrangement in the light adapted state[And05].

Because of photo-induced disorder, the crystal structure for wild type AppA protein is only available in dark state of protein at 2.3 Å resolution (Fig. 3-3) [And05].

In the face of the wild type protein in which the crystal structure is only available in the receptor state, the crystal structure for AppA-C20S, where Cys20 is replaced by Ser, is resolved in the dark and light adapted states recently [Jun06]. It is used to explain the light response mechanism of AppA protein [Jun06]. The supposed hydrogen bond network rearrangement responsible for the observed photo-cycle will be described comprehensively in the discussion chapter.

3.2 Slr1694 from *synechocystis* sp. PCC6803

3.2.1 Physiological function

Cyanobacteria comprise a unique group of bacteria that perform oxygenic photosynthesis. Plant chloroplasts are believed to have evolved from cyanobacteria although their precise origin is not known yet [Ohm01,Bru03,Nar04,Oka04,Kan96,Nak02].

The 17 kDa Slr1694 protein from cyanobacterium *synechocystis* sp. PCC6803 is one of the BLUF proteins with noncovalently bounded FAD as blue-light photoreceptor in its binding pocket [Kan96]. Slr1694 is a 150 amino acids long protein, belonging to short BLUF proteins, where the BLUF domain is nearly the whole protein [Gom02]. The amino acid sequence of Slr1694 is shown in Fig. 3-4 [2].

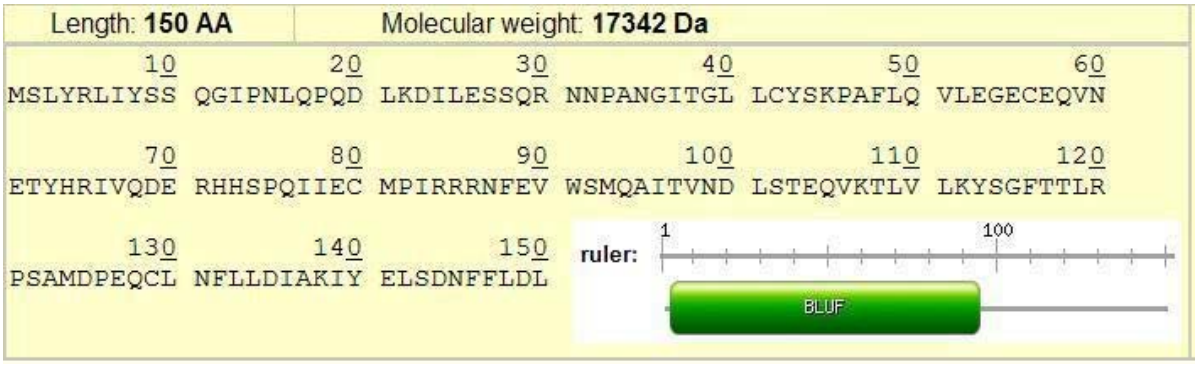

Figure 3-4: Slr1694 amino acid sequence together with graphical view of domain structure (inset) [2].

It is believed that Slr1694 is involved in negative phototaxis in *Synechocystis* [Oka05].

3.2.2 Crystal structure

The crystal structures of Slr1694 in dark and signaling states have become recently available (Fig. 3-5) [Yua06]. This is the first reported crystal structure for wild type protein in both dark and signaling states and therefore of great importance. However it should be mentioned that the crystal structure still suffers from inadequate resolution specially in signaling state [Yua06].

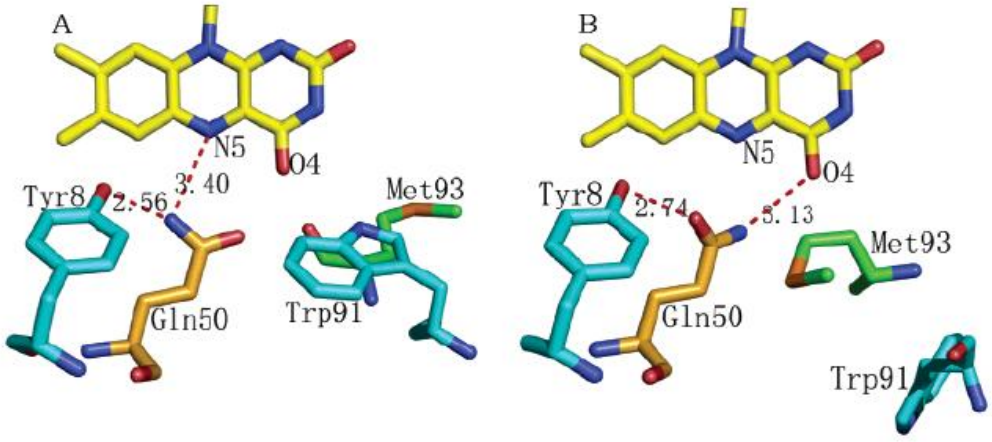

Figure 3-5: Amino acid residues around flavin cofactor in Slr1694 binding pocket according to its crystal structure together with suggested H-bound network in dark (A) and signaling state (B) [Yua06].

3.3 BlrB from *Rhodobacter sphaeroides*

3.3.1 Physiological function

Apart from AppA, the *R. sphaeroides* genome encodes two more BLUF proteins, RSP4060 (134aa) and RSP1261 (140aa) which are known as BlrA and BlrB respectively (for putative blue-light receptors). The physiological function of BlrB protein is not known yet [Jun05]. However due to the protein size, it could be involved in signal transduction via protein-protein interactions [Gom02]. The amino acid sequence of BlrB is depicted in Fig. 3-6 [3].

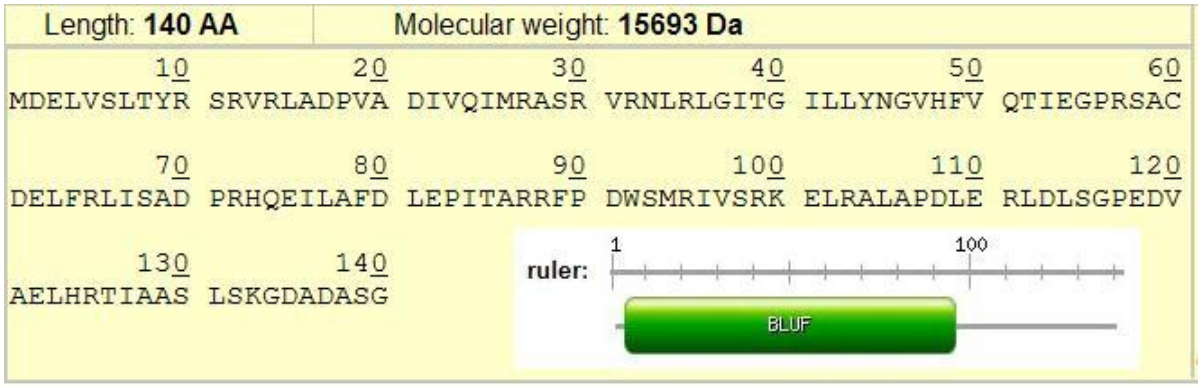

Figure 3-6: Amino acid sequence of BlrB with graphical view of domain structure (inset) [3].

3.3.2 Crystal structure

The crystal structure of BlrB is available in dark at 1.9 Å resolution (Fig. 3-7) [Jun05].

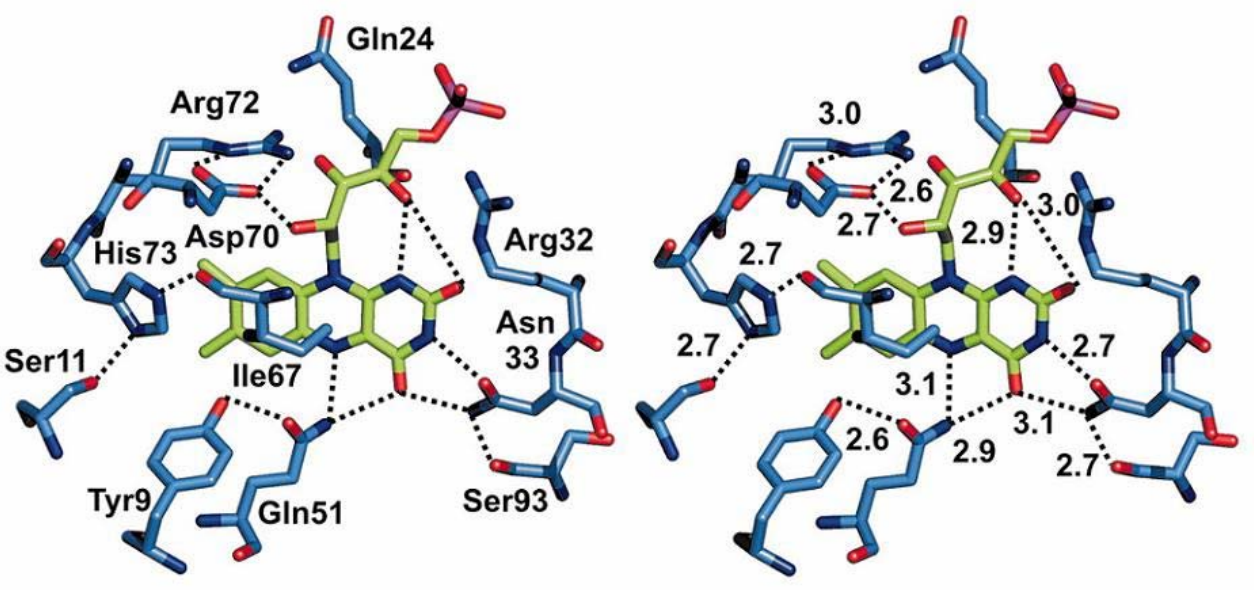

Figure 3-7: Amino acid residues around flavin cofactor in BlrB140 binding pocket according to its crystal structure together with suggested H-bound network in dark state [Jun05].

The crystal structure data will be used in the discussion chapter to compare the spectroscopic properties of the investigated BLUF proteins according to the differences in their binding folds.

4 Fundamentals

In this chapter, a number of processes responsible for excitation and de-excitation of a molecule are briefly introduced. The same nomenclature is used in whole text.

4.1 Absorption

An electronic transition consisting of the promotion of electrons from a lower molecular (or atomic) orbitals to a higher ones triggered by photons is called absorption. The molecule (or atom) is then said to be in an excited state. The characteristics of the molecular orbitals involved in any absorption process (generally any electronic transition) directly influence the properties of the absorption of that special electronic transition [Lac83]. Molecular orbitals are classified according to the spatial overlap of atomic orbitals which they are made of (two atomic s-orbitals or one s- and one p- or two p-orbitals having collinear symmetry axis make σ orbitals whereas lateral overlap of atomic p-orbitals ends up with π orbitals) [Jea93,Atk97]. In addition the multiplicities of the molecular states (e.g. singlet and triplet states defined for spin multiplicities of 1 and 3 respectively) involved in the optical transitions, also affect the absorption properties [Hak00].

The amount of light absorbed or transmitted at a wavelength λ by an absorbing medium is characterized by its absorbance A(λ), or transmission T(λ) (also called pure transmission), in spectroscopy. They are defined as:

$$A(\lambda) = \log\left(\frac{I_0(\lambda)}{I(\lambda)}\right) = -\log T(\lambda)\,, \tag{4-1}$$

$$T(\lambda) = \frac{I(\lambda)}{I_0(\lambda)}\,, \tag{4-2}$$

where $I_0(\lambda)$ and $I(\lambda)$ are the spectral intensities of the light beams at wavelength, λ, entering the absorbing medium and leaving the absorbing medium, respectively.

The absorbance of a sample is related to the concentration of absorbing species C(in mol L^{-1}), absorption path length ℓ (in cm) and extinction coefficient $\varepsilon(\lambda)$(commonly expressed in L mol^{-1} cm^{-1} as molar decadic extinction coefficient) through Beer-Lambert law [Lac83]:

$$A(\lambda) = \varepsilon(\lambda)\ell C\,. \tag{4-3}$$

The decadic absorption coefficient or optical density, *OD(λ)* is defined as the absorbance divided by the sample length, ℓ, as:

$$OD(\lambda) = \frac{1}{\ell} A(\lambda) = \varepsilon(\lambda) C = -\frac{\log(T)}{\ell} . \tag{4-4}$$

In physics instead of the optical density, *OD(λ)*, the absorption coefficient, α(λ), is preferred. It is given by:

$$\alpha(\lambda) = \frac{1}{\ell} \ln \frac{I_0(\lambda)}{I(\lambda)} = OD(\lambda) \ln(10) . \tag{4-5}$$

The absorption coefficient is proportional to the number density, *N*, of the absorbing molecules. The proportionality constant is called the absorption cross-section, *σ(λ)*, and is defined as:

$$\alpha(\lambda) = \sigma(\lambda) N . \tag{4-6}$$

According to eq.(4-6) the absorption cross-section, *σ(λ)*, is the photon-capture area of a molecule. Comparing eqs. 4-4, 4-5 and 4-6 indicate that the absorption cross-section and extinction coefficient are two different forms of the same quantity. This can be easily shown by:

$$\sigma(\lambda) = \frac{1000 \ln(10)}{N_A} \varepsilon(\lambda) \tag{4-7}$$

where N_A, is the Avogadro number ($N_A = 6.022 \times 10^{23}$ mol^{-1}) and other parameters are already defined. Eq. 4-7, is valid when, ε, is measured in L mol^{-1} cm^{-1} and, σ, in cm^2.

4.2 Intrarmolecular interactions

4.2.1 Energy level scheme and relaxation processes

The processes involved in de-populating the excited states can be divided into intramolecular and intermolecular interactions. The energy level scheme suggested by Perrin-Jablonski [Dem06,Val02] (Fig. 4-1) is a simple way to show intramolecular deactivation processes. In Fig. 4-1, the singlet electronic states are denoted with S_0 (for ground state), S_1, S_2,… and the triplet states with T_1, T_2, …**.** Vibrational levels associated with each electronic state are shown with thinner lines. Since the absorption is much faster than all other processes depopulating the excited state, there is no concomitant displacement of the nuclei during the absorption processes (Frank-Condon principle) [Dem06].

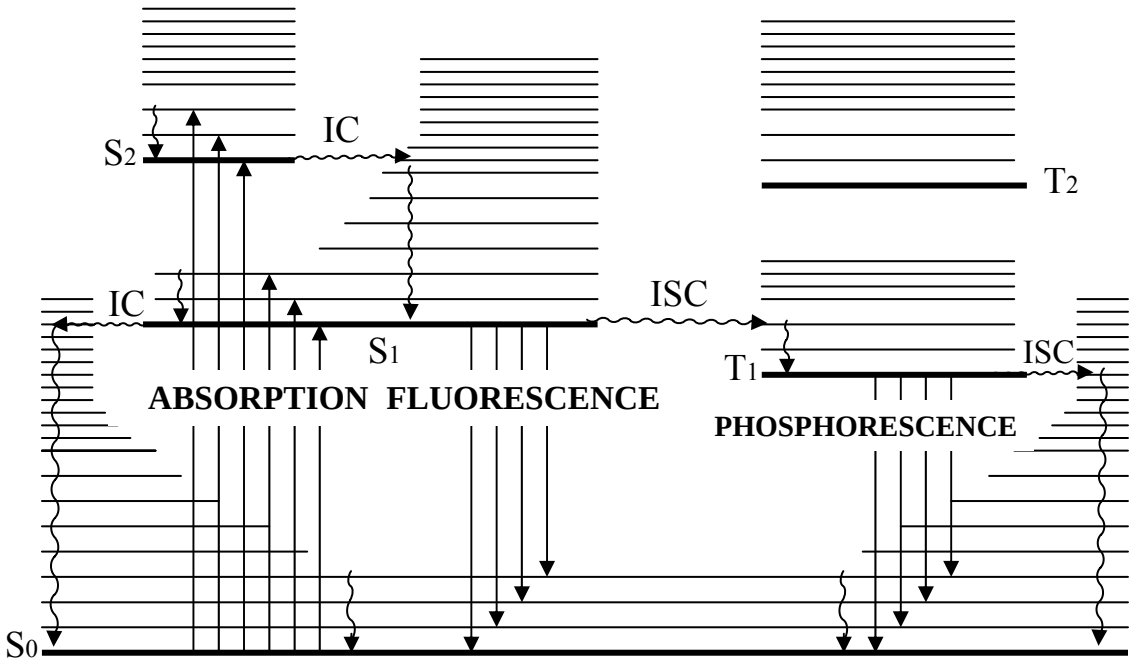

Figure 4-1: Perin-Jablonski diagram for intermolecular de-excitation processes [Val02].

Once a photon is absorbed, the molecule will be in one of the vibrational levels of S_1, S_2, …, where the subsequent excited state de-population processes will compete. Internal conversion (IC), fluorescence, intersystem crossing (ISC), phosphorescence and delayed fluorescence are the de-excitation processes [Lac83,Val02]. Since phosphorescence and delayed fluorescence are not observed experimentally for BLUF proteins, they are not discussed in this text.

Internal conversion is a non-radiative transition between vibrational levels of two different electronic states at the same energy level with the same spin multiplicity. Once a molecule is excited to a higher singlet state ($S_n, n \geq 2$), internal conversion together with vibrational relaxation would lead the molecule to the lowest vibrational level of the S_1 state. This process is normally finished within 10^{-13}-10^{-11}s, where the excess vibrational energy can be transferred to the surrounding solvent molecules by collision. The rate of the internal conversion decreases with increasing energy gap between electronic states involved. Therefore the rate of $S_1 - S_0$ internal conversion is slower than the rate of S_n relaxation to S_1. Typically these rates are of the order of $10^9 - 10^7$ s^{-1} [Lac83,Val02].

Intersystem crossing is a non-radiative transition between two isoenergetic vibrational levels belonging to electronic states of different multiplicity [Val02]. As an example, the molecule in the zero vibrational level of the first singlet excited state can move to a higher vibrational levels

of an excited triplet state, which then would relax to the lowest vibrational level of first electronic triplet excited state by means of internal conversion and vibrational relaxation. Although intersystem crossing is forbidden according to the electric dipole selection rules in approximate theory, it is allowed in the refined theory when spin-orbit coupling is included [Ber00]. The rate of S_1-T_1 intersystem crossing is typically of the order of 10^9-10^7 s^{-1}. It may compete with S_1-S_0 internal conversion in the S_1-state depopulation and lower the fluorescence efficiency [Lac83,Val02]. The intersystem crossing is more efficient in the presence of heavy atoms in the molecule (known as heavy atom effect).

Fluorescence is a radiative transition from an electronic excited state to a lower excited state in the same spin multiplet. Apart from some exceptions, this transition is normally from lowest vibrational level of first electronic singlet excited state to the singlet ground state of the molecule [Lac83].

Since higher excited states relax first to the S_1 state, the fluorescence mostly occurs from this state [Val02]. Due to the dissipation of some part of excitation energy by vibrational relaxation, fluorescence happens at longer wavelengths than absorption which is known as Stokes rule [Gui90].

In addition since at room temperature according to Boltzmann law a small fraction of molecules are in higher vibrational and rotational levels than the 0 level, the absorption and fluorescence spectrums partly overlap. Hence the so called "inner filter effect" which is caused by re-absorption of fluorescence light by the fluorophore itself, should be taken into account (specially in the high chromophore concentration).

4.2.2 Fluorescence lifetime and fluorescence quantum yield

In the absence of intermolecular interactions the de-excitation processes from S_1 to S_0 state can be divided into radiative (fluorescence, rate constant k_r) and non-radiative (internal conversion and intersystem crossing, rate constants k_{ic} and k_{isc} respectively) pathways.

The following differential equation describes the temporal change of the S_1 state population:

$$-\frac{d\left[{}^1A^*\right]}{dt} = \left(k_r + k_{nr}\right)\left[{}^1A^*\right], \tag{4-8}$$

where $\left[{}^1A^*\right]$ is the concentration of excited molecules in the S_1 state and $k_{nr} = k_{ic} + k_{isc}$ is the rate constant for non-radiative processes.

If $\left[{}^1A^*\right]_0$ be the concentration of excited molecules at time 0 after δ-pulse excitation, solving eq. 4-8 would lead to:

$$\left[{}^1A^*\right] = \left[{}^1A^*\right]_0 \exp(-\frac{t}{\tau_F}), \tag{4-9}$$

where τ_F is the excited state lifetime or fluorescence lifetime defined as:

$$\tau_F = \frac{1}{k_r + k_{nr}}. \tag{4-10}$$

If the radiative decay was the only de-excitation pathway from S_1 state, then the excited state lifetime would be $\frac{1}{k_r}$ which is called the radiative lifetime (τ_{rad}). The radiative lifetime can be calculated theoretically by using Strickler-Berg relation [Str62,Bir63]

$$\tau_{rad}^{-1} = \frac{8\pi c_0 n_F^3}{n_A} \frac{\int_{em} E_F(\lambda)\mathrm{d}\lambda}{\int_{em} E_F(\lambda)\lambda^3 \mathrm{d}\lambda} \int_{abs} \frac{\sigma_a(\lambda)}{\lambda}\mathrm{d}\lambda, \tag{4-11}$$

where n_F is the average refractive index in the fluorescence region, n_A is the average refractive index in the region of the first absorption band, $E_F(\lambda)$ is the fluorescence quantum distribution calculated from fluorescence spectrum (see below) and $\sigma_a(\lambda)$ is the absorption cross-section spectrum. The integrals extend over the fluorescence region (*em*) and over the S_0-S_1 absorption band (*abs*).

Another parameter which is often measured in fluorescence studies is the fluorescence quantum yield. It is the ratio of the number of internally emitted photons over the whole emission wavelength region to the number of absorbed photons [Pen87,Hol99]:

$$\phi_F = \frac{\int_{em} S_I(\lambda)d\lambda}{S_{abs}} = \frac{h\nu_L \int_{em} S_I(\lambda)d\lambda}{W_L\left(1 - R_L - T_{RL}\right)} \tag{4-12}$$

where $S_I(\lambda)$ is the intrinsic spectral fluorescence photon density distribution, R_L is the reflectance at the excitation wavelength λ_L, T_{RL} is the transmittance, W_L is the input excitation energy and $\nu_L = C_0/\lambda_L$ is the excitation frequency.

The spectral fluorescence photon density distribution $S_I(\lambda)$ divided by the total number of absorbed excitation photons is defined as fluorescence quantum distribution:

$$E_F(\lambda) = \frac{S_I(\lambda)}{S_{abs}}. \tag{4-13}$$

Using the eqs. 4-12 and 4-13, the eq. 4-14 is obtained between fluorescence quantum distribution and fluorescence quantum yield:

$$\phi_F = \int_{em} E_F(\lambda) d\lambda. \tag{4-14}$$

The intrinsic spectral fluorescence photon density distribution, $S_I(\lambda)$, is experimentally not accessible since it is altered by fluorescence absorption, re-emission, reflection and also geometrical factors. A relation between the measured spectral fluorescence photon density distribution, $S_m(\lambda)$, and $S_I(\lambda)$ is needed for absolute fluorescence quantum yield and fluorescence quantum distribution calculations [Hol99]. This problem is circumvented by application of a reference dye of known fluorescence quantum yield and similar transmission at the same geometrical conditions. The refractive index of the sample and reference solutions have been separately taken into account since for a fixed detection solid angle the measured signal, $S_m(\lambda)$, changes with refractive index of the sample according to [Pen87,Hol99]:

$$S_I(\lambda) \propto S_m(\lambda) \Big/ n_F^2. \tag{4-15}$$

Consequently equations 4-13, 4-14 and 4-15 can be re-written as [Pen87,Hol99]:

$$\phi_F = \frac{\int_{em} S_I(\lambda) d\lambda}{\int_{em} S_{I,R}(\lambda) d\lambda} \frac{(1 - T_{RL,R} - R_{L,R})}{(1 - T_{RL} - R_L)} \phi_R = \frac{\int_{em} S_m(\lambda) d\lambda}{\int_{em} S_{m,R}(\lambda) d\lambda} \frac{(1 - T_{RL,R} - R_{L,R})}{(1 - T_{RL} - R_L)} \frac{n_{F,R}^2}{n_F^2} \phi_R, \tag{4-16}$$

$$E_F(\lambda) = \frac{S_I(\lambda)}{\int_{em} S_{I,R}(\lambda) d\lambda} \frac{(1 - T_{RL,R} - R_{L,R})}{(1 - T_{RL} - R_L)} \phi_R = \frac{S_m(\lambda)}{\int_{em} S_{m,R}(\lambda) d\lambda} \frac{(1 - T_{RL,R} - R_{L,R})}{(1 - T_{RL} - R_L)} \frac{n_{F,R}^2}{n_F^2} \phi_R, \tag{4-17}$$

where $S_{I,R}(\lambda)$, $S_{m,R}(\lambda)$, $T_{RL,R}$ and $R_{L,R}$ are intrinsic spectral fluorescence photon density, the measured spectral fluorescence photon density, transmittance and reflectance of reference respectively.

The fluorescence quantum yield is alternatively defined as the ratio of the emission rate to the total relaxation rate of the excited state de-population [Lac83]:

$$\phi_F = \frac{k_r}{k_r + k_{nr}}. \tag{4-18}$$

Using the definition for fluorescence lifetime and radiative lifetime, fluorescence quantum yield can also be formulated as [Lac83]:

$$\phi_F = \frac{\tau_F}{\tau_{rad}}. \tag{4-19}$$

Eq. 4-19 is only valid if there is a single emitting component. In other words if the eq. 4-19 is not followed, multi-component emission is expected [Val02]. This situation occurs in static fluorescence quenching where part of the emitters are quenched by adjacent quencher molecules and the other part without an adjacent quencher emits with a longer fluorescence lifetime [Sch77].

4.2.3 Fluorescence anisotropy and degree of fluorescence polarization

Chromophores absorb and emit light along a preferred direction (absorption transition dipole moment and emission transition dipole moment respectively) [Val02]. The preferred absorption direction (direction of the transition dipole moment) is generally not same for transitions to different excited states. As a result the degree of fluorescence polarization changes with the excitation light wavelength (according to excitation to different transition states with different direction of transition dipole moments) [Lac83,Val02].

In an isotropic solution, where chromophores are oriented randomly, polarized light excites the chromophores according to the angle which their electric dipole moment makes with the direction of excitation light polarization (photo-selection) [Val02]. This leads to partly polarized fluorescence emission which is reduced by rotational diffusion within the fluorescence lifetime of the excited state [Lac83].

The degree of fluorescence polarization and the fluorescence anisotropy are defined as [Pen87]:

$$P_F = \frac{I_{\parallel} - I_{\perp}}{I_{\parallel} + I_{\perp}}, \tag{4-20}$$

$$r = \frac{I_{\parallel} - I_{\perp}}{I_{\parallel} + 2I_{\perp}}, \tag{4-21}$$

respectively, where $I_{\parallel}$ and $I_{\perp}$ are the fluorescence intensities of the parallel and perpendicular polarized emission with respect to the excitation light polarization direction.

In order to avoid the problem of the dependence of the fluorescence signal on the orientation of the transition dipole moment, for isotropic samples, the magic angle condition is used where the

detection polarizer is at an angle of $\Phi = 54.7°$ with respect to the excitation polarizer (magic angle). Under magic angle condition the fluorescence signal of isotropically oriented molecules is independent of the excitation wavelength and the reorientation of the molecules within the fluorescence lifetime [Val02].

4.3 Intermolecular interactions

In the intermolecular processes, an excited molecule $M*$ is usually de-excited by means of interaction with another molecule Q. Such a reaction is called quenching and the other molecule involved in de-excitation (Q) is known as quencher.

If the quencher molecule is attached to the molecule *M* or is near to the molecule *M*, one speaks of static fluorescence quenching of the excited molecule. On the other hand, if the quencher molecule diffuses to the excited molecules within the excited state lifetime of the excited molecules the process is known as dynamic fluorescence quenching [Eft91].

Quencher molecules interact with the excited molecules by electron transfer or by energy transfer. These processes are discussed in the following.

4.3.1 Electron transfer

Movement of an electron from one substrate (electron donor) to the other (electron accepter) is called electron transfer. It is named photo-induced electron transfer when the process is triggered by absorbing a photon. In other words photo-induced electron transfer is the property of certain molecules which become a stronger oxidizer or reducer upon photo-excitation. As shown in Fig. 4-2, photo-induced electron transfer could be oxidative or reductive.

In most cases electron transfer occurs through an intermediate state in which donor and acceptor molecules are paired. This intermediate state is called *encounter complex* in the case of weak interacting pairs and exciplex (or excimer for chemically same donor and acceptor molecules) for the strong interacting pairs [Kav93,Val02].

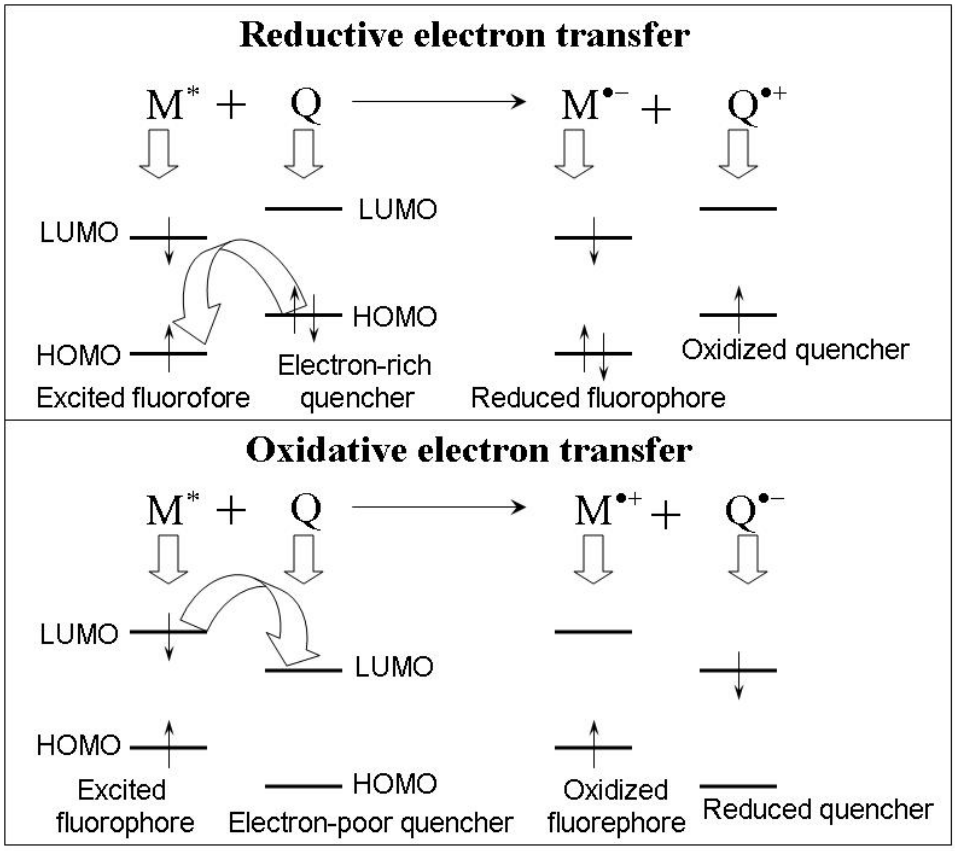

Figure 4-2: (Top): reductive electron transfer, excitation of the molecule M makes electron transfer possible from HOMO of quencher molecule to the HOMO of molecule M. As a result quencher is oxidized and M is reduced. (Bottom): oxidative electron transfer, excitation of molecule M makes transfer of an electron possible from LUMO of molecule M to the LUMO of quencher. As a result M is oxidized and quencher molecule is reduced.

The so-called Rehm-Weller equation, which is based on free energy change of the system upon photo-induced electron transfer are normally used to indicate if the electron transfer process is energetically favored [Kav93]. The free energy change is also used in Marcus theory to estimate the rate of electron transfer (for weak acceptor-donor interaction) [Gil91]:

$$k_{el} = Z \exp(\frac{-\Delta G^*}{RT}), \tag{4-22}$$

where Z is the frequency of collision, R is the gas constant, T is temperature and ΔG^* is the free energy of activation for the electron transfer process.

4.3.2 Excitation energy transfer

Excitation energy can be transfered from an excited molecule (D, donor) to another molecule (A, acceptor) through radiative or non-radiative pathways. In radiative energy transfer, a photon emitted by a donor molecule is reabsorbed by another molecule which is chemically different or same:

$$D^* \rightarrow D + h\nu$$
$$h\nu + A \rightarrow A^* - or - h\nu + D \rightarrow D^* .$$

The radiative energy transfer decreases the fluorescence intensity of the donor molecule in the region of spectral overlap (inner filter effect) [Cro71]. The ratio of the absorbed photons by acceptor molecule to the emitted photons from donor, a, is given by [Val02]:

$$a = \frac{1}{\phi_D^0} \int_0^\infty E_{F,D}(\lambda)(1 - 10^{-\varepsilon_A(\lambda) C_A \ell}) d\lambda , \tag{4-23}$$

where C_A is the concentration of acceptor (in mol dm^{-3}), ϕ_D^0 is the fluorescence quantum yield of donor in the absence of acceptor, ℓ is sample thickness, $E_{F,D}(\lambda)$ is the fluorescence quantum distribution of donor and $\varepsilon_A(\lambda)$ is the extinction coefficient of acceptor.

Non-radiative energy transfer occurs without emission of a photon and results from short range (electron exchange) or long range (dipole-dipole) interactions where in both mechanisms spectral overlap between emission spectrum of donor and absorption spectrum of acceptor is necessary [Lac83].

Long range coulombic dipole-dipole energy transfer was first formulated by Förster (also called Förster type energy transfer) in which energy transfer rate is calculated as [För60]:

$$k_{dd} = k_{F,D} \left[\frac{R_0}{r} \right]^6 = \frac{1}{\tau_{F,D}^0} \left[\frac{R_0}{r} \right]^6 , \tag{4-24}$$

where $k_{F,D}$ and $\tau_{F,D}^0$ are emission rate constant and fluorescence lifetime of donor in the absence of acceptor, r is the distance between donor and acceptor (supposed to be constant during the lifetime of donor), and R_0 the so called critical distance (distance that spontaneous emission and non-radiative dipole-dipole energy transfer rates are same) is defined by:

$$R_0^6 = \frac{9\overline{\kappa^2}\phi_D^0}{128\pi^5 n^4} \int_0^\infty E_{F,D}(\lambda)\sigma_A(\lambda)\lambda^4 d\lambda . \tag{4-25}$$

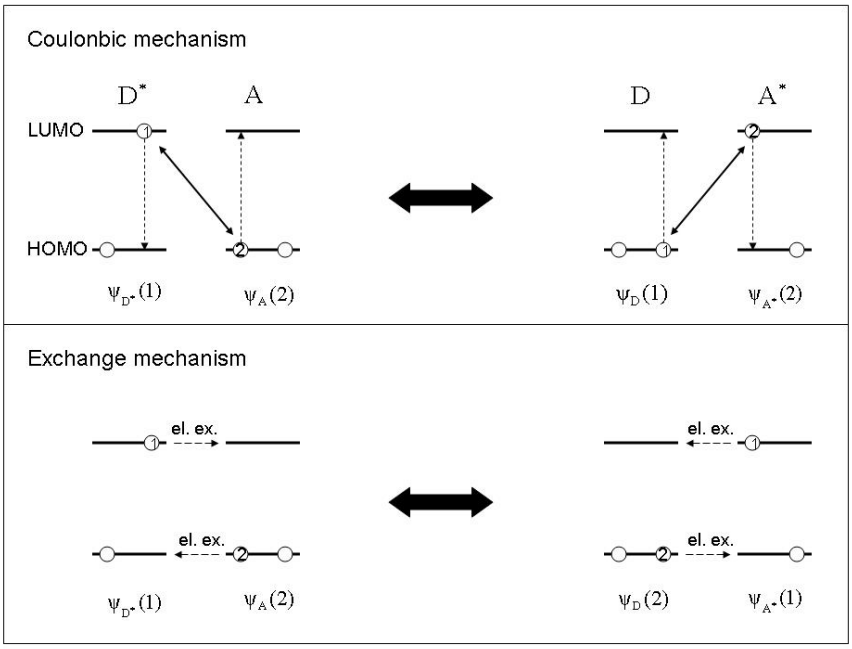

Figure 4-3: (Top): coulombic energy transfer mechanism (Förster type energy transfer), the electron from the LUMO of donor molecule decays non-radiatively and as a result another electron in acceptor molecule is promoted to the excited state (or vise versa). (Bottom): electron exchange mechanism for energy transfer (Dexter type energy transfer), an electron transfer between the LUMO of the donor and acceptor molecules is accompanied by transfer of another electron between their HOMO [Val02].

In the last equation, $\overline{\kappa^2}$ is an orientational factor varying between 0 and 4. For isotropic orientation of the donor and acceptor the orientation factor is, $\overline{\kappa^2} = 2/3$ [Val02].

Short range electron exchange energy transfer mechanism was initially formulated by Dexter in 1953 (also called Dexter type energy transfer) [Dex53]. In contrast to the inverse sixth power dependence of Förster type energy transfer rate constant on distance between acceptor and donor molecules, an exponential dependence is found for the Dexter type energy transfer. In Fig. 4-3 both Dexter and Förster type energy transfer mechanisms are shown schematically. It is worthwhile to note that singlet-singlet energy transfer $\left({}^1D^* + {}^1A \rightarrow {}^1D + {}^1A^*\right)$ is allowed in all types of short range and long range non-radiative energy transfer interactions, while triplet-triplet energy transfer $\left({}^3D^* + {}^1A \rightarrow {}^1D + {}^3A^*\right)$ is only allowed for electron exchange interactions [Val02].

5 Experimental methods

5.1 Absorption measurements

The absorption cross-section spectra of dark adapted samples are determined by transmission measurements with a commercial double-beam spectrophotometer (Beckman type ACTA M IV). Using the relation $T(\lambda) = \exp[-\alpha(\lambda)\ell]$, the transmission spectra $T(\lambda)$ are converted to absorption coefficient spectra $\alpha(\lambda)$, where ℓ is the sample path length.

Absorption cross-section spectra ,$\sigma_a(\lambda)$, are related to the absorption coefficient spectra, $\alpha(\lambda)$, by the relation, $\sigma_a(\lambda) = \alpha(\lambda) / N$, where N is the number density. In the investigated BLUF domains the concentration of the chromophores, FAD, FMN and riboflavin, was not known. Therefore the absorption cross-section spectra were determined by calibration to the absorption cross-section spectra of FAD, FMN or riboflavin (since the absorption cross section spectra of FAD, FMN and riboflavin for the applied pH conditions (pH8) are the same, they all could be equally used for calibration [Hol05]). For this purpose the absorption cross-section integrals ($\sigma_a(\tilde{\nu}) = \alpha(\tilde{\nu}) \int \sigma_{a,R}(\tilde{\nu}) d\tilde{\nu} / \int \alpha_a(\tilde{\nu}) d\tilde{\nu}$, where $\sigma_{a,R}(\lambda)$ is the absorption cross-section spectrum of riboflavin for example, and $\tilde{\nu} = 1/\lambda$ is the wavenumber) extending over the S_0-S_1 and S_0-S_2 absorption band (λ > 310 nm) are set equal since the same chromophore(s) is(are) present [Hol02].

Fig. 5-1 shows the experimental setup used to obtain the absorption coefficient spectra of samples in the signaling-state. The small volume samples (1.5 ×1.5 ×3 mm^3) are exposed with a high pressure mercury lamp through an interference filter (IF). An attenuated tungsten lamp is used as the probe light source. The probe light is focused on sample place by L_1 and L_2 lenses and imaged on the spectrometer by L_3 and L_4 lenses. It is detected with a diode-array photo-detector (tracor DARRS system) after dispersion in the spectrometer.

Whenever necessary to improve the time resolution of dark recovery measurements, two mechanical choppers (Thorlabs, model SH05) are inserted in the excitation and probe paths (see Fig. 5-1). A pulse generator is used for timing of the choppers and detector. Although time resolution of about 10ms is achieved by using the choppers, the real time resolution is much longer (about 15 s due to the time required for data transfer from diode-array to computer).

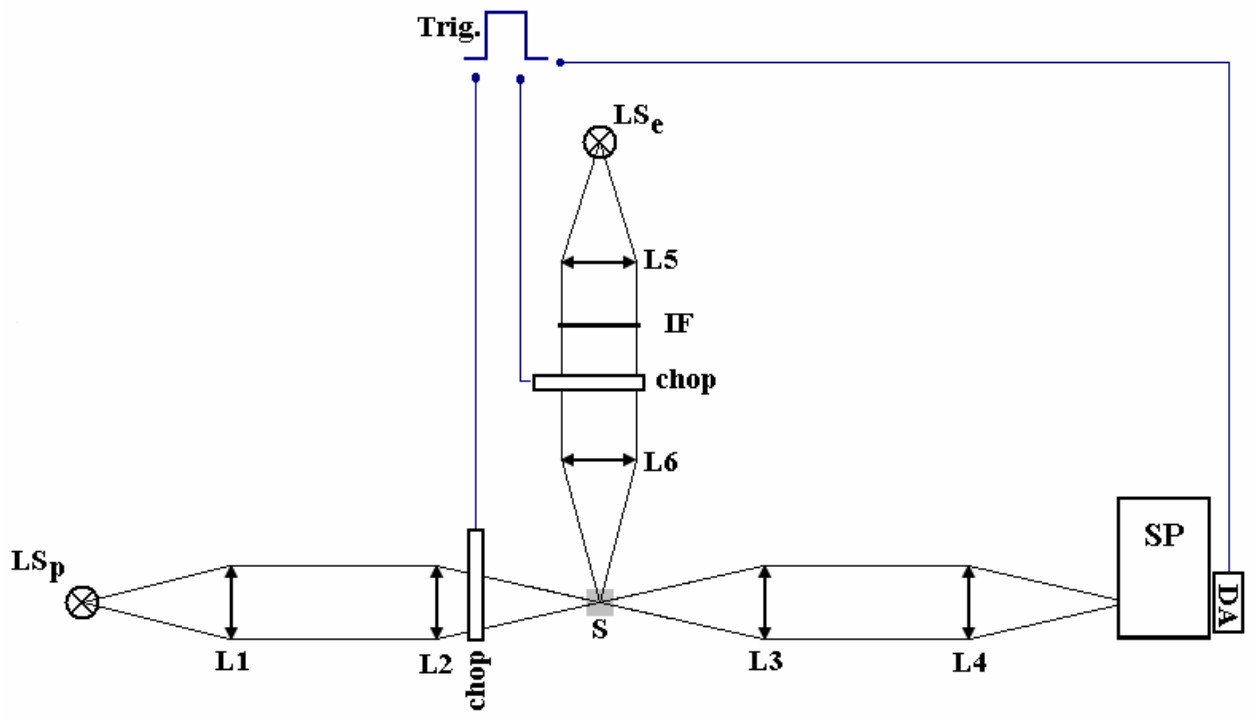

Figure 5-1: Experimental setup for studying temporal development of absorption spectrum. LSp: light source for probe light (tungsten lamp). LS_e: light source for excitation light (high pressure mercury or xenon lamp). L_1-L_6: lenses. IF: interference filter. Chop: triggerable mechanical chopper (used for fast dark recovery studies). SP: spectrometer. DA: diode-array. Trig: pulse generator (for triggering choppers and detector). S: sample.

For those cases where it was not essential to have the complete absorption spectrum, the temporal absorption changes due to the signaling state formation by light switch-on and due to back-recovery by light switch-off were studied by a probe light transmission measurement at a selected wavelength (via interference filter) with a silicon photo-diode as a detector ($1cm^2$ cross-sectional area) and a digital signal recorder (20 sample/sec) (same arrangement as Fig. 5-1, where polychromator and diode-array is replaced with a silicon photodiode and digital signal recorder).

5.2 Spectral fluorescence measurements

The fluorescence spectra were measured with a self-assembled fluorometer in front-face collecting arrangement [Pen87,Hol99] (Fig. 5-2).

In the experimental setup shown in Fig. 5-2 a high pressure mercury lamp is used as excitation light source, where the excitation wavelength is selected by means of an interference filter (IF). The excitation light is focused to the sample place by the lenses L1 and L2. In the detection path

the fluorescence light is collected with L3 and L4 lenses and detected with a diode-array photo-detector (tracor DARRS system) combined with spectrometer.

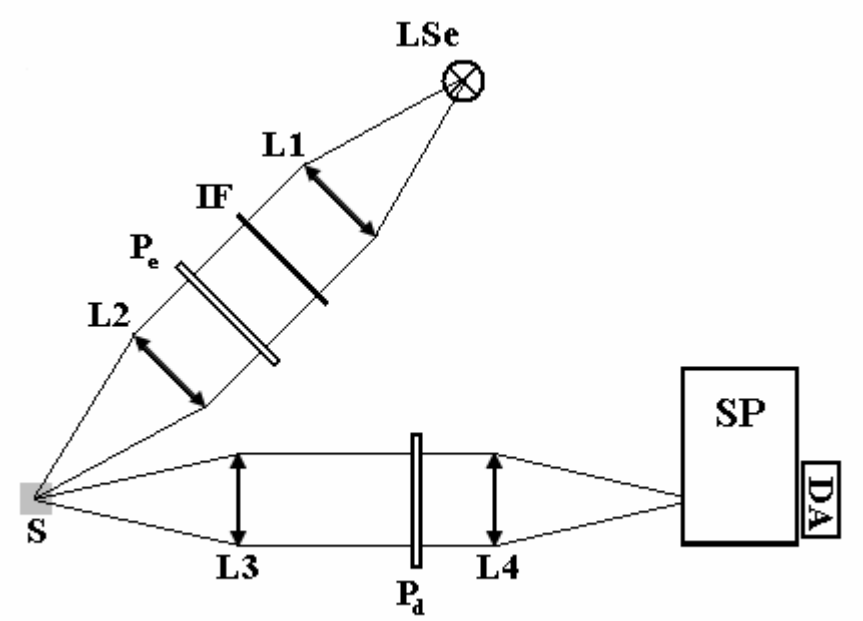

Figure 5-2: Experimental setup used for spectral fluorescence measurements. LSe: light source for excitation (high pressure Mercury lamp or Xenon lamp). L1-L4: lenses. Pe and Pd: polarizers in excitation and detection path respectively. IF: interference filter. SP: spectrometer. DA: diode-array. S: sample.

For fluorescence polarization analysis and also fluorescence quantum yield measurements two polarizer sheets are used in the excitation and detection paths.

The fluorescence quantum distributions, $E_F(\lambda)$ (see theory), were determined by vertical polarized excitation and magic angle detection (the polarizer transmission axis in detection path was set to an angle of 54.74° with respect to the vertical direction of the excitation light [Dam88]). The absolute fluorescence quantum yield and fluorescence quantum distribution for protein samples are obtained by comparing their fluorescence with a dye of known fluorescence quantum yield under the same experimental conditions. Since all the samples which are investigated here contain flavin as a chromophore, lumiflavin in pH8 water (ϕ_F=0.235) is used as reference because of similar fluorescence spectrum and high photostability [Hol05].

The fluorescence degree of polarization is determined by measuring fluorescence spectrums parallel, $I_{\parallel}$, and perpendicular, $I_{\perp}$, to the excitation light polarization direction (polarization sensitivity of detection system considered in calculations). The arrangement shown in Fig. 5-2 is also used for fluorescence measurement of long-time exposed samples.

5.3 Temporal fluorescence measurements

The temporal fluorescence behavior of the samples is studied in different time ranges: Sub-nanosecond to nanosecond (real time fluorescence life time measurement) and sub-picosecond to picosecond regions (with fluorescence up-conversion technique).

5.3.1 Real time fluorescence measurements

The experimental setup used for real time fluorescence life time measurement is shown in Fig 5-3, where frequency doubled (using a BBO crystal) short laser pulses from Ti:sapphire femtosecond oscillator-amplifier laser system (laser system Hurricane from Spectra-Physics, Darmstadt, Germany) at 400 nm are used for excitation.

The laser was operated with a pulse duration of $\Delta t_L = 4\,ps$ (FWHM) and a micro channel plate photomultiplier (MCP) (type R1564-U01 from Hamamatsu photonics Deutschland, Heidelberg, Germany) together with a high-speed digital oscilloscope (type DSO 9362 from LeCroy Deutschland, Heidelberg, Germany) were used for fluorescence detection. The fluorescence light is imaged on MCP via L_3 and L_4 lenses where the 400nm excitation light is blocked by an interference filter. For signaling-state fluorescence lifetime measurement the samples were excited using a high pressure mercury lamp (wavelength of which is selected by an interference filter and focused on the sample via L_1 and L_2 lenses) before the picosecond pulse excitation and fluorescence trace recording. The development of the fluorescence traces during long-time excitation was studied by continuous exciting the samples with high intensity light and taking fluorescence traces by single picosecond pulse excitations at certain time intervals. In addition the photodiodes PD1 and PD2 placed before and after sample enable transmission measurement during fluorescence trace recording.

The response function of detection system is obtained by recording a strongly attenuated laser pulse (obtained 1/e-time constant is $\tau_{resp} \approx 370$ ps).

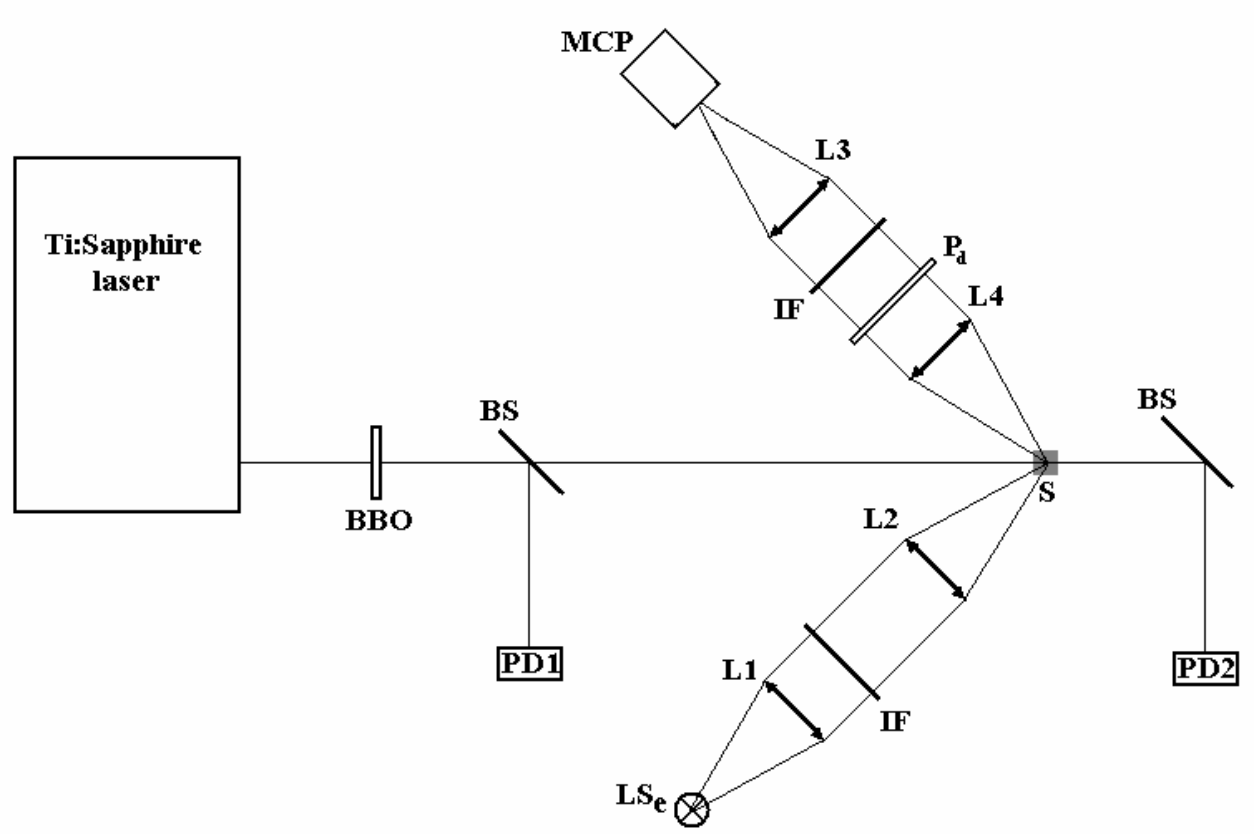

Figure 5-3: Experimental setup used for real time fluorescence lifetime measurement. BBO: beta-BaB_2O_4 nonlinear optical crystal for second harmonic generation (400 nm light generation). BS: beam splitter. L_1-L_4: lenses. P_d: polarizer. IF: interference filter. LS_e: excitation light source (high pressure mercury or xenon lamp). MCP: micro channel plate. PD: photodiode. S: sample.

5.3.2 Fluorescence up-conversion

For fluorescence lifetime measurements at sub-picosecond to picosecond region the fluorescence up-conversion technique is used (Fig. 5-4). The principle of this technique is based on phase matched frequency mixing of the fluorescence light (excited by the frequency doubled femtosecond laser pulses) with a suitably time delayed fundamental laser beam in a nonlinear optical crystal. The so called up-conversion takes place only when the delayed laser pulse and fluorescence signal are both present at the BBO_u crystal (where nonlinear up-conversion occurs). As a result the time resolution is limited to the laser pulse width [Dam88,Sch01].

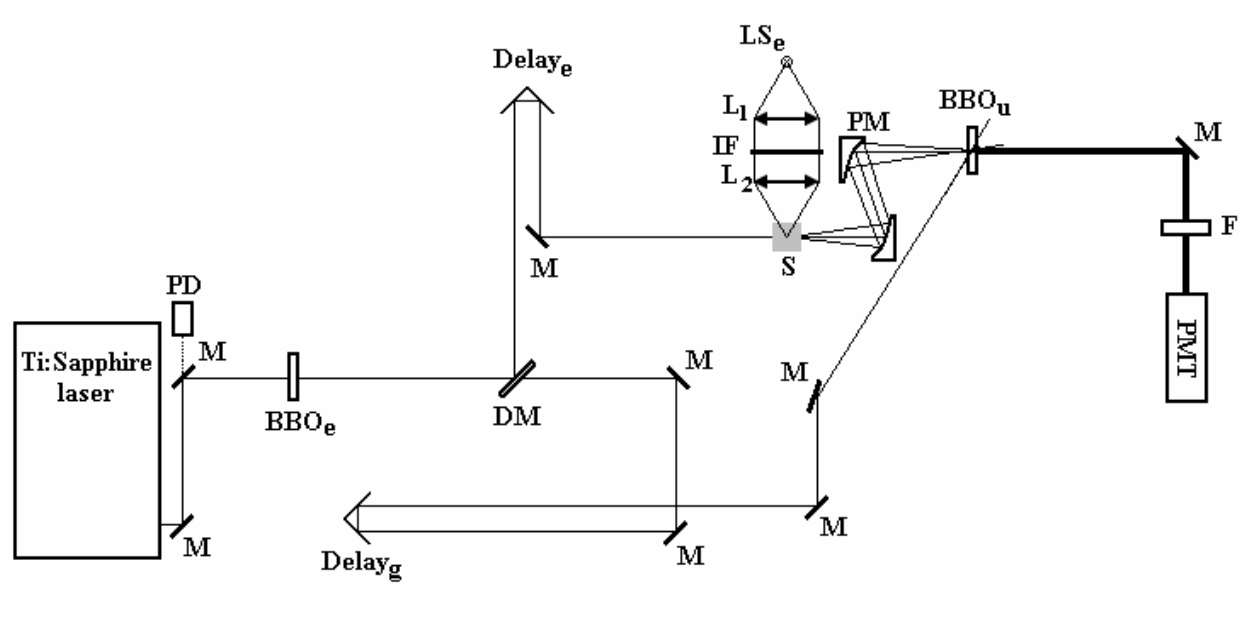

Figure 5-4: Experimental setup used for fluorescence lifetime measurement with up-conversion technique. M: mirror. BBO_e: BBO crystal used for frequency doubling (400 nm light generation). BBO_u: BBO crystal for sum frequency generation (up-converting fluorescence and gate beams). DM: dichroic mirror (reflecting 400 nm and transmitting 800 nm). $Delay_g$: manual delay line for gate pulse (delay length 1 m).$Delay_e$: stepper motor driven delay line (delay length 50cm). PM: parabolic mirror. F: filter (270-380 nm). LS_e: excitation light source (high pressure Mercury lamp). L_1-L_2: lens. IF: interference filter. PD: photodiode. PMT: photomultiplier. S: sample.

For measuring fluorescence lifetime with the up-conversion technique the laser was operated with 110 fs pulse duration. The samples were excited with frequency doubled (400 nm) femtosecond laser pulses, where a dichroic mirror was used to separate fundamental and frequency doubled beams. The generated fluorescence signal is collected by parabolic mirrors and focused on the second BBO crystal (0.2 mm thick) where the frequency mixing with the fundamental laser pulse takes place (type II phase matching [Boy92]: $\nu_F(e)+\nu_G(o)\rightarrow\nu_S(e)$, *o*: ordinary polarized light and *e*: extraordinary polarized light, *G*: gate beam (here fundamental) and *F*: 400 nm excited fluorescence). The 400 nm beam is time delayed relative to the gate beam by using a stepper motor driven linear translation stage. The up-converted signal is passed through a broad band filter (Schott glass UG11 of 10mm thickness, transmission window from 270 nm to 380 nm) and is detected with a photomultiplier tube (Valvo, type PM2254B) and a high speed digital oscilloscope (LeCroy, type DSO 9362). The second delay line ($Delay_g$ in Fig. 5-4) which is changed manually allows to increase the delay length of the system to follow the fluorescence decay over longer times, when necessary.

To measure fluorescence lifetime of the signaling state, the high pressure mercury lamp (wavelength of which is selected by an interference filter and focused on the sample by L_1 and L_2 lenses) is used to prepare the signaling state before femtosecond pulse excitation.

6 Results

6.1 AppA

The BLUF domains $AppA_{148}$ (amino acid residues 1-148, see Fig. 3-1) and $AppA_{126}$ (amino acid residues 1-126) from R. *sphaeroides* are studied.

6.1.1 Chromophore composition

Fig. 6-1 shows the thin-layer-chromatogram (TLC) analysis used for revealing mole fraction of non-migrating isoalloxazine derivatives, riboflavin, FMN and FAD. The extracted mole fractions are listed in Table 6-1 [Zir05].

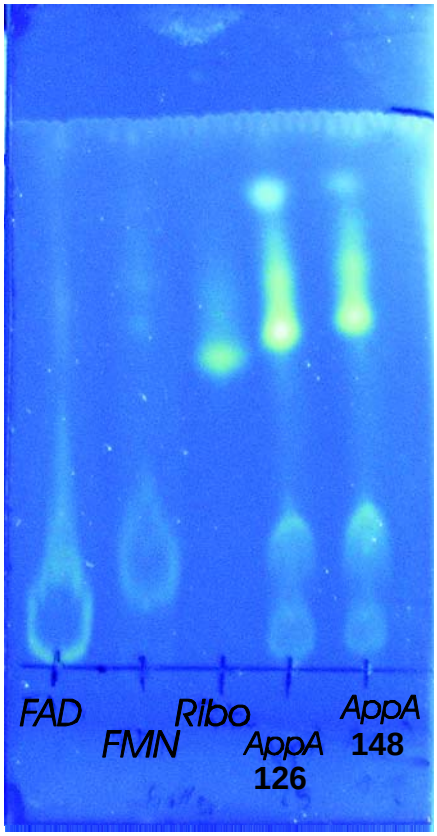

Figure 6-1: Thin-layer-chromatogram traces of FAD, FMN, Riboflavin (Ribo), $AppA_{126}$ and $AppA_{148}$

6.1.2 Absorption studies

The absorption coefficient spectra for $AppA_{148}$ in the dark-state and signaling-state (prepared with excitation for 3 min at λ_{exc} = 428 nm, light intensity $I_{exc} \approx 0.01 W cm^{-2}$) are shown in Fig. 6-2. They are calculated from transmission measurements as described in chapter 5. As illustrated in Fig. 6-2, the S_0-S_1 absorption band of the signaling-state is 16nm red-shifted compared to that of the dark-state.

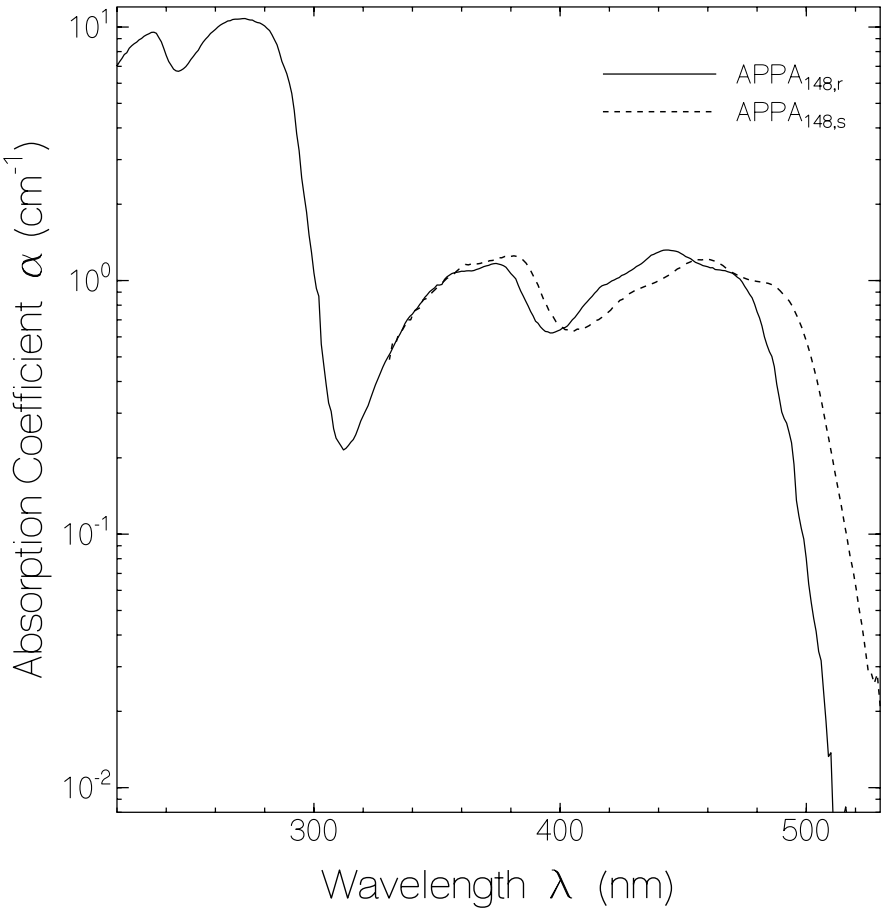

Figure 6-2: Absorption coefficient spectra for $AppA_{148}$ in dark-state ($AppA_{148,r}$) and $AppA_{148}$ in the signaling-state ($AppA_{148,s}$) in aqueous solution buffered to pH8. The S_0-S_1 absorption peak is 16 nm red-shifted compared to that of dark state.

The absorption coefficient spectra are used to calculate the absorption cross-section where the absorption cross-section spectrum of riboflavin is employed for calibration, as described in chapter 5.

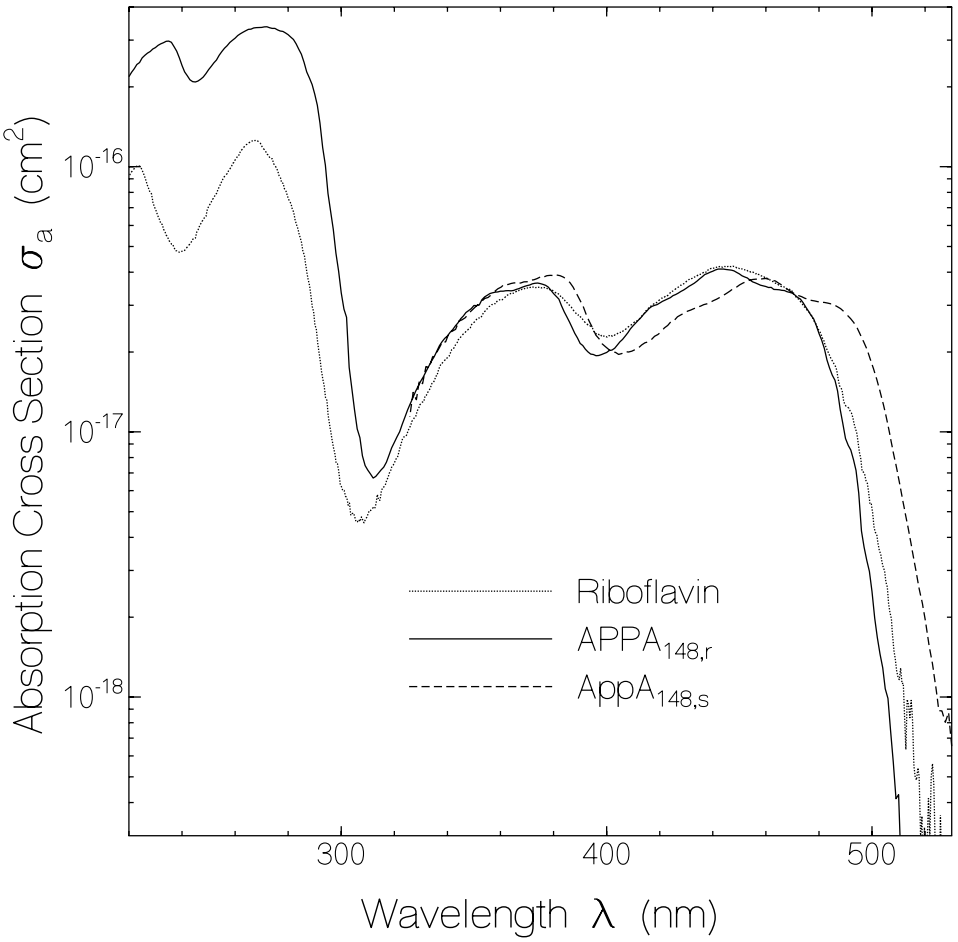

Figure 6-3: Absorption cross-section spectra of riboflavin, AppA$_{148,r}$, and AppA$_{148,s}$, in the aqueous solution at pH8.

Fig. 6-3 shows the absorption cross-section spectra for AppA$_{148}$ in the dark-state and signaling-state together with the absorption cross-section of riboflavin [Drö02] for comparison. The absolute absorption cross-section spectra of the signaling state of AppA BLUF are extracted from the intersection point at 454nm where the absorption cross-section of the dark adapted and light adapted forms are the same. Fig. 6-3 shows that the absorption cross-section spectra of AppA$_{148,r}$ and riboflavin are quite similar and only below 310 nm absorption cross-section of AppA$_{148}$ is larger (mainly because of absorption contribution of aromatic amino acids [Leh93]). In addition the vibronic structures of the S_0-S_1 and S_0-S_2 absorption bands (444nm and 374nm respectively) are more pronounced for AppA than for riboflavin.

Similar absorption cross-section spectra for the dark-state and signaling state of AppA$_{126}$ are obtained (data not shown).

6.1.3 Fluorescence studies

The fluorescence quantum distributions are calculated from spectral fluorescence measurements as described in chapters 4 and 5. The absolute intrinsic fluorescence quantum distributions, $E_F(\lambda)$, are determined using riboflavin in water buffered to pH 7 ($\phi_{F,R} = 0.26$ [Hol05]) as reference (by means of eqs. 4-12 and 4-13). Fig. 6-4a shows the absolute intrinsic fluorescence quantum distributions for dark-state and signaling-state proteins ($AppA_{148}$ and $AppA_{126}$) in buffer solution at pH 8 together with that of riboflavin and FAD in aqueous solution at pH 7 for comparison. As Fig. 6-4 shows, dark-adapted fluorescence spectra for $AppA_{148}$ and $AppA_{126}$ are approximately 16nm blue-shifted compared to free flavins FAD and riboflavin.

The fluorescence quantum yields are calculated from $E_F(\lambda)$ with the relation $\phi_F(\lambda) = \int E_F(\lambda) d\lambda$ (see chapter 4) and are listed in table 6-1. They are $\approx 2\%$ and $\approx 0.1\%$ for dark- and signaling-states of $AppA_{148}$ and $\approx 2\%$ and $\approx 0.2\%$ for dark- and signaling-states of $AppA_{126}$ respectively. The measured fluorescence quantum yields are much lower than fluorescence quantum yields for FMN, FAD and riboflavin in aqueous solution and at the same pH [Hol05].

The degree of fluorescence polarization spectra for dark and light adapted proteins ($AppA_{148}$ and $AppA_{126}$) are shown in Fig. 6-4b. They are listed in Table 6-1 for dark-state and signaling-state proteins. The degrees of fluorescence polarization are reasonably high, compared to that of free flavin in aqueous solution (e.g. $P_F \approx 0.0146$ for riboflavin in neutral aqueous solution [Leh93]), indicating that the non-covalently bound flavin chromophores are hindered in free rotation by the protein binding pocket.

In addition to the spectral fluorescence measurements, temporal fluorescence measurements are carried out to possibly understand the mechanism/s leading to the fluorescence quenching of the flavins inside protein binding pocket.

Fig. 6-5 shows the fluorescence traces excited with picosecond laser pulses ($\lambda_L = 400$ nm, $\Delta t_L = 4$ ps) and fluorescence detected with a micro-channel-plate photomultiplier and a fast digital oscilloscope (real time lifetime measurement, see chapter 5). The response function of the detection system is shown by the dotted curve (approximately Gaussian shape with 1/e-time constant of $\tau_{resp} \approx 370$ ps). Outside the response-function region the fluorescence signals fit reasonably well with single exponential decay function. The best fitting decay times are given in the Fig.6-5a for $AppA_{148}$ and Fig. 6-5b for $AppA_{126}$ and are listed in Table 6-1. They are about

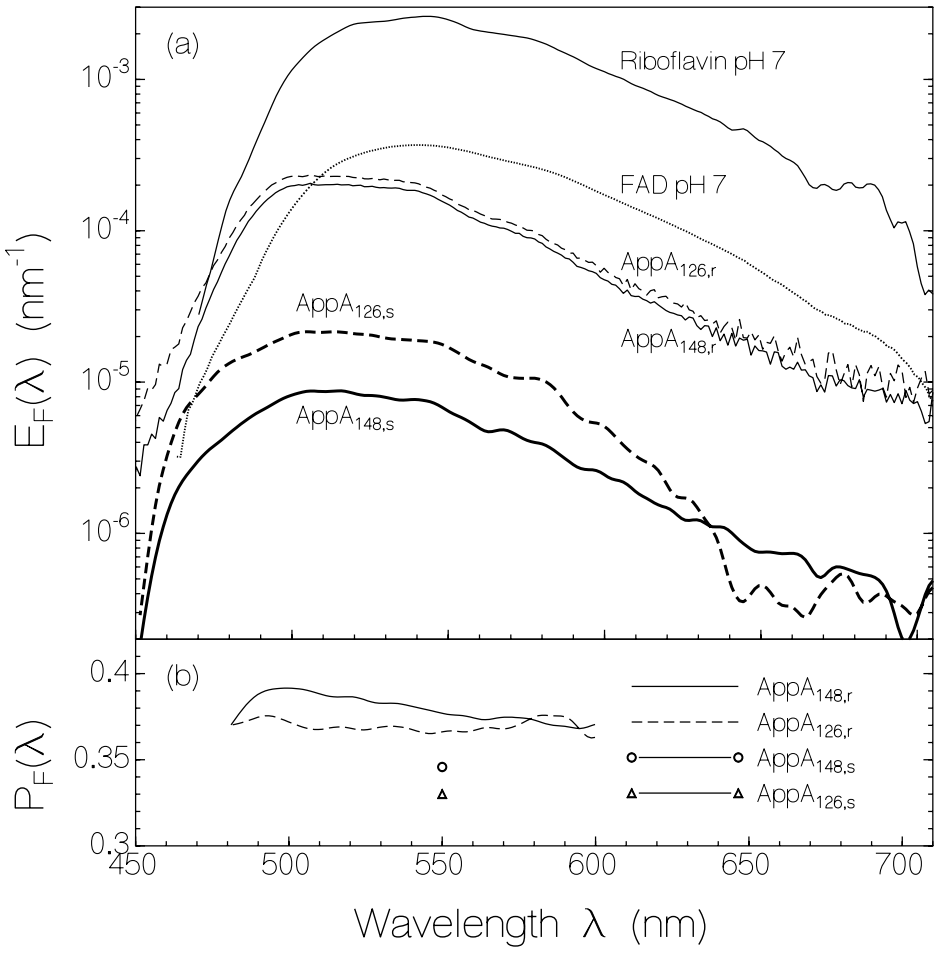

Figure 6-4: (a) Fluorescence quantum distrbution, $E_F(\lambda)$, of dark-state and signaling-state $AppA_{148}$ and $AppA_{126}$ in aqueous solution at pH 8 together with fluorescence quantum distribution of riboflavin and FAD in aqueous solution at pH 7. (b) Degree of fluorescence polarization, $P_F(\lambda)$, of dark-state signaling-state $AppA_{148}$ and $AppA_{126}$ in aqueous solution at pH 8. The fluorescence degree of polarization is shown in a single wavelength for the proteins in the signaling-state, due to the lower quality of the degree of fluorescence polarization spectra in this state.

$\tau_{F,r,sl} \approx 900$ ps for the dark-state, and $\tau_{F,nc} \approx 1.1$ ns to 1.6 ns for the signaling-state of the $AppA_{148}$ and $AppA_{126}$ proteins.

The measured fluorescence lifetimes do not agree with average fluorescence lifetimes which are calculated by the eq. 4-19 (e.g. the average fluorescence lifetime of about 490 ps is calculated for $AppA_{148,r}$ while the fluorescence lifetime is measured to be 938 ps). This discrepancy is due to the presence of components with shorter fluorescence lifetimes [Fle86,Sch87,Eck82] which are

not resolved in the applied real-time measurements (due to not enough time resolution). In order to resolve these fast component/s fluorescence up-conversion measurements were employed.
In Fig. 6-6 ($AppA_{148}$ and $AppA_{126}$ in the dark-state) and Fig. 6-7 ($AppA_{148}$ and $AppA_{126}$ in the signaling-state) the temporal fluorescence development was recorded by non-linear optical up-conversion of the fluorescence light with variable time-delayed fundamental femtosecond laser pulses in a BBO crystal (see chapter 5). The line-connected circles are measured.

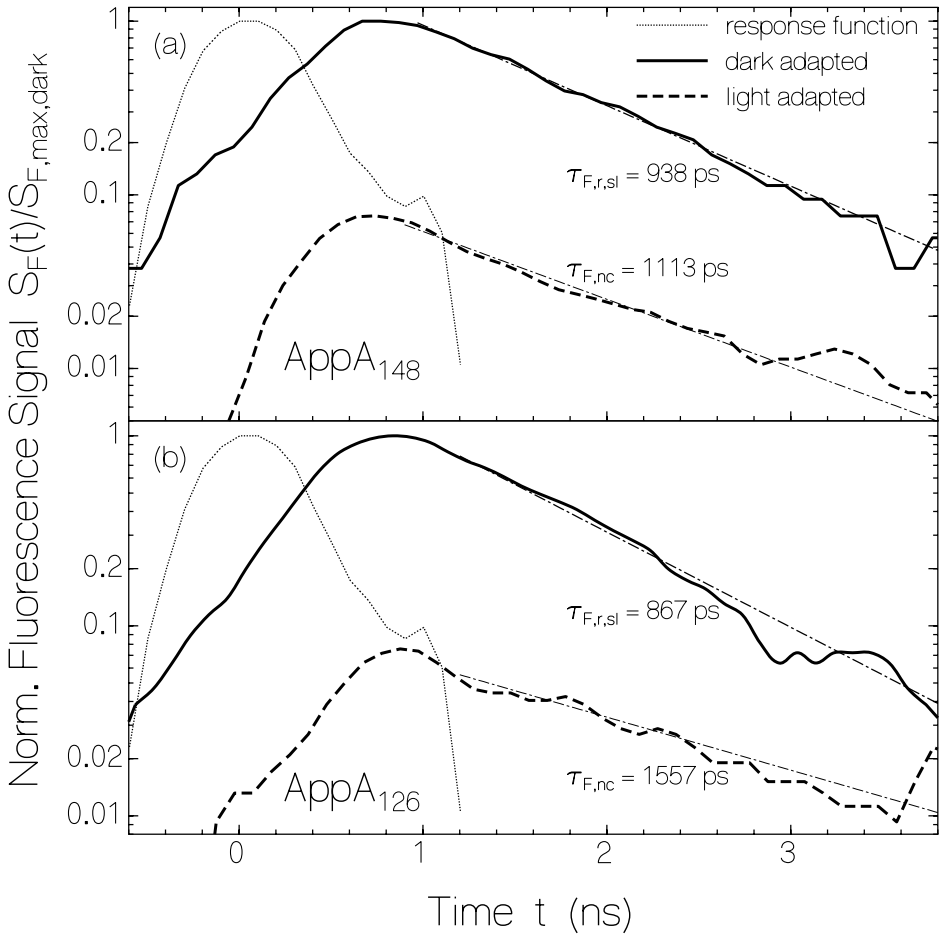

Figure 6-5: Normalized temporal fluorescence signals, $S_F(t)/S_{F,max,dark}$, of dark-adapted (thick solid curve) and light-adapted (thick dashed curves) of (a) $AppA_{148}$ and (b) $AppA_{126}$ in aqueous solution at pH 8 buffer. Fluorescence excitation with femtosecond laser system (λ_L = 400 nm, pulse duration Δt_L = 4 ps, beam diameter at sample 3.5 mm, pulse energy attenuated to micro-channel-plate photomultiplier signal height in the 5 mV to 50 mV range). Dotted line shows experimental response function of the detection system. Dash-dotted lines are single-exponential decay fits according to $S_F(t) = S_F(t_0)\exp[-(t-t_0)/\tau_F]$. The fit parameters are given in the figure.

The dotted curves show the response function of the measurement system (nearly triangular shaped with a decay half-width of $\tau_{resp} \approx 300$ fs).

These measurements reveal a component with a short fluorescence lifetime of $\tau_{F,r,f} \approx 230$ ps for $AppA_{148}$ and of $\tau_{F,r,f} \approx 120$ ps for $AppA_{126}$ together with a slow fluorescence lifetime components of $\tau_{F,r,sl} \approx 940$ ps for $AppA_{148}$ and of $\tau_{F,r,sl} \approx 870$ ps for $AppA_{126}$. On the other hand Fig. 6-7 shows fluorescence lifetimes of $\tau_{F,s,f} \approx 2.8$ ps and $\tau_{F,s,sl} \approx 48$ ps for $AppA_{148}$ and of $\tau_{F,s,f} \approx 2.2$ ps and $\tau_{F,s,sl} \approx 32$ ps for $AppA_{126}$ in the signaling-state.

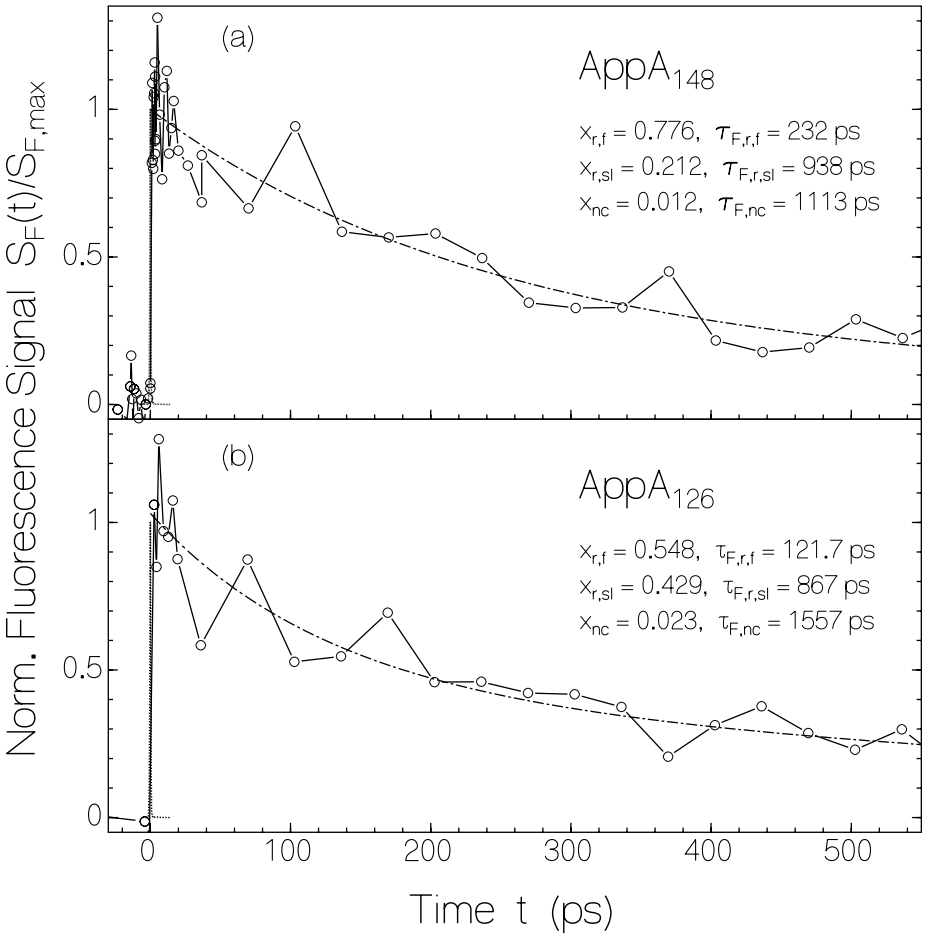

Figure 6-6: Femtosecond laser up-converted fluorescence signal versus femtosecond pulse delay time, *t*, for dark-state $AppA_{148}$ (a) and $AppA_{126}$ (b) in aqueous solution at pH 8 and at room temperature. Line-connected points are measured. Dash-dotted curve is a three-component exponential fit according to eq. 6-2 with parameters given in the figure. Dotted lines give response function of the system.

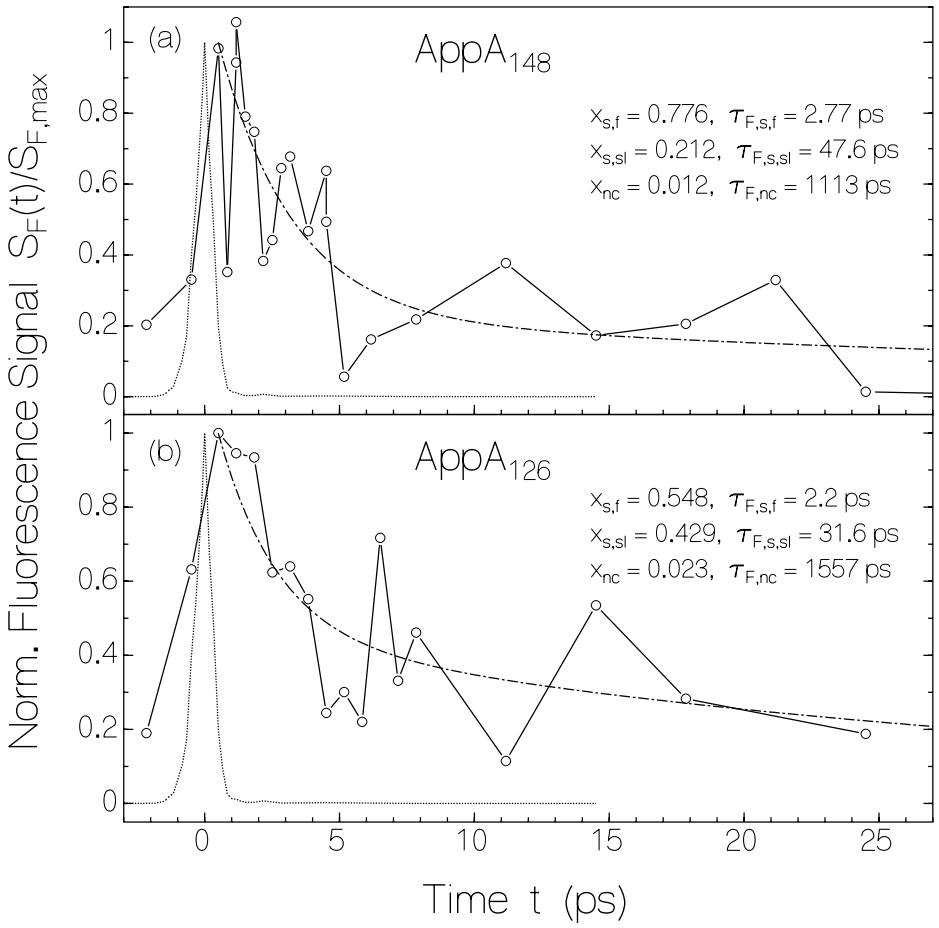

Figure 6-7: Femtosecond laser up-converted fluorescence signal versus femtosecond pulse delay time, *t*, for signaling-state (a) $AppA_{148}$ and (b) $AppA_{126}$ in aqueous solution at pH 8 and at room temperature. Line-connected points are measured. Dash-dotted curves are three-component exponential fit according to eq 6-2 with parameters given in the figure. Dotted lines give response function of the system.

The dash-dotted curves in Figs. 6-6 and 6-7 result from three-component exponential fits using the relation:

$$S_F(t) = S_F(t_0) \sum_{i=f,sl,nc} x_i \exp[-(t-t_0)/\tau_{F,i}], \tag{6-1}$$

where x_i is the mole-fraction of component *i* with fluorescence lifetime $\tau_{F,i}$ ($\sum_{i=f,sl,nc} x_i = 1$). The fit parameters x_i and $\tau_{F,i}$ are listed in Figs. 6-6 and 6-7 and are collected in Table 6-1. The three-component fit of the AppA BLUF domains implies that the fluorescence quantum efficiency, ϕ_F, of the domains is also composed of three components according to:

$$\phi_F = \sum_{i=f,sl,nc} x_i \phi_{F,i} = \sum_{i=f,sl,nc} x_i \frac{\tau_{F,i}}{\tau_{rad}}. \tag{6-2}$$

In the regression fits of Figs. 6-6 and 6-7 the mole fractions, x_i, of AppA conformations are assumed to be the same in the dark-state and the signaling-state (three distinct components). The time-constant of the longest-time component, $\tau_{F,nc}$, is assumed to be the same for the dark-adapted and the light-adapted states (no formation of a signaling state, time constants taken from Fig. 6-5a and Fig. 6-5b for $AppA_{148}$ and $AppA_{126}$ respectively). The other two components are thought to make conformational changes in conversion from the dark-adapted state to the light-adapted state (rearrangement of hydrogen bonds, see discussion). The time constants, $\tau_{F,r,sl}$, of the slow dark-adapted forms are taken from Fig. 6-5a and Fig. 6-5b for $AppA_{148}$ and $AppA_{126}$ respectively. In addition eq. 6-2 is used to implicitly determine the mole-fraction of one component in the dark-adapted and the light-adapted state. The other parameters are determined in the fits. A component with mole fractions of about 1% for $AppA_{148}$ and about 2% for $AppA_{126}$ which has the same decay time in the dark-state and signaling-states could be explained if it is supposed that this component does not participate in signaling-state formation upon light exposure. It is likely that this small fraction of chromophore is adsorbed to the protein surface and is not in the protein binding pocket. It dominates the fluorescence when the proteins are in their signaling-states. This will also explain the rather low degree of fluorescence polarization in the signaling-state with respect to the dark-state and also the higher fluorescence quantum yields for dark-state and specially signaling-state of $AppA_{126}$ compared to $AppA_{148}$ ($AppA_{126}$ has more fraction of this component compared to the $AppA_{148}$, see Figs. 6-6 and 6-7).

6.1.4 Photo-cycle dynamics

The absorption coefficient change at λ_p = 493.1 nm during high intensity light exposure, I_{exp} = 0.01 W cm^{-2} at λ_{exp} = 428nm, for $AppA_{148}$ and $AppA_{126}$ are displayed in Fig. 6-8a.

According to Fig .6-8a, the signaling state is formed quickly, but after formation the absorption during long-time exposure remains constant which indicates a high photo-stability of the light-adapted form. Fig. 6-8a, allows the determination of the quantum yield of photo-degradation of the chromophores in the signaling-state, $\phi_{D,s}$, for $AppA_{148}$ and $AppA_{126}$. It is defined as the number of degraded molecules to the number of absorbed photons and is determined by the relation:

$$\phi_{D,s} = \frac{N_{s,D}}{n_{ph,abs}}. \qquad (6\text{-}3)$$

Thereby $N_{s,D} = \int_0^l N_{s,D} dz$ is the length-integrated number density of degraded signaling state molecules, ℓ is the sample length, $N_{s,D}$, is the number density of degraded molecules, and $n_{ph,abs}$ is the density of absorbed photons at the excitation wavelength λ_{exc}. Assuming that the degraded molecules do not absorb at the probe wavelength, then $N_{s,D}$ is given by:

$$N_{s,D} = \frac{[\overline{\alpha}_{a,s,p}(t_1) - \overline{\alpha}_{a,s,p}(t_2)]\ell}{\sigma_{a,s,p}}, \tag{6-4}$$

in which $\overline{\alpha}_{a,s,p}(t_1) = -\ln[T_{s,p}(t_1)]/l$ and $\overline{\alpha}_{a,s,p}(t_2) = -\ln[T_{s,p}(t_2)]/l$ are the length-averaged absorption coefficients at time t_1 and t_2. The number of absorbed photons per cross-sectional area within the time interval $t_2 - t_1$ is:

$$n_{ph,abs} = \frac{(t_2 - t_1) I_{exc}(1 - \overline{T}_{exc})}{h\nu_{exc}}, \tag{6-5}$$

where I_{exc} is the input light intensity and $\overline{T}_{exc} = [T_{exc}(t_1) + T_{exc}(t_2)]/2$ is the average transmission at λ_{exc} during the time period $t_2 - t_1$.

Although Fig. 6-8a shows no absorption coefficient decrease of the probing wavelength during long time exposure, taking the experimental accuracy into account, an upper limit for the quantum yield of photo-degradation of $\phi_{D,s,max} \approx 1\times10^{-6}$ is estimated for $AppA_{148,s}$ and $AppA_{126,s}$. The dark recovery of $AppA_{148}$ after 1 min exposure and of $AppA_{126}$ after 318 sec excitation at room temperature and at 493.1 nm are shown in Fig. 6-8b. There the function:

$$\alpha(\lambda_p, t) = \alpha(\lambda_p, \infty) + \left[\alpha(\lambda_p, 0) - \alpha(\lambda_p, \infty)\right] \exp\left(-\frac{t}{\tau_{d,rec}}\right) \tag{6-6}$$

is used to fit the absorption decrease where $\tau_{d,rec}$ is the signaling state recovery time in dark at room temperature. The best fittings give 16.7 min for $AppA_{148}$ and 18.8 min for $AppA_{126}$.

The finite dark recovery to the initial conformation at room temperature indicates some ground-state barrier. The barrier height may be estimated using an Arrhenius-type function for the rate of transfer from the signaling state to the receptor state [Sch87,Mas02]:

$$k_{d,rec} = \frac{1}{\tau_{d,rec}} = k_0 \exp\left(-\frac{W_b}{k_B \vartheta}\right), \tag{6-7}$$

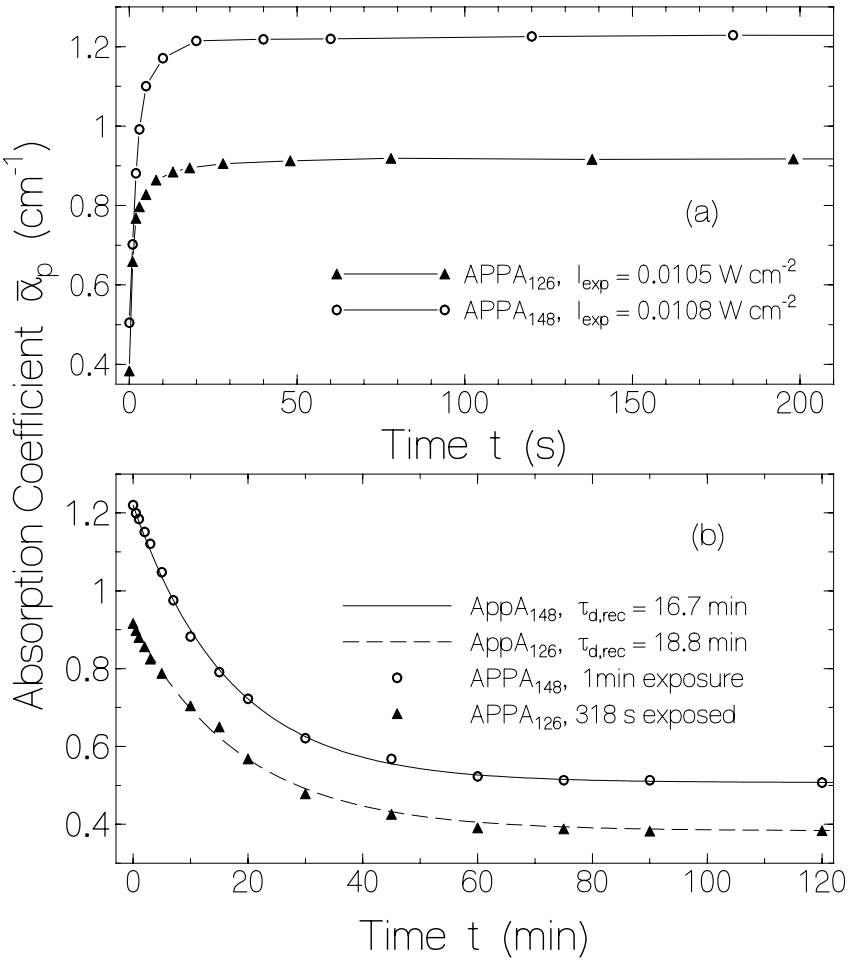

Figure 6-8: (a) Temporal absorption coefficient increase at λ_p = 493.1 nm due to light exposure at λ_{exc} = 428 nm with an intensity of I_{exc} = 0.0108 W cm^{-2} for AppA$_{148}$ and of I_{exc} = 0.0105 W cm^{-2} for AppA$_{126}$. (b) Temporal absorption coefficient recovery in the dark at λ_p = 493.1 nm after light exposure at λ_{exc} = 428 nm. Data points are measured and curves are calculated by eq. 6-6 with recovery time constant, τ_{rec}, as fit parameter. Circles and solid curve: AppA$_{148}$, time of light exposure t_{exp} = 1 min, excitation intensity I_{exc} = 0.0108 W cm^{-2}, τ_{rec} = 16.6 min. Triangles and dashed curve: AppA$_{126}$, t_{exp} = 318 s, excitation intensity I_{exc} = 0.0105 W cm^{-2}. τ_{rec} = 18.8 min.

where k_0 is the attempt frequency of barrier crossing, W_b is the energy barrier height from the signaling ground-state to the receptor ground-state, k_B is the Boltzmann constant, and ϑ is the temperature. The attempt frequency is given by the oscillation frequency of the potential well of the signaling state along the signaling-state to the receptor-state coordinate. It is typically of the order of 10^{12} Hz to 10^{13} Hz [Laa03,Web66a]. Using an attempt frequency of $k_0 = 10^{13}$ s^{-1}, barrier heights of $W_b = 1.5016\times10^{-19}$ J (7554 cm^{-1}) for AppA$_{148}$ and $W_b = 1.5064\times10^{-19}$ J (7579 cm^{-1}) for AppA$_{126}$ are calculated.

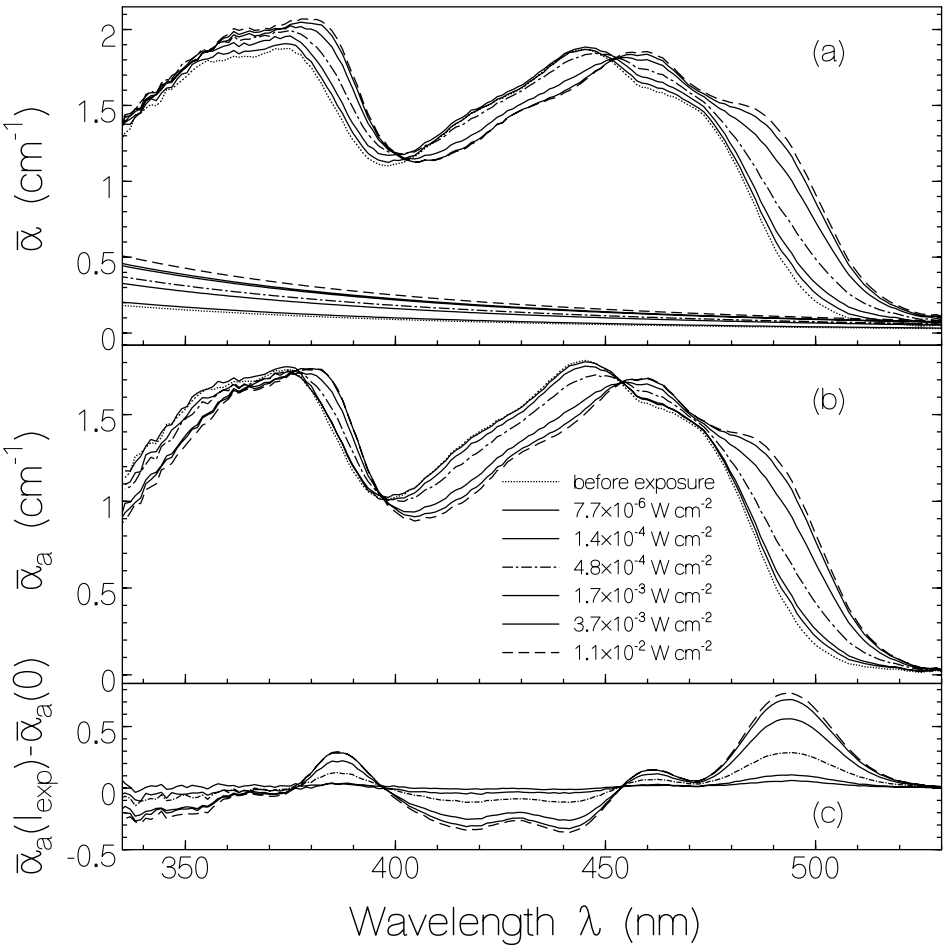

Figure 6-9: Dependence of absorption spectra of $AppA_{148}$ on the excitation light intensity. Excitation wavelength λ_{exc} = 428 nm, cell thickness ℓ = 1.5 mm, cell area, 1.5 mm × 3.5 mm. Exposure time, t_{exp} = 1 min. Time interval between exposures is 30 min for $I_{exc} \le 1.6\times10^{-3}$ W cm^{-2}, and 40 min for $I_{exc} > 1.6\times10$-3 W cm^{-2}. (a) Length-averaged total absorption spectra, $\bar{\alpha}(\lambda) = -\ln[T(\lambda)]/\ell = \bar{\alpha}_a(\lambda) + \alpha_s(\lambda)$, including pure absorption, $\bar{\alpha}_a(\lambda)$, and scattering contribution, $\alpha_s(\lambda)$, together with approximate scattering specta , $\alpha_s(\lambda)$. (b) pure absorption spectra, $\bar{\alpha}_a(\lambda)$. (c) difference absorption spectra, $\bar{\alpha}_d(\lambda) = \bar{\alpha}_a(\lambda, I_{exc}) - \bar{\alpha}_a(\lambda,0)$.

Conformational changes leading to hydrogen bond exchanges between chromophore and nearby amino acid residues have been discussed to stabilize the signaling state [Laa03].

The excitation intensity dependence of absorption coefficient spectra for $AppA_{148}$ is shown in Fig 6-9. There, part (a) shows the total absorption spectra, $\bar{\alpha}(\lambda) = \bar{\alpha}_a(\lambda) + \alpha_s(\lambda)$, including the pure absorption, $\bar{\alpha}_a(\lambda)$, and the scattering part $\alpha_s(\lambda) = \alpha_s(\lambda_0)\,(\lambda_0/\lambda)^4$ [Boh83]. Part (b) shows the pure absorption spectrum, $\alpha_a(\lambda)$, where scattering contribution is subtracted and part (c) shows the difference absorption spectra of exposed and unexposed samples. Below 380nm the

extrapolated scattering contribution is not exact which causes some inaccuracy in the difference spectra there.

Similar absorption changes due to the excitation with different light intensities were obtained for $AppA_{126}$ (data not shown).

The difference absorption spectra between exposed and unexposed samples, as shown in Fig .6-9c, have their maximum at λ_p = 493.1nm. The difference absorption coefficient at 493.1nm as a function of excitation intensity, are shown in Fig. 6-10 for $AppA_{148}$ and $AppA_{126}$. They are used to extract the quantum yields of photo-induced signaling state formation, ϕ_s (eqs. 6-8, 6-9 and 6-10, see below).

Based on the performed absorption and fluorescence studies a scheme of the photo-cycle dynamics of the two photo-active components together with an inactive component of the AppA BLUF domains are shown in Fig. 6-11 (for both $AppA_{148}$ and $AppA_{126}$ proteins).

As illustrated by Fig. 6-11, the receptor state excitation is the first event in photo-cycle. The excited chromophore could return back to the ground state by radiative or non-radiative processes or causes chromophore-protein rearrangement leading to a putative signaling-state formation (red-shift in absorption spectrum). The signaling-state recovers back to the receptor state at room temperature with a time constant, τ_{rec}. No further chemistry is observed due to photo-excitation indicating a high photo-stability of the proteins.

Following the suggested photo-cycle scheme, the temporal development of the active receptor and signaling state number densities are given by the following rate equation system:

$$\frac{\partial N_s}{\partial t} = \phi_s \frac{\sigma_{a,exc} I_{exc}}{h\nu_{exc}} (N_0 - N_{nc} - N_s) - \frac{N_s}{\tau_{d,rec}}, \tag{6-8}$$

$$\frac{\partial I_{exc}}{\partial z} = -\sigma_{a,exc}(N_0 - N_s) I_{exc} - \sigma_{a,s,exc} N_s I_{exc} - \alpha_{s,exc} I_{exc}, \tag{6-9}$$

where z is the coordinate along the propagation direction, $\sigma_{a,exc}$ is the absorption cross-section of the dark-adapted sample at the excitation wavelength λ_{exc}, $\sigma_{a,s,exc}$ is the absorption cross-section of the light-adapted sample at λ_{exc} ,$\tau_{d,rec}$ is the signaling state recovery time in the dark, $\alpha_{s,exc}$ is the scattering coefficient at the excitation wavelength and N_0 , N_s and N_{nc} are the total number density of chromophores, the number density of chromophores in the signaling-state, and the number density of the chromophores which are not in protein binding pocket respectively.

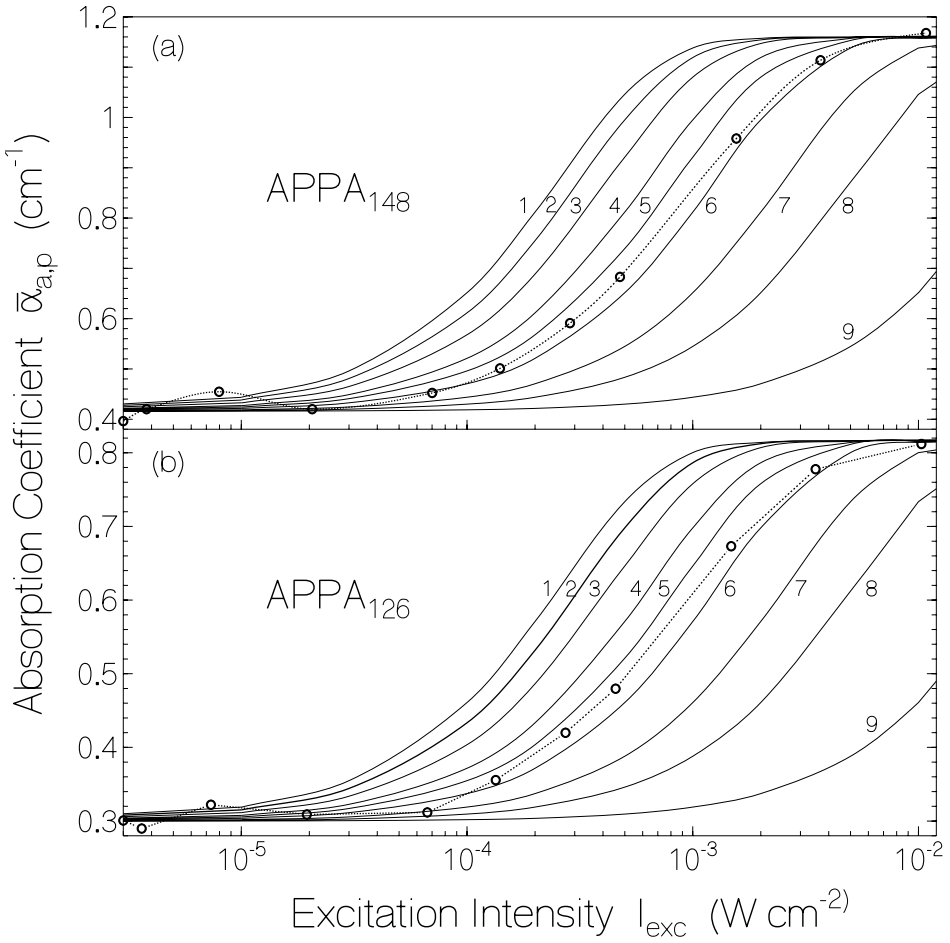

Figure 6-10: Intensity dependent increase of absorption coefficient of $AppA_{148}$ (a) and $AppA_{126}$ (b) at wavelength λ_p = 493.1 nm due to light exposure at λ_{exc} = 428 nm (dot-connected circles). Solid curves are calculated by use of eqs. 6-8 till 6-10. quantum yield, ϕ_s, of signaling-state formation is varied: (1) ϕ_s = 1, (2) 0.8, (3) 0.6, (4) 0.4, (5) 0.3, (6) 0.2, (7) 0.1, (8) 0.05 and (9) 0.01.

The solid curves in Fig. 6-10 are calculated for different quantum yields, ϕ_s, by numerical solution of the equation system (6-8,9) and application of:

$$\alpha_{a,p}(t) = [N_r(t) + N_{nc}]\sigma_{a,p} + N_s(t)\sigma_{a,s,p}. \qquad (6\text{-}10)$$

for the absorption coefficient ,$\alpha_{a,p}(t)$, at the exposure time , t, and probe wavelength, λ_p, where $N_r(t) = N_0 - N_s(t) - N_{nc}$ is the number density of chromophores in protein with receptor state conformation. The best fits to the experimental data give $\phi_s(AppA_{148})$ = 0.24 and $\phi_s(AppA_{126})$ = 0.25.

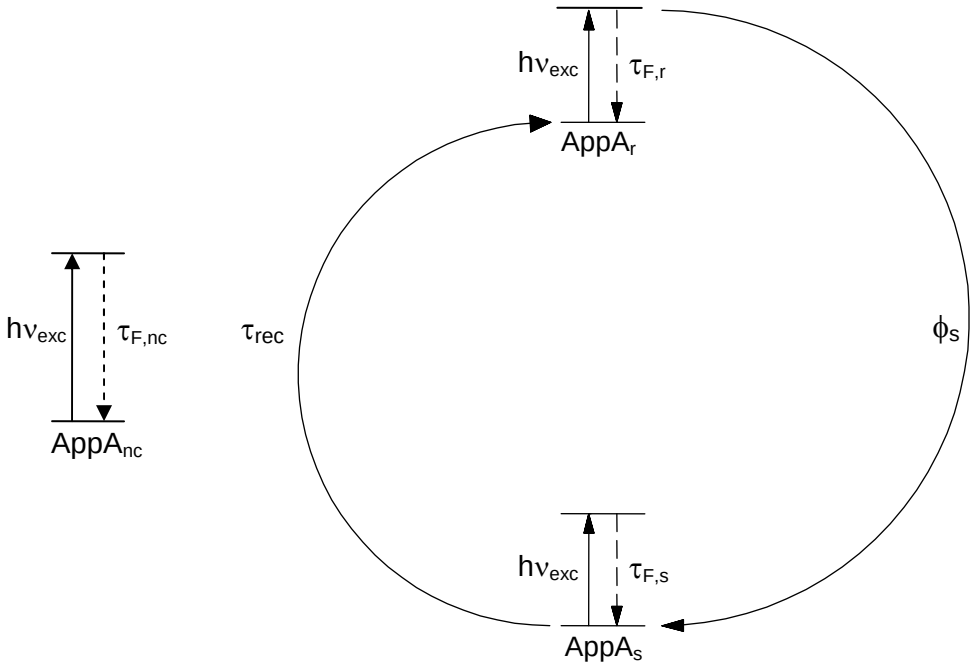

Figure 6-11: Photo-cycle scheme of photo-active BLUF domains (right) and photo-excitation scheme of BLUF domains not taking part in receptor state – signaling state photo-cycle dynamics (left).

Table 6-1. parameters of AppA BLUF domains in aqueous solution at pH 8 and at room temperature. λ_{exc} = 428 nm; λ_p = 493.1 nm. Error bars are estimates taking experimental accuracy into account.

Parameter	$AppA_{148}$		$AppA_{126}$		Comments
Chromophore composition					
x_{FAD}	0.085±0.03		0.15±0.04		TLC
x_{FMN}	0.22±0.04		0.12±0.03		TLC
x_{Rf}	0.54±0.04		0.67±0.05		TLC
x_{iso}	0.155±0.03		0.06±0.02		TLC
Domain composition					
x_f	0.776±0.03		0.548±0.03		Figs. 6-6, 6-7
x_{sl}	0.212±0.02		0.429±0.03		Figs. 6-6, 6-7
x_{nc}	0.012±0.004		0.023±0.004		Figs. 6-6, 6-7
Photo-cycle characterization					
ϕ_s	0.24±0.03		0.25±0.03		Fig. 6-10
$\tau_{d,rec}$ (min)	16.7±0.5		18.8±0.5		Fig. 6-8(b)
$Wb/(hc_0)$ (cm^{-1})	7554±10		7579±10		eq. (6-7)
State dependent parameters					
	Dark-adapted	Light-adapted	Dark-adapted	Light-adapted	
ϕ_F	0.02±0.002	$(9.1±0.5)\times10^{-4}$	0.0235±0.002	$(2.2±0.2)\times10^{-3}$	Fig. 6-4
$\phi_{F,f}$	≈0.012	≈0.00015	≈0.0064	≈0.00012	eq. (6-2)
$\phi_{F,sl}$	≈0.049	≈0.0025	≈0.046	≈0.0017	eq. (6-2)
$\phi_{F,nc}$	≈0.059	≈0.059	≈0.082	≈0.082	eq. (6-2)
P_F	0.385±0.01	0.37±0.01	0.345±0.01	0.33±0.01	
$\tau_{F,f}$ (ps)	232±20	2.77±1	121.7±20	2.2±1	Figs. 6-6, 6-7
$\tau_{F,sl}$ (ps)	938±50	47.6±15	867±50	31.6±10	Figs. 6-6, 6-7
$\tau_{F,nc}$ (ps)	1113±100	1113±100	1557±100	1557±100	Fig. 6-5
$\sigma_{a,exc}$ (cm2)	3.39×10^{-17}	2.76×10^{-17}	3.22×10^{-17}	3.15×10^{-17}	Fig. 6-3
$\sigma_{a,p}$ (cm2)	9.3×10^{-18}	2.62×10^{-17}	9.2×10^{-18}	2.54×10^{-17}	Fig. 6-3
ϕ_D		$< 1\times10^{-6}$		$< 1\times10^{-6}$	eq. 6-3 Fig. 6-8(a)

Abbreviations: x_{FAD}, x_{FMN}, x_{Rf}, x_{iso}, mole-fractions of FAD, FMN, riboflavin, and non-movable isoalloxazine moiety, respectively. x_f, x_{sl}, x_{nc}, mole-fractions of BLUF domain conformations with fast fluorescence lifetime, slow fluorescence lifetime and the component non-convertible to signaling state correspondingly.

6.2 AppAH44R mutant

The results of absorption and emission spectroscopic studies on the AppA-H44R mutant protein are reported where the positively charged amino acid residue Histidine at position 44 (H44) is replaces with another positively charged amino acid residue Arginine (R) [Zir07].

6.2.1 Chromophore composition

Fig. 6-12 shows the High-Pressure-Liquid-Chromatography (HPLC) diagram to extract the chromophore composition of the investigated AppA-H44R protein. The revealed mole fractions are listed in table 6-2.

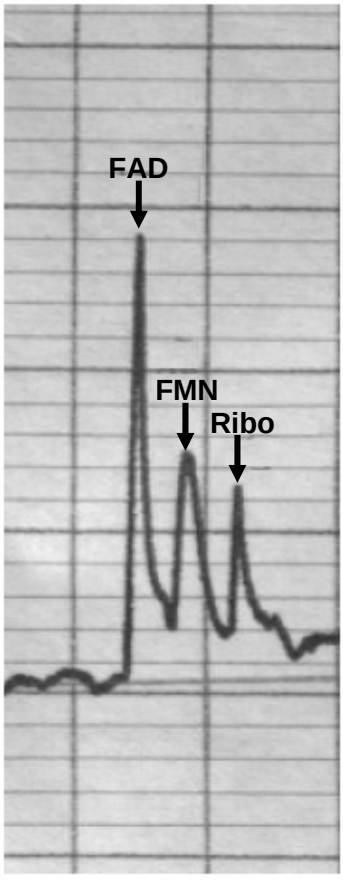

Figure 6-12: HPLC analysis for mole fraction of FAD, FMN and riboflavin (Ribo) in AppA-H44R

6.2.2 Absorption studies

Fig. 6-13 shows the absorption cross-section spectra of dark-adapted AppA mutant (AppA-H44R$_r$) and saturated light-adapted protein (AppA-H44R$_s$ prepared by excitation with 350-440 nm, $I_{exc} \approx 0.17 Wcm^{-2}$, and exposure time $\Delta t_{\exp} = 20s$). They are calculated from absorption coefficient spectra of the dark- and signaling-states of the protein where the absorption cross-section spectrum of FMN at pH 7 [Isl03] is used to calibrate the spectra as described for the wild-type AppA protein in the last section.

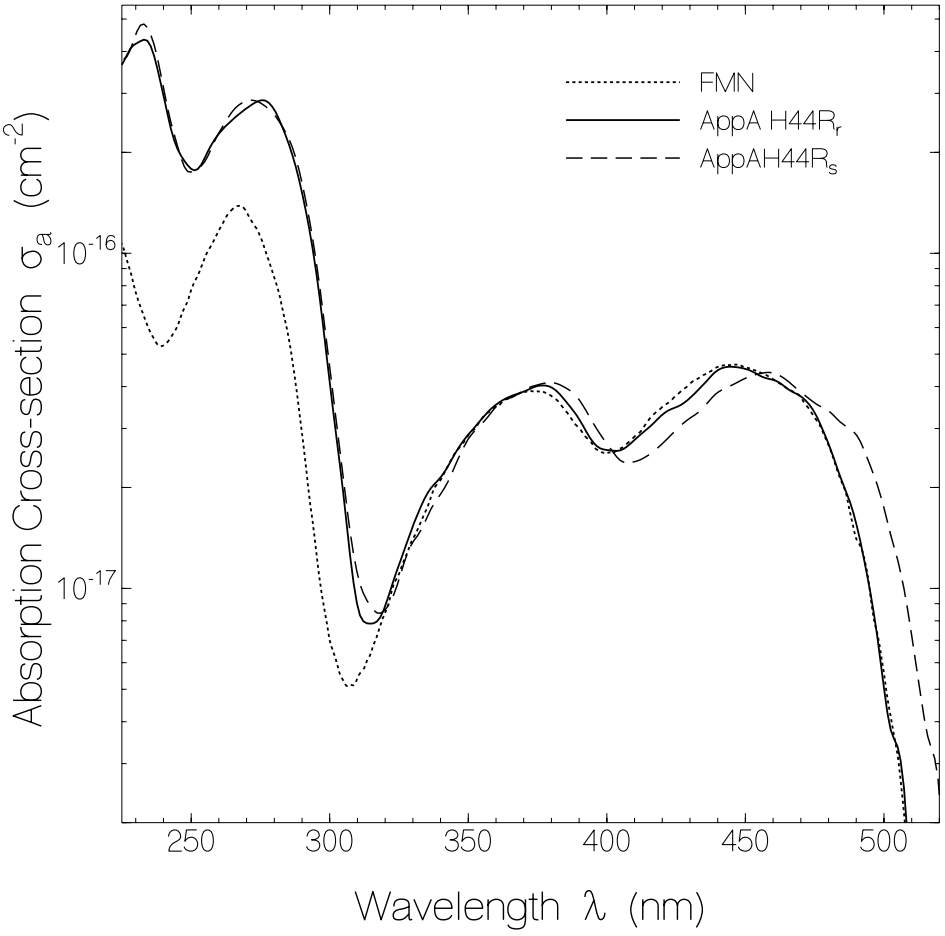

Figure 6-13: Absorption cross-section spectra, $\sigma_a(\lambda)$, of: AppA-H44R$_r$ (dark-state), AppA-H44R$_s$(signaling-state) and FMN in aqueous solution at pH 7 [Isl03].

Similar to the light adapted wild-type AppA, the light-adapted AppA-H44R spectrum is also red-shifted with respect to the dark adopted spectrum. This shows that independent of the mutation the domain is still photo-active.

6.2.3 Fluorescence studies

The fluorescence quantum distributions, $E_F(\lambda)$, of AppA-H44R$_r$ in the dark state (receptor state, excitation with $I_{exc} \approx 0.001$ W cm^{-2} in a cell with magnetic stirrer to avoid signaling-state formation and photodegradation), in the signaling state (excitation with 0.0067 W cm^{-2} for 1.5 min and signal accumulation for 5 min at 0.003 W cm^{-2} in a small-volume cell), and after 30 min of light exposure at $I_{exc} \approx 0.09$ W cm^{-2} are shown in Fig. 6-14. The absolute intrinsic fluorescence quantum distributions, $E_F(\lambda)$, were determined by using lumiflavin in water buffered to pH7 as reference.

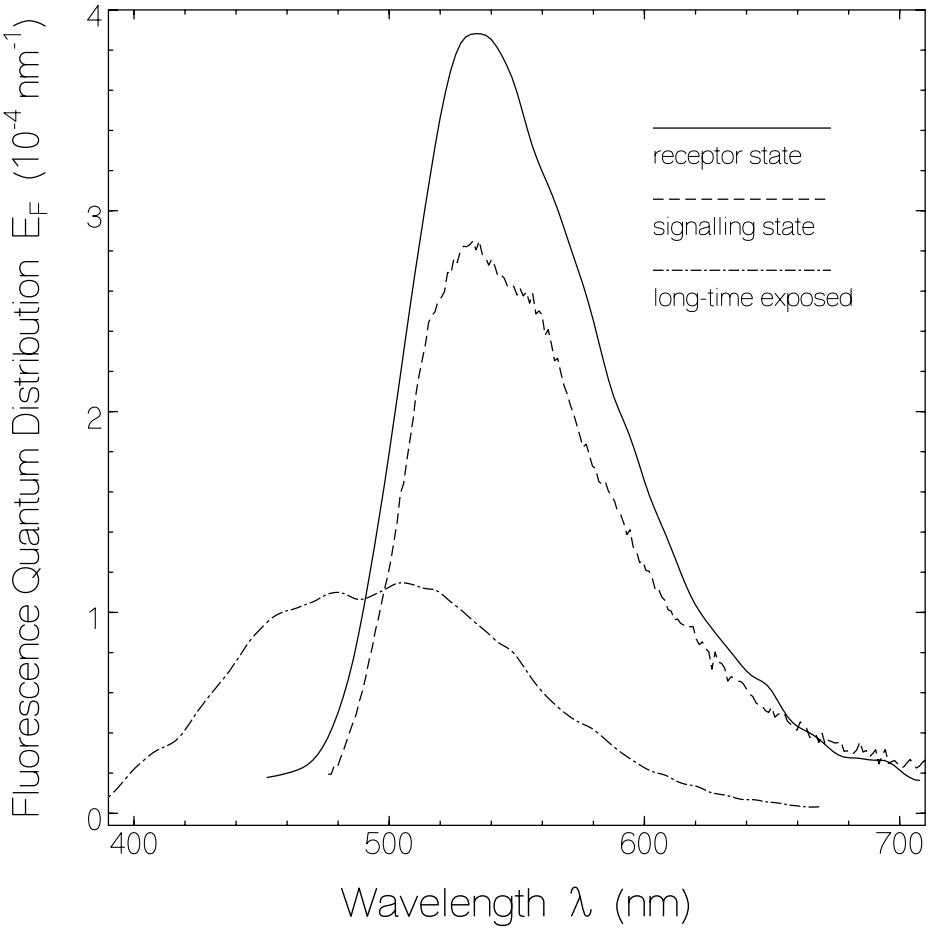

Figure 6-14: Fluorescence quantum distributions of AppA-H44R. Solid curve: protein in receptor state (excitation wavelength: λ_{exc} = 428 nm, excitation intensity: I_{exc} = 1 mW cm^{-2}, accumulation time: t_{acc} = 5 min, solution circulation with magnetic stirrer). Dashed curve: protein in signaling state (λ_{exc} = 350-440 nm, I_{exc} = 6.7 mW cm^{-2} over 1.5 min and then fluorescence detection with I_{exc} = 3 mW cm^{-2} over 5 min). Dash-dotted curve: partly degraded sample (λ_{exc} = 350-440 nm, I_{exc} = 0.09 W cm^{-2}, t_{exp} = 30 min, fluorescence excitation at 365 nm).

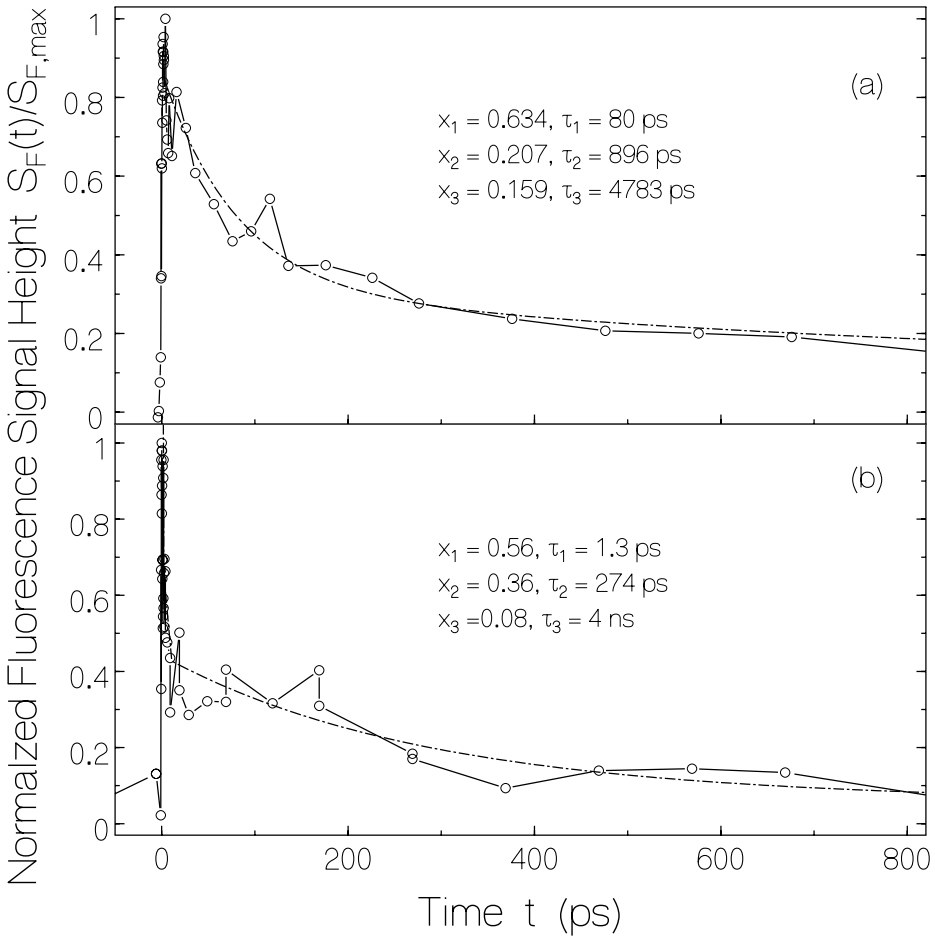

Figure 6-15: Normalized temporal fluorescence signals, $S_F(t)/S_{F,max}$, of AppA-H44R determined by fluorescence up-conversion experiments. Line-connected circles are measured. Dash-dotted curves are three-component single-exponential fits. (a) Sample is in dark state. (b) Sample is in saturated light-adapted state (and partially degrading during measurement). Sample is continuously excited at λ_{exc} = 470 nm with I_{exc} = 0.023 W cm^{-2} for a duration of 30 min (up-conversion measurements are carried out during this time)

The absolute fluorescence quantum yields, ϕ_F, are calculated from $E_F(\lambda)$ using the relation $\phi_F = \int E_F(\lambda) d\lambda$ and are listed in table 6-2. The smaller fluorescence of the signaling-state observed immediately after illumination shows that the fluorescence efficiency of the signaling state is smaller than that of the receptor state. The fluorescence signal after 30 min ofexposure is attributed the emission of lumichrome which is known to be formed by photo-degradation of free flavins [Hol05].

Fluorescence up-conversion was used to measure temporal fluorescence traces of AppA-H44R$_r$ (dark -state, in a cell with magnetic stirrer) and AppA-H44R$_s$ (signaling-state, with partial free flavin degradation). The obtained fluorescence signals are shown in Fig. 6-15. The signal heights

are normalized to the signal maxima, i.e. $S_F(t)/S_{F,max}$, and plotted versus time. The system response function (not shown) had a symmetric trapezoid shape with 2 ps half-width, 0.4 ps rise time, and 0.4 ps decay time on the 80 % to 20 % level. It was obtained by white-light generation [Hol99] using the same experimental arrangement with 1 mm cell filled with pH 8 buffer solution and stronger pump laser focusing.

The experimental fluorescence data points are fitted by a three-component exponential function (eqs. 6-1,2). Similar to the wild-type AppA the regression fit revealed two photocycle-active components with slow and fast decay times together with a third component which belongs to the free flavin. The fit reveals the presence of a mole fraction of $x_{free} \approx 0.16$ free flavin in dark-state of the protein, whereas the amount of free flavin is found to be smaller for the protein in the signaling-state, Fig. 6-15b, due to free flavin photo-degradation mainly to lumichrome [Hol05]. The mole fractions and fluorescence lifetimes for these three components in the dark-state and signaling-state of AppA-H44R are listed in table 6-2.

The presence of free flavin indicates an equilibrium between holo-AppA-H44R (containing flavin), apo-AppA-H44R (without flavin), and free flavin according to $\text{holo} - \text{AppA} - \text{H44R} \leftrightarrow \text{apo} - \text{AppA} - \text{H44R} + \text{flavin}$. The dissociation constant, K_d, of this reaction is given by [Hol04]:

$$K_d = \frac{[\text{apo} - \text{AppA} - \text{H44R}][\text{flavin}]}{[\text{holo} - \text{AppA} - \text{H44R}]} = \frac{x_{free}^2}{1 - x_{free}} C_0 , \qquad (6\text{-}11)$$

where C_0 is the total AppA-H44R concentration. Using the experimental values of $C_0 = 3.12\times10^{-4}$ mol dm^{-3} and $x_{free} \approx 0.16$ one gets $K_d \approx 9.5\times10^{-6}$ mol dm^{-3}.

6.2.4 Photo-cycle dynamics

The absorption coefficient spectra of AppA-H44R after 20 s exposure with different excitation intensities at λ_{exc} = 350-440 nm are displayed in Fig. 6-16.

It is seen that with rising excitation intensity the absorption spectra are more and more shifted to the longer wavelengths. Fig. 6-16 is used to extract the excitation intensity dependence of the absorption coefficients, α_p, at λ_p =492 nm (wavelength position of largest absorption change between exposed and unexposed samples) in Fig. 6-17 (dot-connected circles). The quantum yield of photo-induced signaling-state formation, ϕ_s, is extracted from the excitation intensity

dependence of the absorption coefficient, α_p, depicted in Fig. 6-17. The eqs. 6-8,9,10 are used for the calculation of quantum yield of signaling-state formation where the free flavin contribution is excluded (similar calculations are carried out for AppA protein in which the contribution of photo-cycle inactive component was excluded).

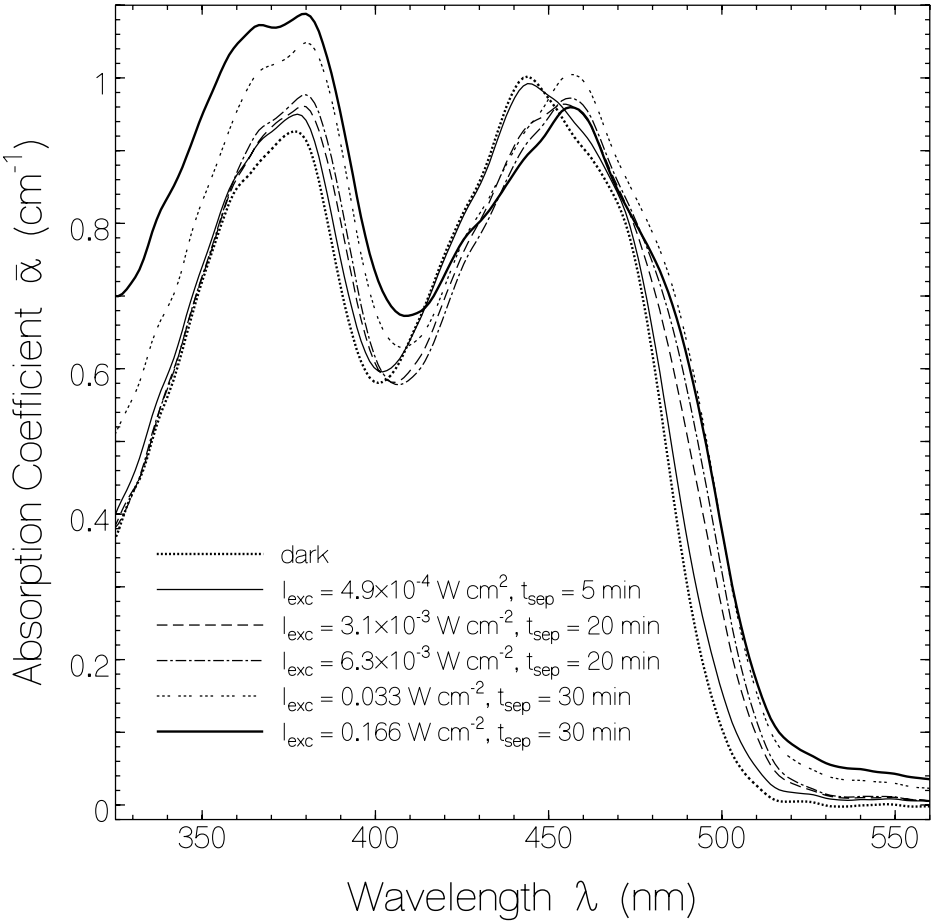

Figure 6-16: Dependence of absorption spectra of AppA-H44r on excitation intensity. Temperature ϑ = 21.8 °C. $\bar{\alpha}(\lambda) = -\ln[T(\lambda)]/\ell$ is the length-averaged absorption coefficient. Excitation wavelength λ_{exc} = 350-440 nm. Cell thickness, ℓ = 1.5 mm. Cell area 1.5 mm × 4 mm. Exposure time t_{exp} = 20 s. Excitation intensity, I_{exc}, and time intervals between exposures, t_{sep}, are given in the figure.

The solid curves in Fig. 6-17 are calculated for different quantum yields, ϕ_s, by numerical solution of the equation system (6-8,9) and application of eq. 6-10. The best fit to the experimental data at low excitation intensities gives ϕ_s = 0.3±0.05. The deviation of the experimental data from the calculated intensity dependence at higher excitation intensities is thought to be due to photo-degradation and light scattering.

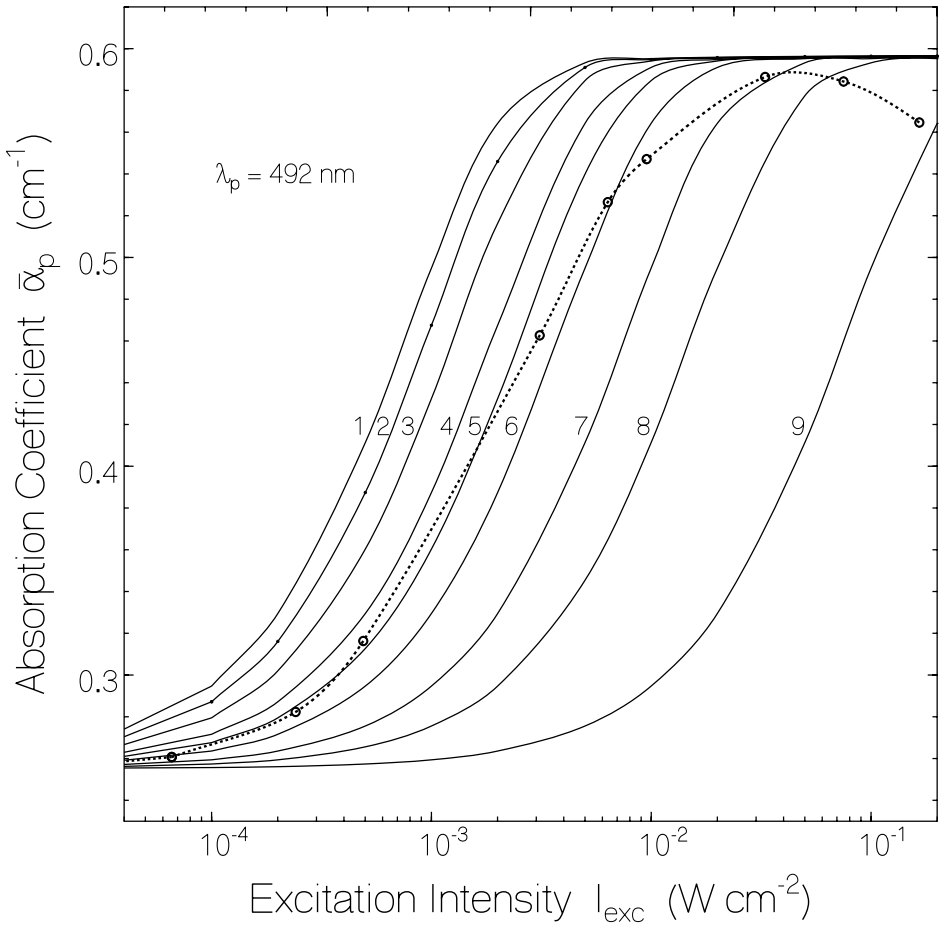

Figure 6-17: Intensity dependent increase of absorption coefficients of AppA-H44R at wavelength λ_p = 492 nm due to light exposure at λ_{exc} = 350-440 nm. Exposure time t_{exp} = 20 s. Temperature ϑ = 21.8 °C. Experimental data are taken from Fig. 6-16. Curves are calculated by use of Eqs. 6-8,6-9 and 6-10 with parameters of Figs. 6-16,17 and N_0 = 2.18×1016 cm^{-3}, $\sigma_{a,p}$ = 1.17×10-17 cm^2, $\sigma_{a,s,p}$ = 3.15×10^{-17} cm^2, $\sigma_{a,exc}$ = 3.3×10^{-17} cm^2, τ_{rec} =390 s. The used quantum yields of signaling state formation, ϕ_s, are (1) 1, (2) 0.8, (3) 0.6, (4) 0.4, (5) 0.3, (6) 0.2, (7) 0.1, (8) 0.05, and (9) 0.0

The spectral absorption recovery of AppA-H44R$_s$, after 20 s exposure at λ_{exc} = 350-440 nm with an intensity of I_{exc} = 0.17 W cm^{-2}, to AppA-H44R$_r$ is illustrated in Fig. 6-18a. The sample temperature was set to 21.8 °C. In addition the spectral changes, $\alpha(\lambda,t_d)$ - $\alpha(\lambda,t_{exp} = 0)$, are depicted in part (b) of the same Figure. In the long-wavelength range, λ > 430 nm, the signaling-state absorption spectrum recovers nearly back to the dark-state spectrum. But in the short-wavelength part, λ < 430 nm, additional absorption is built up during signaling-state relaxation to

the receptor state mainly due to free flavin photo-degradation to lumichrome [Hol05] during exposure.

The true signaling-state absorption coefficient spectrum is shown by the thick solid curve in Fig. 6-18a. It is given by $\alpha_s = \alpha(t_{exp} = 20\ s) - [\alpha(t_d = 75\ min) - \alpha(t_{exp} = 0)]$. The absorption change of the signaling-state versus time after light switch-off and at $\lambda_p = 491.9$ nm is shown in Fig. 6-19b, while Fig. 6-19a gives the excitation light profile.

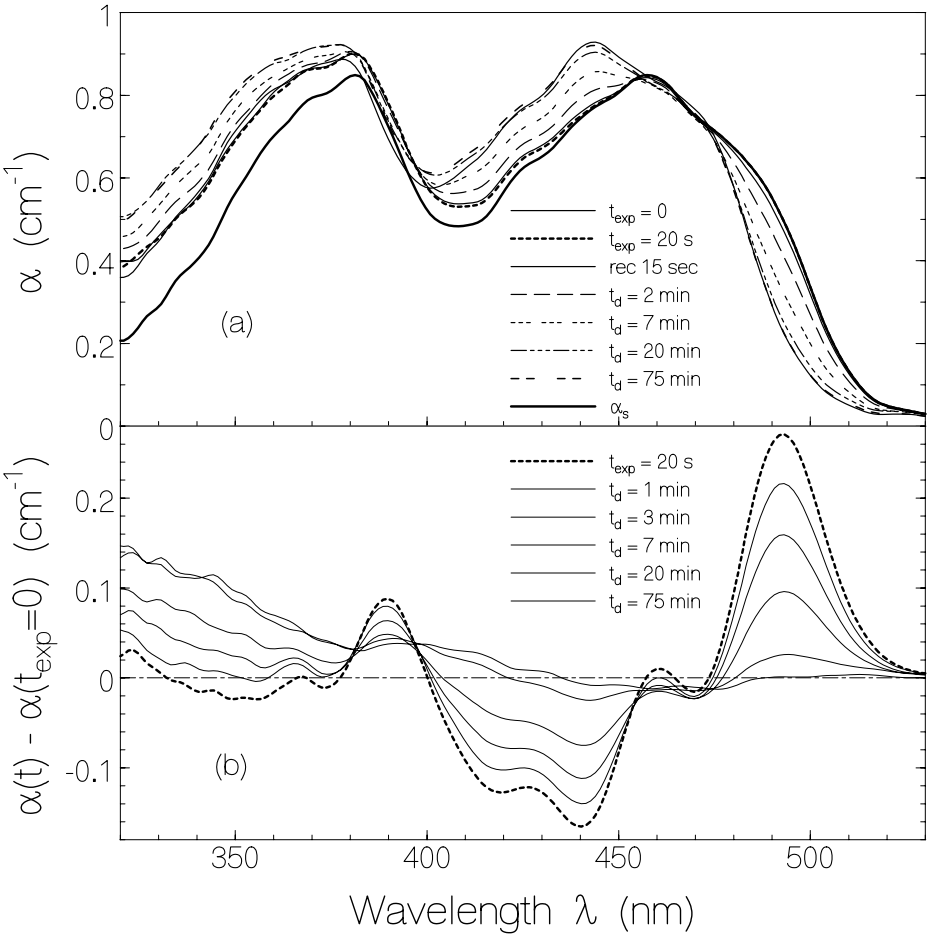

Figure 6-18: Absorption behaviour of AppA-H44R after light switch-off. Sample was excited at λ_{exc} = 350-440 nm with I_{exc} = 0.17 W cm^{-2} for t_{exp} = 20 s. Temperature was ϑ = 21.8 °C. (a) Absorption coefficient spectrum. (b) Difference spectrum $\alpha(\lambda,t) - \alpha(\lambda,t_{exp} = 0)$.

In Fig. 6-19b curves are presented for three different sample temperatures, ϑ = 12.3 °C, 21.8 °C and 31.5 °C. The absorption recoveries at λ_p = 491.9 nm are fitted by single-exponential functions (eq. 6-6). The obtained recovery times are shown in Fig. 6-19 and listed in table 6-2.

As described for AppA, domain recovery from the signaling to the dark-state can be explained by a barrier height, W_b, between the signaling-state and dark-state. Using the Arrhenius-type equation (eq. 6-7) at two temperatures, ϑ_1 and ϑ_2, gives:

$$W_b = \frac{k_B \vartheta_1 \vartheta_2 \ln\left[\tau_{d,rec}(\vartheta_2)/\tau_{d,rec}(\vartheta_1)\right]}{\vartheta_1 - \vartheta_2}. \qquad (6\text{-}12)$$

Inserting experimental data into eqs. 6-7 and 6-12 the barrier height and attempt frequency are calculated to be $W_b = 1.36\times10^{-19}$ J ($\tilde{\nu}_b = W_b/(hc_0) = 6846$ cm^{-1}) and $k_0 = 8\times10^{11}$ s^{-1}.

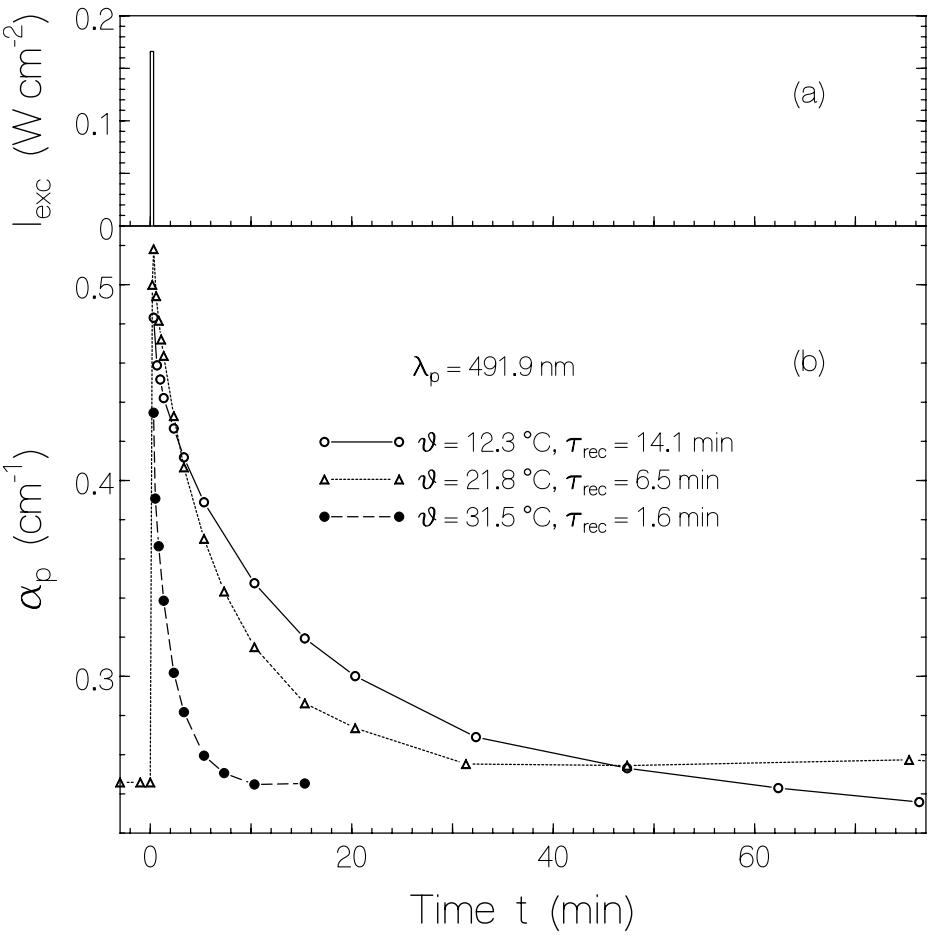

Figure 6-19: Temporal absorption behavior due to pulsed light exposure (duration 20 s, intensity 0.17 W cm^{-2}) for three different temperatures, , ϑ = 12.3 °C (open circles), 21.8 °C (triangles), and 31.5 °C (filled circles). (a) Excitation intensity profile. (b) Absorption coefficient development at probe wavelength, λ_p = 491.9 nm.

The signaling-state photo-degradation due to long-time exposure is seen in Fig. 6-20. The sample is exposed for 60 min at λ_{exc} = 470 nm with an intensity of I_{exc} = 0.023 W cm^{-2}. For exposure times longer than 10 min light scattering gets more and more severe.

Two corrected curves are included in Fig. 6-20 for the exposure times of 36 min and 60 min where the scattering contribution is subtracted ($\alpha_{cor}(\lambda) = \alpha_{measure}(\lambda) - \alpha_{scatter}(\lambda)$ with $\alpha_{scatter}(\lambda) = \alpha_{measure}(\lambda_0)(\lambda_0/\lambda)^4$ [Ker69] where λ_0 is in the transparent region, here λ_0 = 550 nm is used). The photoproduct absorption at 60 min of light exposure is obtained by subtracting the signaling state absorption contribution from the scattering-corrected absorption spectrum at that time. The obtained photoproduct spectrum has the same spectral shape as the lumichrome absorption cross-section spectrum (Fig. 2-3).

The quantum efficiency of photo-degradation, ϕ_D, is estimated from the ratio of the length-integrated number density of photo-degraded flavin molecules to the number density of absorbed photons:

$$\phi_D = \frac{\Delta N_D}{\Delta n_{ph,abs}}. \tag{6-13}$$

The length-integrated number density of the degraded molecules (converted to lumichrome) is approximately given by:

$$\Delta N_D = N_0 \ell \frac{\alpha_p(t_1) - \alpha_p(t_2)}{\alpha_{p,ini}}. \tag{6-14}$$

N_0 is the total number density of flavin molecules in the sample, given by $N_0 = -\alpha_0(\lambda)/\sigma_{a,r}(\lambda)$. $\alpha_p(t_i) = -\ln[T_p(t_i)]/\ell$, is the absorption coefficient at the probe wavelength, λ_p, at time t_i. $T_p(t_i)$ is the transmission at wavelength λ_p and time t_i. $\alpha_{p,ini}$ is the absorption coefficient at λ_p before degradation (initial signaling state absorption for AppA-H44R$_s$, or initial receptor state absorption for AppA-H44R$_r$). The number density of absorbed photons is given by the eq. 6-5. The analysis of the absorption coefficient development with time, depicted in Fig. 6-21 for λ_p = 456 nm (data taken from Fig. 6-20), gives $\phi_{s,D} = (2.0\pm0.3)\times10^{-4}$ ($N_0 = 3.12\times10^{16}$ cm^{-3}, ℓ = 0.15 cm, I_{exc} = 0.023 W cm^{-2}, λ_{exc} = 470 nm) in the time interval between t_1 = 1 min and t_2 = 5 min. There free flavin is dominantly photo-degraded. Using an initial fraction of free flavin of $x_{free} \approx 0.16$ (Fig. 6-15a) a quantum yield of free flavin degradation of $\phi_{D,free} \approx 0.00125$ is estimated in reasonable agreement with free flavin photo-degradation studies [Hol05]. In the time range from 10 min to 36 min the absorption decrease gives $\phi_{s,D} = (5.9\pm1)\times10^{-5}$. Here the degradation is thought to be due to flavin

release from the protein binding pocket in the signaling-state and subsequent degradation. The photo-degraded flavin is likely also accepted by the protein.

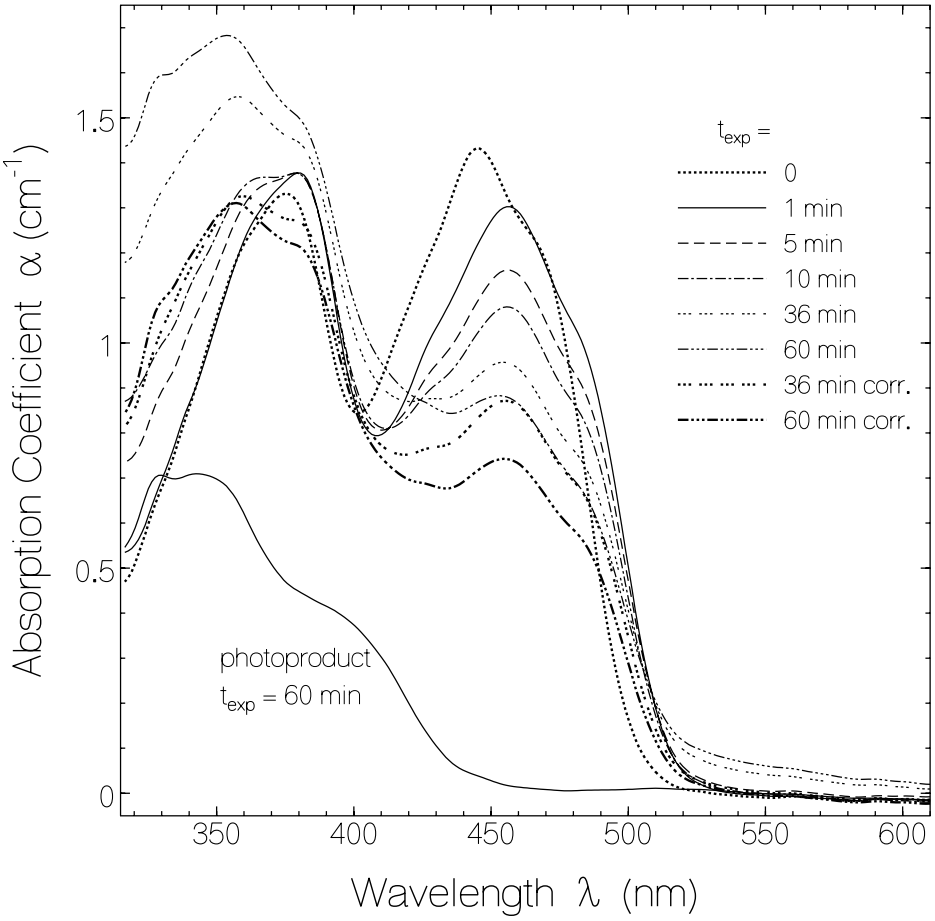

Figure 6-20: Absorption spectra development due to long-time light exposure at λ_{exc} = 470 nm with I_{exc} = 0.023 W cm^{-2}. Corrected curves belonging to 36 min and 60 min of exposure are included (the scattering contribution is subtracted ($\alpha_{sca}(\lambda) = \alpha_{sca}(\lambda_0)(\lambda_0 / \lambda)^4$). For t_{exp} = 60 min also the photoproduct contribution is shown (subtraction of signaling-state contribution from the corrected spectrum). Its shape agrees with the lumichrome absorption spectral shape.

The above suggested model for degradation of flavin outside of the protein binding pocket, flavin release from the protein binding pocket in the signaling state and subsequent degradation is further supported by the fluorescence quantum yield measurement during intense long-time exposure.

The temporal development of the fluorescence quantum yield in the case of intense long-time exposure is shown in Fig. 6-22.

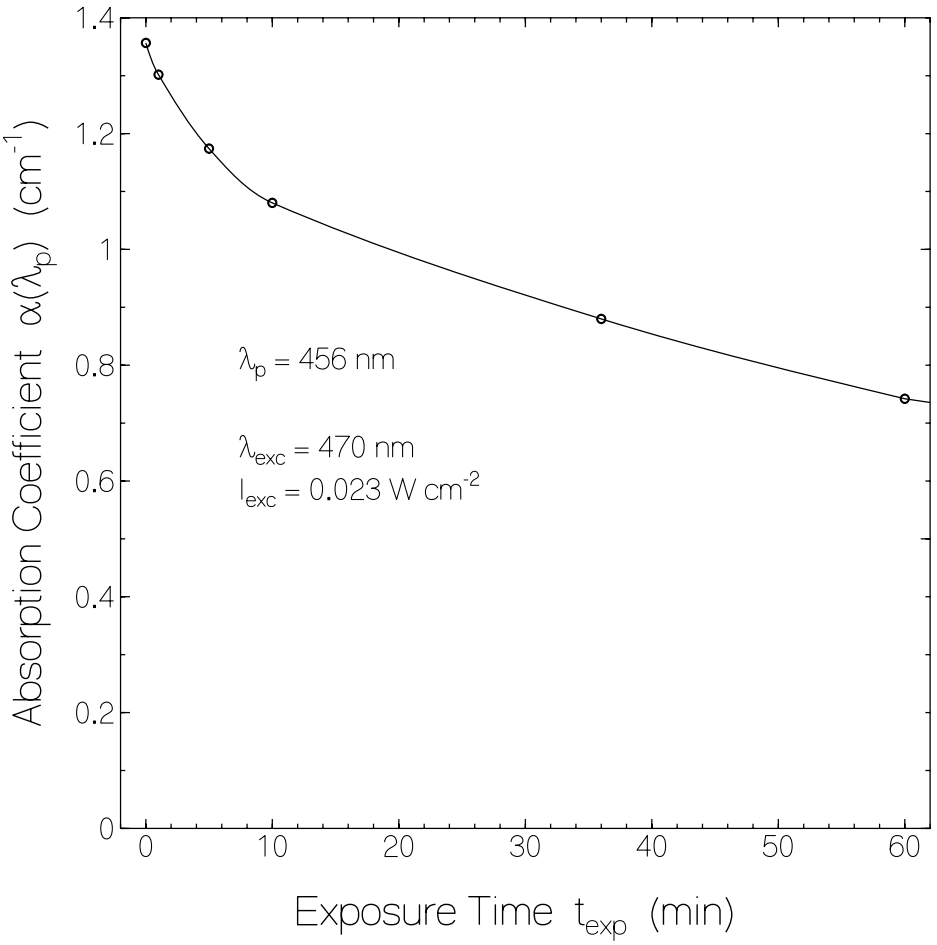

Figure 6-21: Temporal absorption coefficient development at probe wavelength, λ_p = 456 nm due to the long-time light exposure at λ_{exc} 470 nm with I_{exc} = 0.023 W cm^{-2}.

The dependence was obtained by: continuous excitation with a mercury lamp in the wavelength region from 350 nm to 440 nm (broadband interference filter, intensity I_{exc} = 0.12 W cm^{-2}), recording the temporal fluorescence traces by 3 ps pulse excitation at 400 nm, and finally fluorescence signal detection in the 500 nm to 600 nm region with a micro-channel-plate photomultiplier (the same experimental arrangement as shown in Fig. 5-3).

The initial reduction of fluorescence efficiency within the first 30 s is due to signaling state formation and photo-degradation of free flavin mainly to lumichrome [Hol05]. Then it continues reduction of fluorescence efficiency by photo-degradation of free flavin mainly to lumichrome. The slight rise of fluorescence quantum yield with time after about 6 min of exposure is thought to be due to photo-degradation of free coiled FAD to lumichrome, and due to release of non-covalently bound flavin to free flavin with subsequent conversion to lumichrome. It should be noted that FAD is more photo-stable than FMN or riboflavin [Hol05].

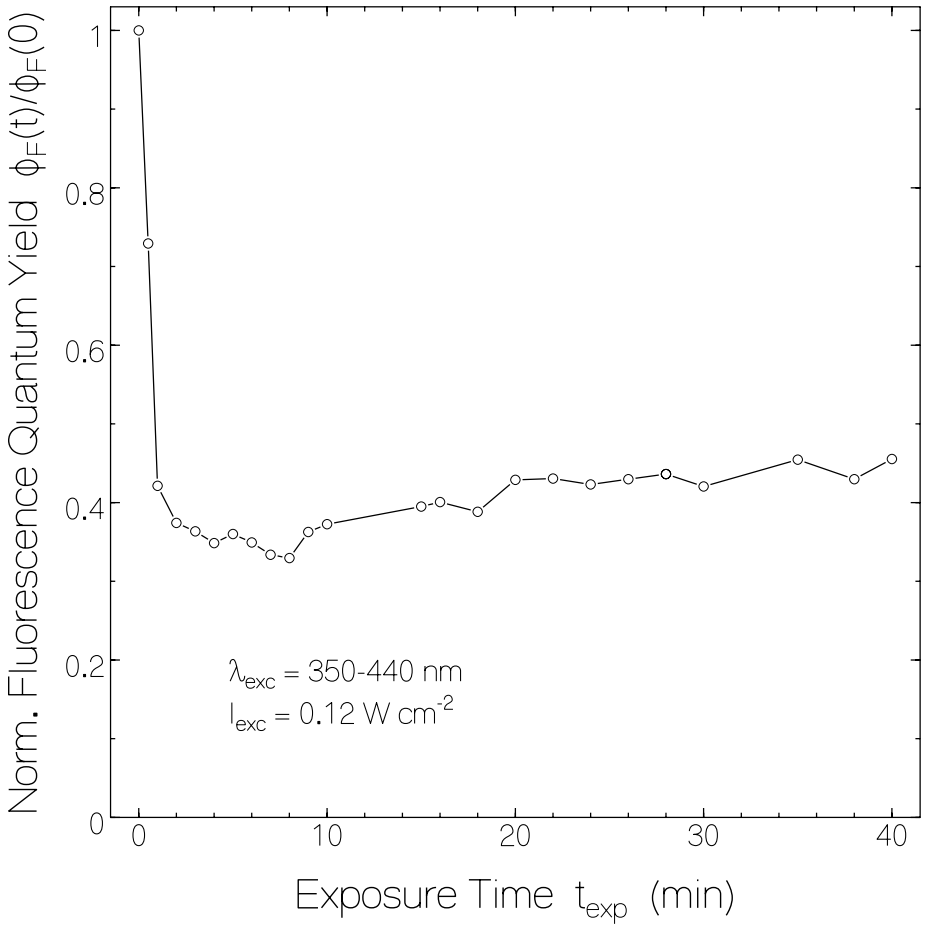

Figure 6-22: Temporal development of normalized fluorescence quantum yield, $\phi_F(t)/\phi_{F,dark}$, due to long-time light exposure. Excitation wavelength λ_{exc} = 350-440 nm, excitation intensity I_{exc} = 0.12 W cm^{-2}.

The performed spectral and time-resolved studies lead to the following photo-dynamics behaviour which is illustrated in Fig. 6-23: The AppA-H44R holoprotein is in thermodynamic equilibrium with AppA-H44R apoprotein and free flavin. Photo-excitation of dark adapted AppA-H44R holoprotein (called AppA-H44R$_r$) leads to excited singlet state population (S_1-state). From there fluorescence emission occurs with a quantum efficiency of ϕ_F(AppA-H44R$_{r,f}$) = $\tau_{F,f,r}/\tau_{rad} \approx 0.004$ and ϕ_F(AppA-H44R$_{r,sl}$) = $\tau_{F,sl,r}/\tau_{rad} \approx 0.046$. The photo-excitation leads to the AppA-H44R signaling state formation (called AppA-H44R$_s$) showing up in absorption red-shift and enhanced fluorescence quenching.

The fluorescence quantum yields of the flavins in the signaling state conformations of AppA-H44R$_s$ are rather small, i.e. $\phi_{F,f}$(AppA-H44R$_s$) = $\tau_{F,f,s}/\tau_{rad} \approx 6.7\times10^{-5}$ and $\phi_{F,sl}$(AppA-H44R$_s$) = $\tau_{F,sl,s}/\tau_{rad} \approx 0.018$. The AppA-H44R mutant in the signaling- state relaxes back to the initial receptor state in the dark with a time constant of $\tau_{rec} \approx 6.5$ min at room temperature (21.8 °C),

while that of wild-type AppA is about 17 min at the same temperature. The photo-excitation of flavin in the mutant domain, both in the receptor state and in the signaling state, causes some protein aggregation likely via apoprotein denaturation. The aggregation shows up in light scattering (light scattering efficiency is proportional to degree of aggregation[4] [Ker69]). During and after the photo-degradation process of AppA-H44R it is thought that there is again a thermodynamic equilibrium establishment between the free flavin including lumichrome and the non-covalently bound flavin (lumichrome is thought to be accepted in the domain binding pocket). Decreasing the free flavin (FAD, FMN and riboflavin) content explains the decrease of quantum yield of photo-degradation with exposure time.

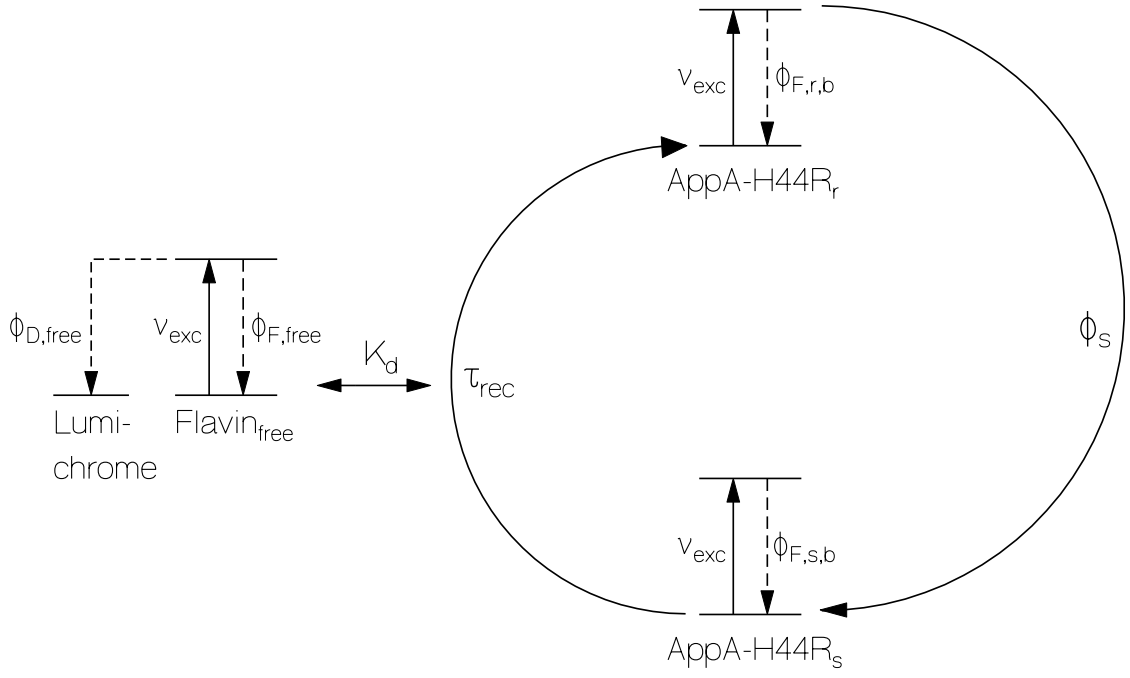

Figure 6-23: Suggested photo-cycle for AppA-H44R together with photodegradation scheme (see text)

[4] Number of the monomers in the aggregate.

Table 6-2: Determined parameters for $AppA_{1-148}$-H44R BLUF domain mutant in aqueous solution at pH 8 and at room temperature

Parameter	$AppA_{1-148}$-H44R$_r$	$AppA_{1-148}$-H44R$_s$	Comments to mutant data
Chromophore composition:			
x_{FAD}	0.50±0.05		HPLC
x_{FMN}	0.27±0.04		HPLC
x_{Rf}	0.23±0.04		HPLC
Domain composition ($x_f + x_{sl} + x_{free} = 1$):			
x_f	0.63±0.03	0.695	Fig. 6-15
x_{sl}	0.21±0.02	0.227	Fig. 6-15
x_{free}	0.16±0.02	0.078	Fig. 6-15
Photo-cycle characterization:			
ϕ_s	0.30±0.05		Fig. 6-17
τ_{rec} (min)		6.5±0.5	Fig. 6-19, at 21.8° C
$W_b/(hc_0)$ (cm^{-1})		6846±100	Eq. 6-12
$\delta\lambda_{s,r}$ (nm)	12±1		Fig. 6-13
State dependent parameters:			
ϕ_F	0.04±0.005	0.03±0.005	Fig. 6-14
$\phi_{F,b}$	≈ 0.014	≈ 0.0041	See text
$\phi_{F,f}$	≈0.004	≈6.7×10^{-5}	$\tau_{F,f}/\tau_{rad}$
$\phi_{F,sl}$	≈0.046	≈0.018	$\tau_{F,sl}/\tau_{rad}$
$\phi_{F,free}$	≈0.245		$\tau_{F,free}/\tau_{rad}$
$\tau_{F,f}$ (ps)	80±10	1.3±0.2	Fig. 6-15
$\tau_{F,sl}$ (ps)	896±50	350±100	Fig. 6-15
$\tau_{F,free}$ (ps)	4780±100	4700±1000	Fig. 6-15
$\phi_{D,0}$		(2±0.3)×10^{-4}	Fig. 6-21

Abbreviations: x_{FAD}, x_{FMN}, x_{Rf} mole-fractions of FAD, FMN, and riboflavin. x_f, x_{sl}, x_{free}, mole-fractions of flavin in BLUF domain conformations with fast fluorescence lifetime, slow fluorescence lifetime, and not bound to protein, respectively. ϕ_s, quantum yield of signaling state formation. τ_{rec} is the recovery time of BLUF domains after light exposure from signaling state back to receptor state in the dark. $W_b/(hc_0)$, energy barrier from signaling state to receptor state (h is Planck constant, c_0 is vacuum light velocity). ϕ_F is total fluorescence quantum yield. $\phi_{F,f}$, $\phi_{F,sl}$, $\phi_{F,free}$ are fluorescence quantum yields of fast and slow conformation of the BLUF domains, and of free flavin, respectively. $\phi_{F,b}$ is average fluorescence quantum yield of non-covalently bound flavin [$\phi_{F,b} = (x_f\phi_f + x_{sl}\phi_{sl})/(x_f + x_{sl})$]. $\tau_{F,f}$, $\tau_{F,sl}$, $\tau_{F,free}$, fluorescence lifetimes of fast, and slow BLUF conformations and of free flavin, respectively. $\phi_{D,0}$ is initial quantum yield of photo-degradation.

6.3 BlrB

The BLUF protein BlrB (amino acid residues 1-140, see Fig. 3-6) from R. *sphaeroides* as expressed from E. *Coli* with non-covalently bound FAD, FMN and riboflavin (named $BlrB_I$) and also the reconstituted protein with only FAD as chromophore (named $BlrB_{II}$) is studied [Zir06a].

6.3.1 Chromophore composition

The chromophore compositions of the BlrB proteins are revealed by thin-layer chromatography (TLC) and are listed in Table 6-3. The thin layer chromatogram for $BlrB_I$ and $BlrB_{II}$ are shown in Fig. 6-24a and 6-24b respectively.

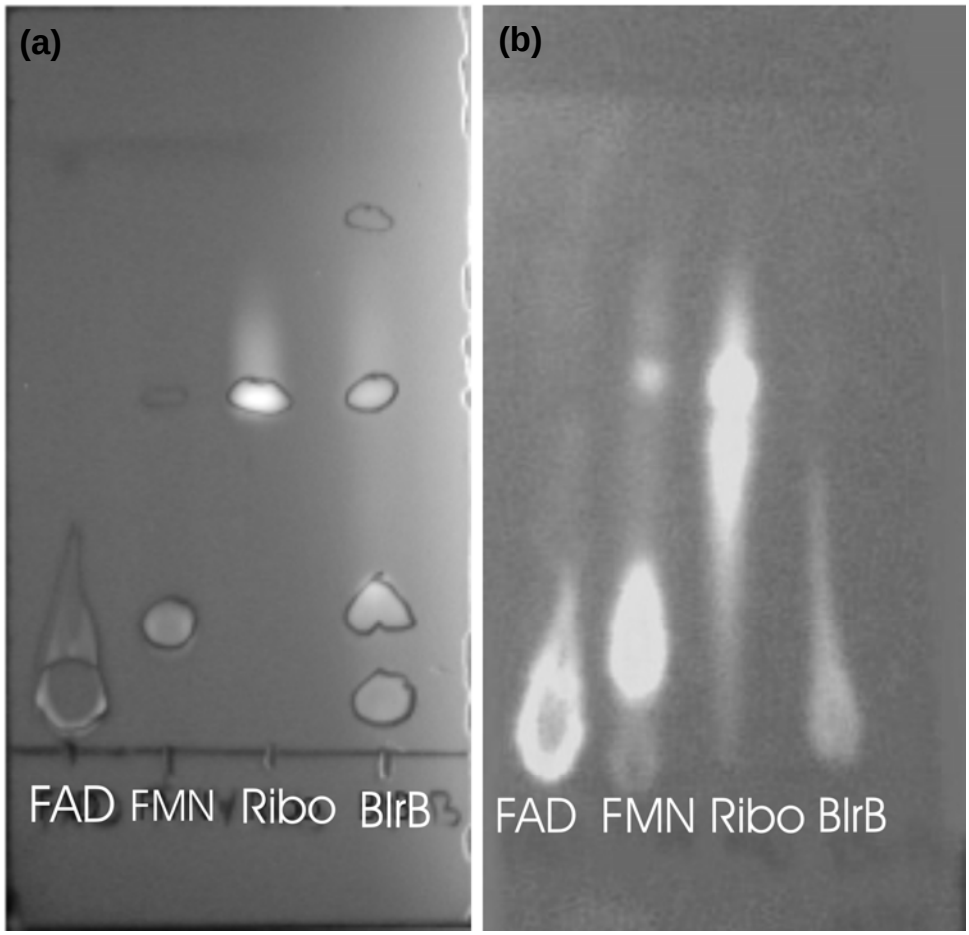

Figure 6-24: Thin-layer-chromatography analysis of: (a) $BlrB_I$ and (b) $BlrB_{II}$. together with traces for FAD, FMN and riboflavin (Ribo) for comparison.

6.3.2 Absorption studies

Fig. 6-25 shows the absorption cross-section spectra for $BlrB_I$ in the fresh dark-state ($BlrB_{I,r}$) and signaling-state ($BlrB_{I,s}$, prepared by excitation at 350-440 nm for 4 s, I_{exc} = 0.35 W cm^{-2}). They are calculated from the absorption coefficient spectra for $BlrB_I$ in the dark- and signaling-state as described for wild-type AppA and are calibrated to the absorption cross-section spectrum of FMN at pH 7 [Isl03] (see chapter 5). As shown in Fig. 6-25, except more pronounced vibronic structures of S_0-S_1 (around 450 nm) and of the S_0-S_2 absorption band (around 375 nm) the shapes of the absorption cross-section spectra of $BlrB_{I,r}$ and FMN are quite similar. Like the other BLUF proteins the $BlrB_{I,s}$ absorption spectrum is shifted to longer wavelengths compared to the $BlrB_{I,r}$ spectrum. Within our experimental accuracy the same absorption cross-section spectra were obtained for $BlrB_{I,}$ and $BlrB_{II}$ (curves only shown for $BlrB_I$).

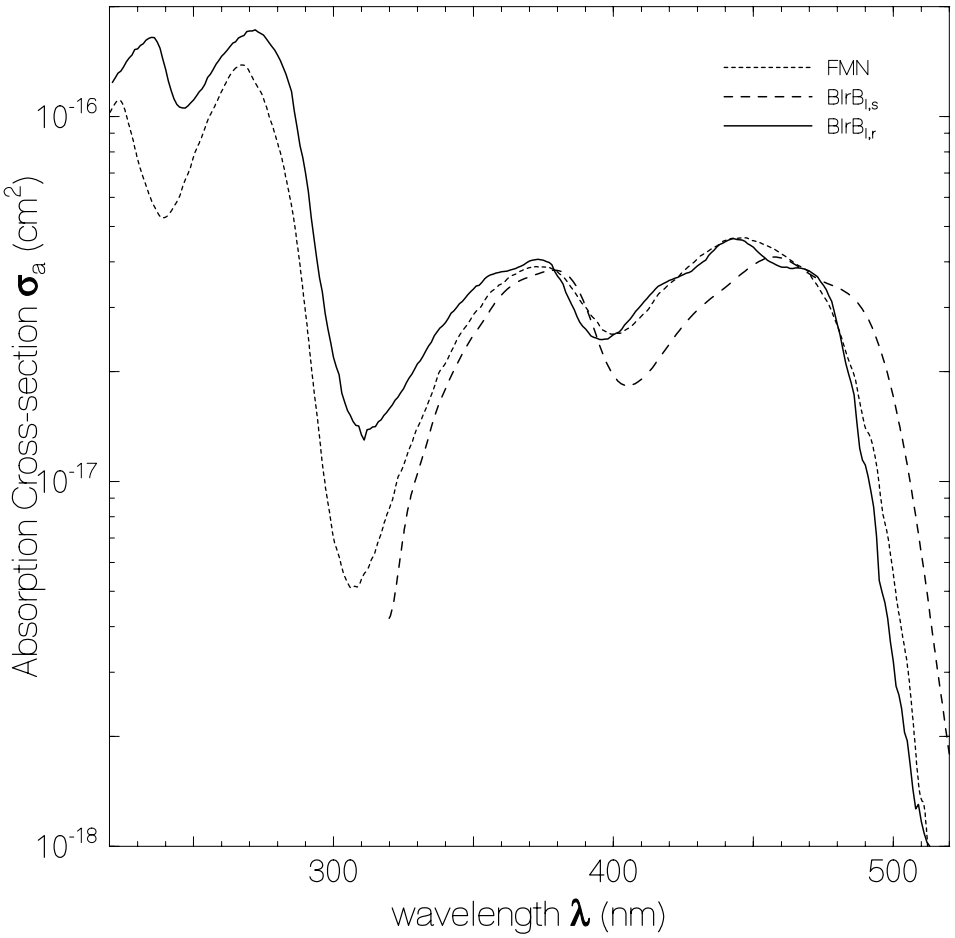

Figure 6-25: Absorption cross-section spectra of fresh dark-state of $BlrB_I$ (called $BlrB_{I,r}$) and photo-induced signaling-state of $BlrB_I$ (called $BlrB_{I,s}$) in aqueous solution buffered to pH8, and FMN in aqueous solution at pH 7 for comparision.

6.3.3 Fluorescence studies

The absolute fluorescence quantum distributions, $E_F(\lambda)$, of dark-adapted $BlrB_I$ ($BlrB_{I,r}$), $BlrB_I$ in the signaling state ($BlrB_{I,s}$), and of photo-degraded $BlrB_{II}$ ($BlrB_{II,d}$) in aqueous solution at pH 8 are shown in Fig. 6-26. They are calibrated using lumiflavin in aqueous solution at pH 7 (ϕ_F = 0.235 [Hol05]) as reference. The fluorescence quantum distributions of FAD in neutral aqueous solution and that of lumichrome in aqueous solution at pH 8 are included in Fig. 6-26 for comparison. The fluorescence quantum yields, ϕ_F, are calculated from $E_F(\lambda)$ (see chapter 4) and are listed in Table 6-3. The fluorescence spectrum of the dark-adapted $BlrB_I$ protein is 16 nm blue-shifted compared to the fluorescence spectrum of FAD.

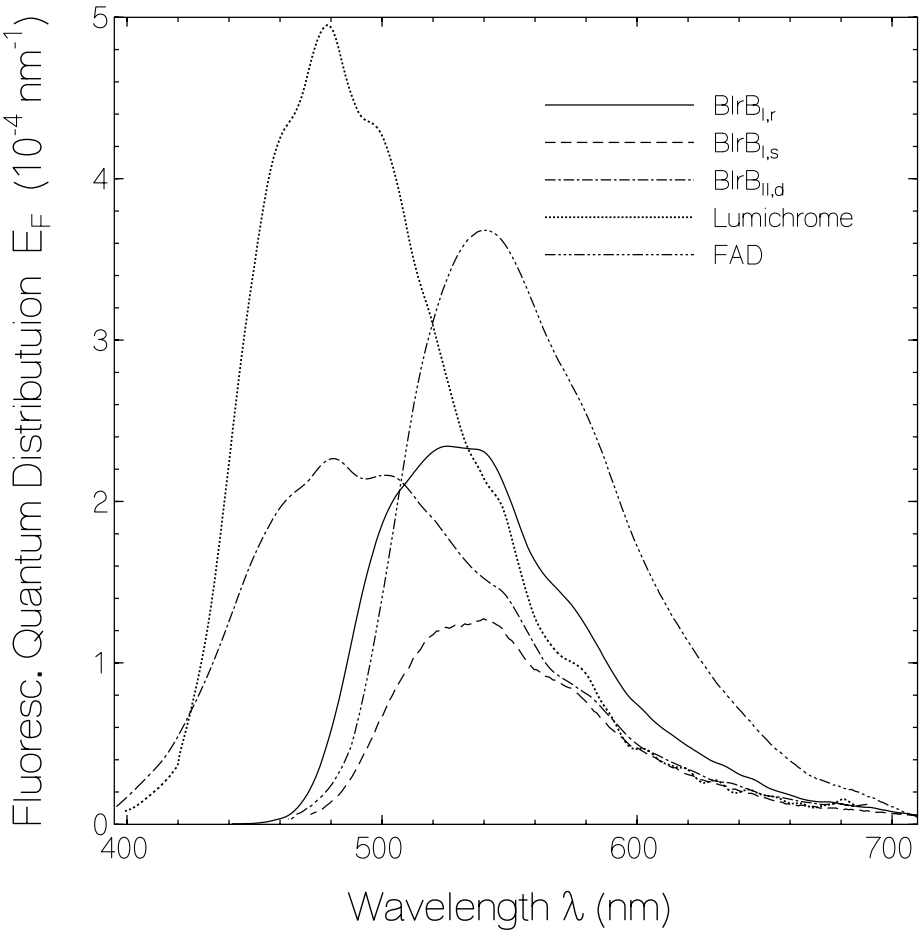

Figure 6-26: Fluorescence quantum distribution, $E_F(\lambda)$, of $BlrB_{I,r}$, $BlrB_{I,s}$, $BlrB_{II,d}$, lumichrome in aqueous solution at pH 8 and FAD in neutral aqueous solution.

The fluorescence quantum distribution of photo-degraded BlrB is broadened to the short-wavelength side resembling the fluorescence spectra of photo-degraded flavins where lumichrome and lumiflavin derivatives were identified [Hol05].

Fig. 6-27 shows temporal fluorescence traces of $BlrB_I$. The thick solid line belongs to $BlrB_{I,r}$ and the thick dashed line belongs to $BlrB_{I,s}$. The dotted line shows the system response function (approximately Gaussian shape with 1/e-time constant of $\tau_{resp} \approx 370$ ps). For $BlrB_{I,r}$ the fluorescence trace is composed of bound flavin emission (short-time contribution) and free flavin emission (long-time emission of FMN and riboflavin). For $BlrB_{I,s}$ only the long-time free flavin emission is observed.

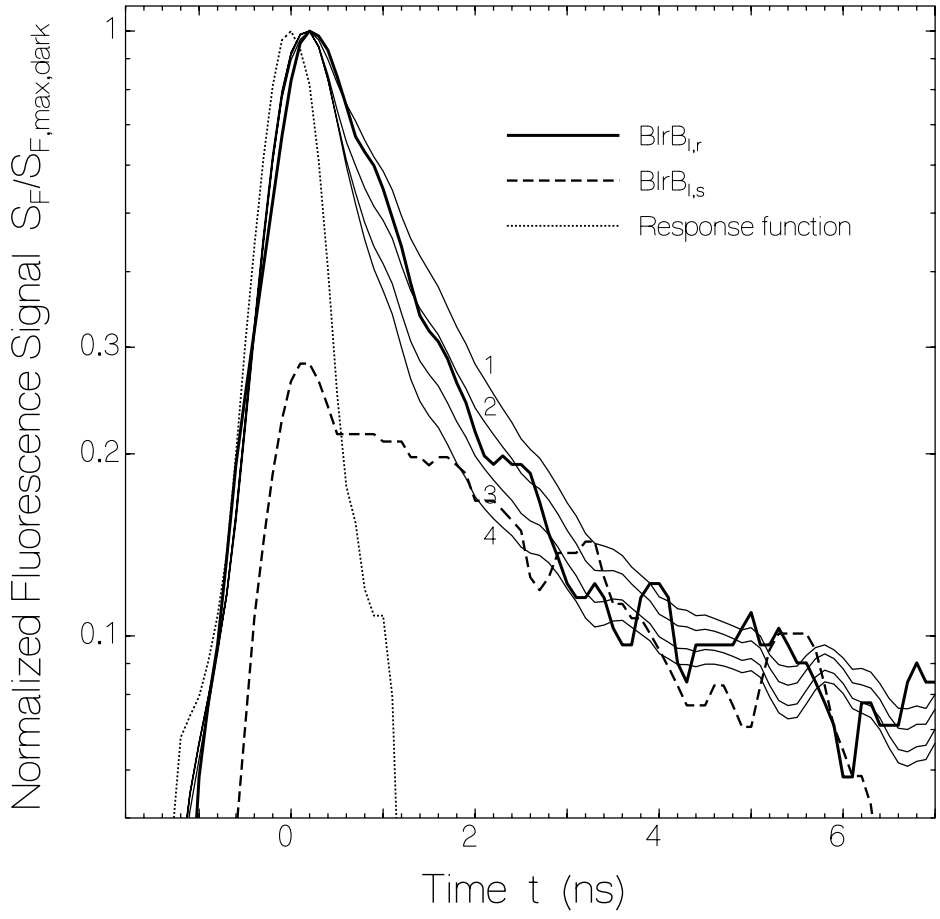

Figure 6-27: Normalized temporal fluorescence signal, $S_F(t)/S_{F,max,dark}$, of $BlrB_I$ in aqueous solution at pH 8. Thick solid curves belong to $BlrB_r$, thick dashed curves belong to $BlrB_s$. Dotted curves show response function of detection system. Thin solid curves are calculated convolution curves (eqs. 6-1,15). $X_{free} = 0.08$. Concentration = 9.3×10^{-5} mol dm^{-3} (0.093 mM). Convolution curves are calculated for $\tau_{F,FMN} = 5$ ns, $\tau_{F,FAD} = 0.7$ ns, $\beta_{FAD} = 0.42$, $\tau_{F,sl} = 700$ ps and (1): $x_{sl} = 0.3$, $x_f = 0.62$, $\tau_{F,f} = 22.6$ ps; (2): $x_{sl} = 0.2$, $x_f = 0.72$, $\tau_{F,f} = 116.7$ ps; (3): $x_{sl} = 0.1$, $x_f = 0.82$, $\tau_{F,f} = 187.8$ ps; (4): $x_{sl} = 0$, $x_f = 0.92$, $\tau_{F,f} = 243.5$ ps.

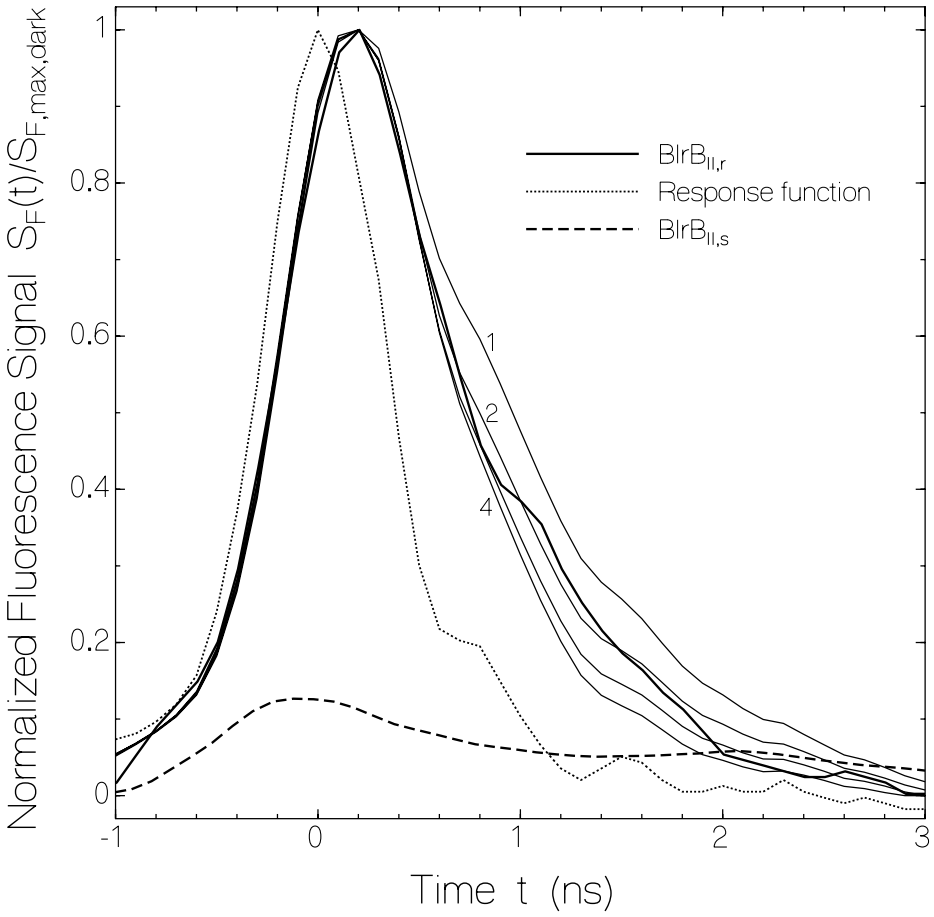

Figure 6-28: Normalized temporal fluorescence signals, $S_F(t)/S_{F,max,dark}$ of $BlrB_{II}$ in aqueous solution at pH8 C_0 = 1.05×10^{-4} mol dm^{-3} (0.105 mM). Convolution curves are calculated for $\tau_{F,FAD}$ = 0.7 ns, β_{FAD} = 1, $\tau_{F,sl}$ = 700 ps and (1): x_{sl} = 0.3, x_f = 0.62, $\tau_{F,f}$ = 64.35 ps; (2): x_{sl} = 0.2, x_f = 0.72, $\tau_{F,f}$ = 152.6 ps; (3): x_{sl} = 0.1, x_f = 0.82, $\tau_{F,f}$ = 219.4 ps; (4): x_{sl} = 0, x_f = 0.92, $\tau_{F,f}$ = 271.6 ps.

In Fig. 6-28 the temporal fluorescence behaviour of $BlrB_{II,r}$ the fluorescence trace for $BlrB_{II,s}$ (dashed curve) together with the corresponding response function (dotted curve) are shown. The fluorescence traces are mainly dominated by free flavin emission.

The measured decay times of the fluorescence traces, Figs. 6-27 and 6-28, do not agree with the average fluorescence lifetimes determined from eq. 4-19 (e.g. the average fluorescence lifetime for $BlrB_{I,r}$ is calculated to be 452 ps while the fluorescence decay time of 700 ps is measured). As a result the fluorescence signal traces of BlrB can be considered as a composition of at least three dominant components, free flavin contributions (mole-fraction x_{free}) and contributions from two dominant BlrB conformations with mole-fraction x_f of conformation $BlrB_f$ with shorter fluorescence lifetime (faster decay) and mole-fraction x_{sl} of conformation $BlrB_{sl}$ with longer

fluorescence lifetime (slower decay). Therefore the true fluorescence signal of the BlrB can be written as a three component exponential decay function, eq. 6-1, where the experimental signal, $S_F(t)$, is the convolution of the δ-function fluorescence signal, $S_{F,\delta}(t)$, with the system response function, $g(t)$, according to:

$$S_F(t) = \int_{-\infty}^{t} g(t')S_{F,\delta}(t-t')dt' . \qquad (6\text{-}15)$$

The total fluorescence efficiency is also composed of the three components, revealed in fluorescence decay analysis, according to the eq. 6-2.

The mole-fraction, x_{free}, of free flavin is determined approximately by the long-time fluorescence signal of BlrB protein in the signaling-state. The mole fraction, x_f, of BlrB with fast fluorescence decay time is determined by comparing with calculated convolution curves. The mole-faction x_{sl} of BlrB with slower fluorescence relaxation is given by $x_{sl} = 1 - x_{free} - x_f$. The time constants, $\tau_{F,free}$ and $\tau_{F,sl}$, are predetermined by a regression fit in the range t > 700 ps. The fast fluorescence lifetime, $\tau_{F,f}$, is determined by the relation:

$$\tau_{F,f} = \frac{\phi_F \tau_{rad} - x_{free}[(1-\beta_{FAD})\tau_{F,FMN} + \beta_{FAD}\tau_{F,FAD}] - (1 - x_{free} - x_f)\tau_{F,sl}}{x_f}, \qquad (6\text{-}16)$$

which is derived from eq. 6-2. β_{FAD} is the fraction of FAD in the flavin cofactor (from TLC analysis). Some convolution curves are shown in Figs. 6-27 and 6-28 (thin solid curves). The applied parameters are listed in the caption of the Figures. The parameters fitting to the experiments are listed in Table 6-3.

The existence of the free flavin can be interpreted as an equilibrium between the holoprotein holo-BlrB (protein containing flavin), the apoprotein apo-BlrB (protein without flavin) and the free cofactor, flavin, according to $holo - BlrB \leftrightarrow apo - BlrB + flavin$. The dissociation constant, K_d, of this reaction is given by eq. 6-11. Inserting the experimental data: $C_0 = 9.3\times10^{-5}$ mol dm^{-3} (1 mol dm^{-3} = 1 molar =1 M) and $x_{free} = 0.08$, gives $K_d = 6.5\times10^{-7}$ mol dm^{-3}.

6.3.4 Photo-cycle dynamics

The length-averaged absorption coefficient spectra, $\overline{\alpha}(\lambda)$, at different excitation light intensities after 4 s of light exposure (at λ_{exc} = 428 nm for I_{exc} < 0.014 W cm^{-2} and λ_{exc} =350-440 nm for I_{exc}

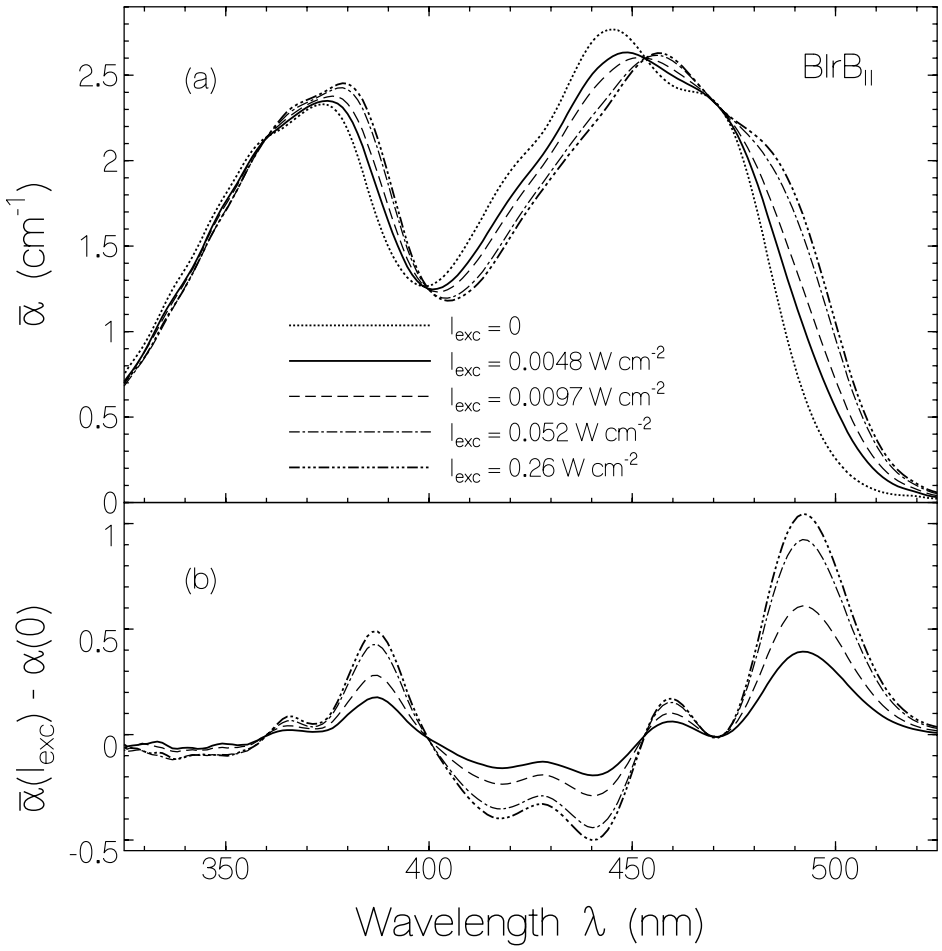

Figure 6-29: Intensity dependent signaling state formation of $BlrB_{II}$ in aqueous solution at pH 8. Cell thickness ℓ = 1.5 mm; cell area, 1.5 mm × 3.5 mm. Exposure time, t_{exp} = 4 s. Excitation intensity, I_{exc} is varied. Excitation wavelength is selected with interference filters to λ_{exc} = 428 nm (3.4 nm FWHM) for $I_{exc} \le 0.014$ W cm^2, and to λ_{exc} = 350-440 nm for $I_{exc} \ge 0.014$ W cm^2. Time interval between exposures is t_{sep} = 2 min for $I_{exc} \le 3.5\times10^{-4}$ W cm^{-2}, and t_{sep} = 10 min for $I_{exc} > 3.5\times10^{-4}$ W cm^{-2}. (a) Length-averaged absorption coefficient spectra, $\overline{\alpha}(\lambda) = -\ln[T(\lambda)]/\ell$ (T is transmission, ℓ is sample length) at various excitation intensities. (b) Absorption coefficient difference spectra, $\overline{\alpha}(\lambda, I_{exc}) - \overline{\alpha}(\lambda,0)$ for various excitation intensities (data taken from part (a)).

> 0.014 W cm^{-2}) are shown in Fig. 6-29a for $BlrB_{II}$. The temperature was set to ϑ = 22.5 °C. A 12 nm spectral red-shift from the receptor-state ($BlrB_{II,r}$) to the signaling state ($BlrB_{II,s}$) (at higher intensities) is clearly seen. The difference spectra, $\overline{\alpha}(\lambda, I_{exc}) - \overline{\alpha}(\lambda,0)$ are displayed in Fig. 6-29b. The most pronounced absorption change takes place at 493.1 nm. The excitation intensity dependence of the absorption coefficient, $\overline{\alpha}_p$, at λ_p = 493.1 nm is displayed by the dot-connected filled circles in Fig. 6-30a for $BlrB_{II}$ and in Fig. 6-30b for $BlrB_I$.

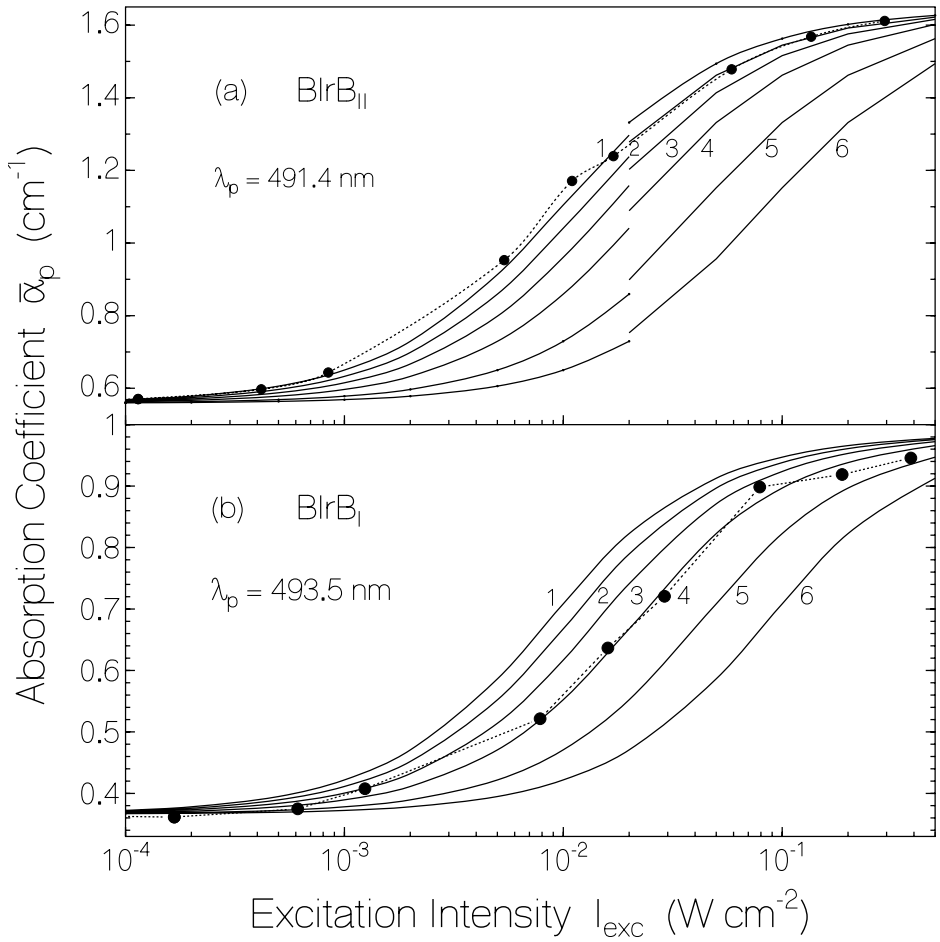

Figure 6-30: Intensity dependent increase of absorption coefficients of $BlrB_{II}$ (a) and $BlrB_I$ (b) due to light exposure. Curves are calculated by use of eqs. 6-28 till 6-30. Quantum yield, ϕ_s, of signaling state formation is varied: (1) ϕ_s = 1, (2) 0.8, (3) 0.6, (4) 0.4, (5) 0.2, and (6) 0.1. (a) $BlrB_{II}$. Probe wavelength, λ_p = 491.4 nm. Excitation wavelength, λ_{exc} = 428 nm for I_{exc} < 0.014 W cm^{-2} and λ_{exc} = 350-440 nm for I_{exc} ≥ 0.014 W cm^{-2}. Experimental data are taken from Fig.6-29a. (b) $BlrB_I$: λ_p = 493.5 nm, λ_{exc} = 350-440 nm.

The rise in absorption will be exploited below (eqs. 6-29, 6-30, 6-31) to extract the quantum efficiency of signaling state formation.

The temporal development of the absorption coefficients at probe wavelength λ_{exc} = 493.1 nm, $\bar{\alpha}_p$, upon high intensity irradiation of $BlrB_{II}$ at λ_{exc} = 350-440 nm over a period of 4 s is displayed in Fig. 6-31. In part (a) the intensity profile of the excitation pulse is shown where in part (b) the temporal development of the absorption coefficient, $\bar{\alpha}_p(t)$, is shown for the sample at three different temperatures. The signaling state forms quickly and remains constant within the exposure time.

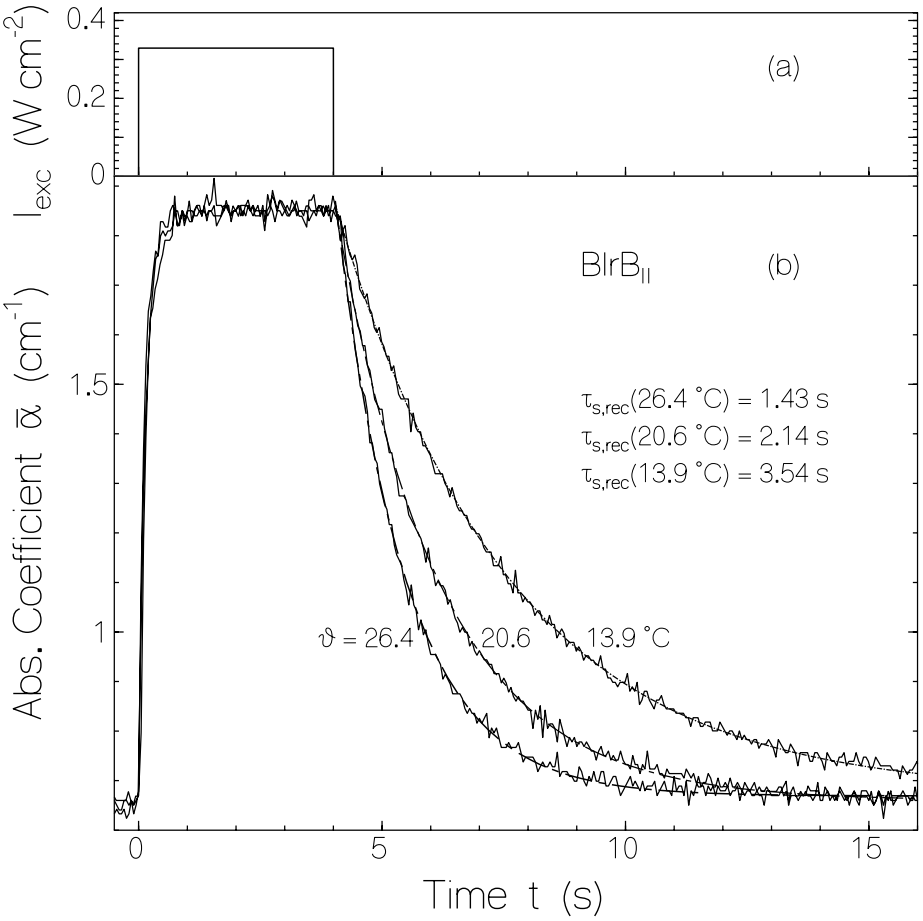

Figure 6-31: Photo-induced intermediate signaling-state formation and its recovery after light switch-off to the initial dark state of $BlrB_{II}$ in aqueous solution at pH 8. (a) Excitation intensity profile. Excitation wavelength range λ_{exc} = 350-440 nm. (b) Temporal absorption coefficient dependence at λ_p = 493.1 nm. Curves are shown for three different sample temperatures. They fit to single-exponential decays, eq. 6-6, with time constants, $\tau_{s,rec}$, listed in the figure.

The signaling state dark recovery to the original receptor state obeys a single-exponential decay (eq. 6-6). The decay time, $\tau_{s,rec}$, fastens with rising temperature. At ϑ = 22 °C the recovery time is $\tau_{s,rec}$ = 1.93 s. Practically the same absorption recovery time of $\tau_{s,rec}$ = 2.05 s was measured for $BlrB_I$ at $\vartheta \approx$ 22 °C.

The temperature dependent dark recovery of $BlrB_{II,s}$ is used to calculate the barrier height, W_b, between the signaling-state and dark-state of the protein, by use of eqs. 6-7 and 6-12. Inserting experimental data for $BlrB_{II}$ a barrier height of $W_b = 8.617\times10^{-20}$ J ($\tilde{\nu}_b = W_b/(hc_0) = 4338$ cm^{-1}) and an attempt frequency of $k_{s,rec,0} = 8\times10^8\,s^{-1}$ are calculated. In Fig. 6-32a absorption coefficient

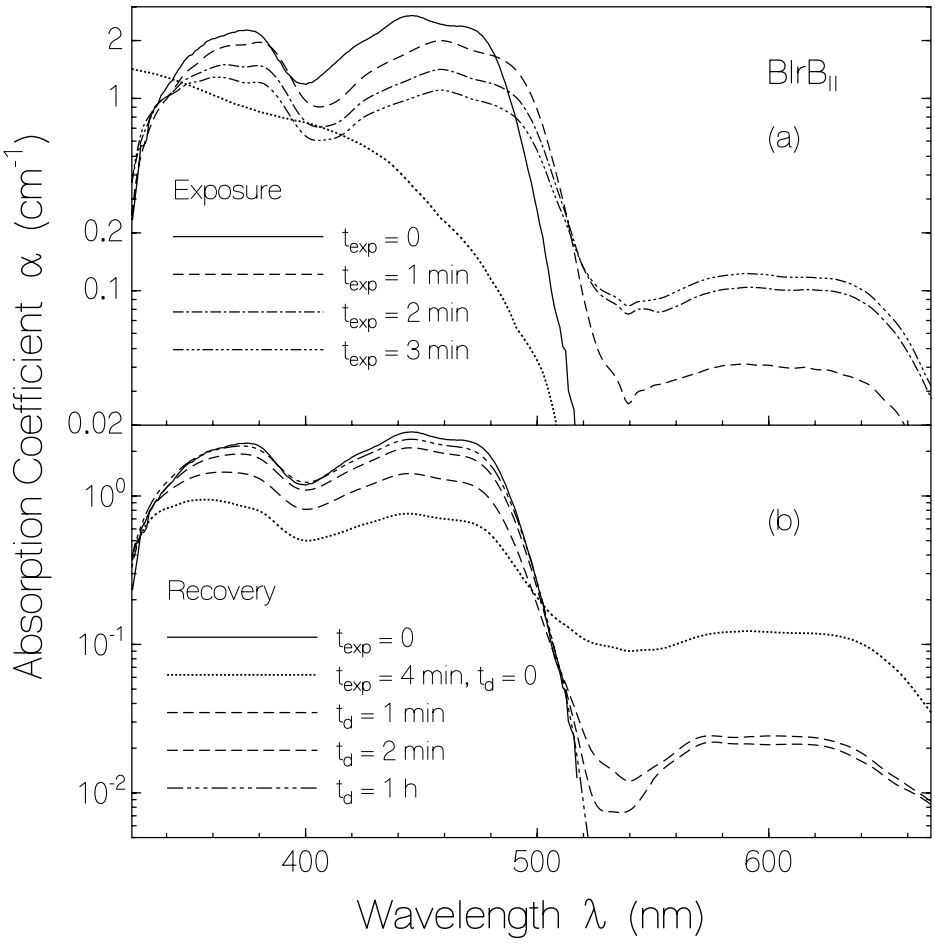

Figure 6-32: Absorption spectra development of $BlrB_{II}$ in aqueous solution at pH 8 during light exposure (a) and after light switch-off (b). (a) Excitation intensity I_{exc} = 0.354 W cm^{-2}. Excitation wavelength range λ_{exc} = 350-440 nm. Dotted curve shows expected absorption coefficient spectrum of sample composed of 1,5-dihydro-flavin. (b) Recovery after 4 min of light exposure at λ_{exc} = 350-440 nm with I_{exc} = 0.354 W cm^{-2}. Dark time t_d is varied.

spectra of $BlrB_{II}$ at different times of high-intensity light exposure are shown. These times are long compared to the signaling-state recovery time, $\tau_{s,rec}$. The sample was excited at λ_{exc} = 350-440 nm with an intensity of I_{exc} = 0.354 W cm^{-2}.

The absorption bands centred at 450 nm (S_0-S_1 transition) and 375 nm (S_0-S_2 transition) decrease and a new absorption band centred at 610 nm appears. There the S_0-S_1 absorption band of neutral flavin-semiquinone is located (see Fig. 2-6). The absorption recovery of $BlrB_{II}$ after 4 min of light exposure at λ_{exc} = 350-440 nm with I_{exc} = 0.354 W cm^{-2} is displayed in Fig. 6-32b. The dominant part of the neutral flavin-semiquinone absorption in the wavelength range > 520 nm disappears with a time constant of about 10 s, and the oxidized flavin absorption in the range from 500 nm to 330 nm recovers with a time constant of about 1.5 min.

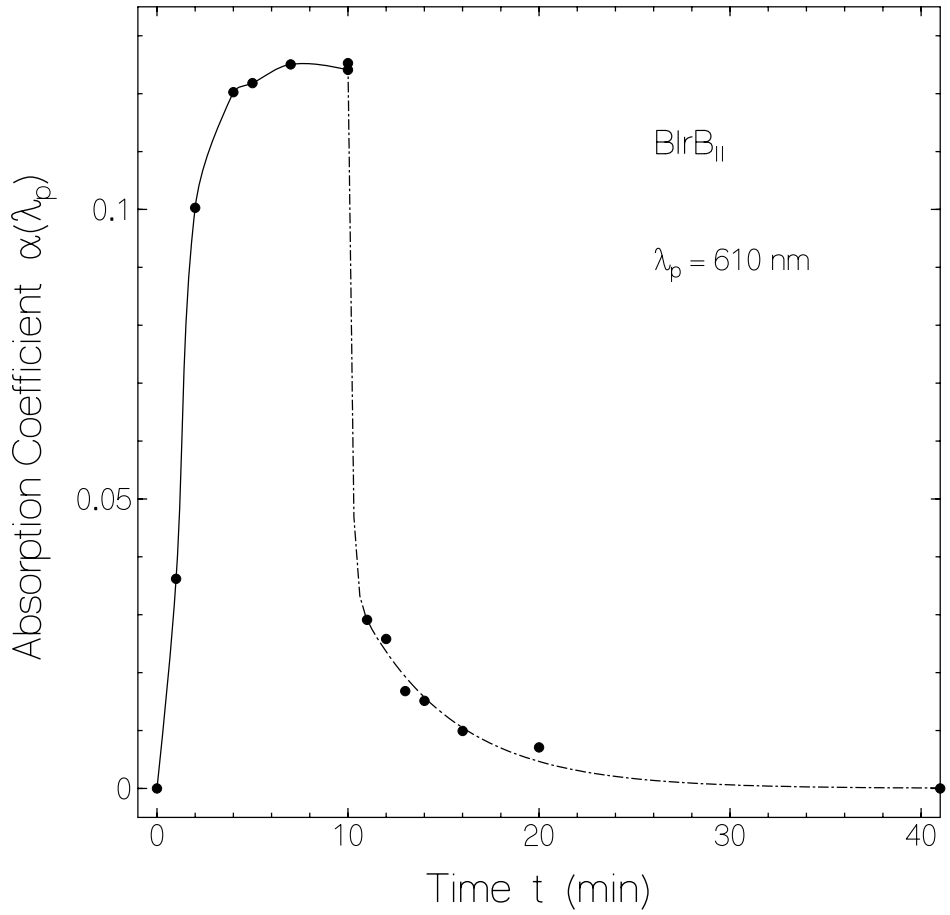

Figure 6-33: Dynamics of FAD-semiquinone formation and decay in $BlrB_{II}$. Sample is exposed for 10 min at λ_{exc} = 350-440 nm with I_{exc} = 0.354 W cm^{-2}. Probe wavelength λ_p = 610 nm. Points measured during light exposure are spline-interpolated. Absorption in the dark is fitted by $\alpha_p(t) = \alpha_p(t_0)$ $\{\beta_1 \exp[-(t-t_0)/\tau_{sq,1}]+(1-\beta_1) \exp[-(t-t_0)/\tau_{sq,2}]\}$ with t_0 = 10 min, β_1 = 0.718, $\tau_{sq,1}$ = 9.5 s, and $\tau_{sq,2}$ = 6.84 min.

The temporal absorption behaviour at λ_p = 610 nm (S_0-S_1 absorption band of flavin-semiquinone) due to light exposure (for a duration of 10 min at λ_{exc} = 350-440 nm, I_{exc} = 0.354 W cm^{-2}) is displayed in Fig. 6-33.

Upon excitation the absorption rises steeply to a plateau value from which it decays bi-exponentially after light switch-off with time constants of $\tau_{sq,1} \approx 9.5$ s (fraction $\beta_1 = 0.72$) and $\tau_{sq,2} \approx 6.8$ min (fraction $\beta_2 = 0.28$). The FAD-semiquinone (5-hydro-FAD) is thought to fully reduce with these two time constants to 1,5-dihydro-FAD. The reduced flavin, recovers back to the receptor state in the dark at room temperature.

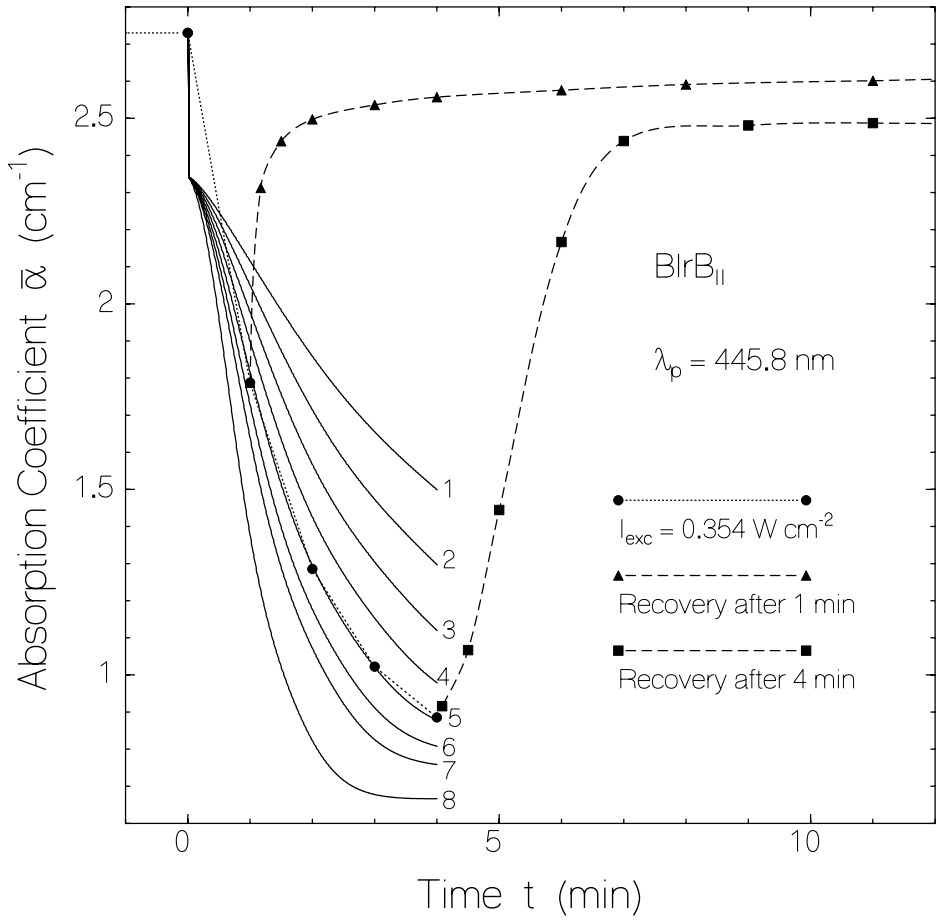

Figure 6-34: Temporal absorption behaviour, $\overline{\alpha}_p(t)$, at λ_p = 445.8 nm of $BlrB_{II}$. Light exposure at λ_{exc} = 350-440 nm with I_{exc} = 0.354 W cm^{-2}. (Data partly extracted from Fig. 6-32). Curves are calculated (eqs. 6-19 till 6-26) with parameters in Table 6-3, $\sigma_{a,r,exc} = 3.08\times10^{-17}$ cm^2, $\sigma_{a,s,exc} = 3.22\times10^{-17}$ cm^2, $\sigma_{a,sq,exc} = 2.52\times10^{-17}$ cm^2, $\sigma_{a,re,exc} = 0$, $\sigma_{a,d,exc} = 2.38\times10^{-17}$ cm^2, $\sigma_{a,r,p} = 4.28\times10^{-17}$ cm^2, $\sigma_{a,s,p} = 3.61\times10^{-17}$ cm^2, $\sigma_{a,sq,p} = 2.18\times10^{-17}$ cm^2, $\sigma_{a,re,p} = 0$, $\sigma_{a,d,p} = 1.05\times10^{-17}$ cm^2, and (1) $\phi_{sq} = 1\times10^{-3}$, (2) 1.2×10^{-3}, (3) 1.4×10^{-3}, (4) 1.6×10^{-3}, (5) 1.8×10^{-3}, (6) 2×10^{-3}, (7) 2.2×10^{-3}, (8) 2.8×10^{-3}.

The temporal absorption behaviour of $BlrB_{II}$ at λ_p = 445.7 nm is shown in Fig. 6-34 for 1 min and 4 min of light exposure (λ_{exc} 350-440 nm, I_{exc} = 0.354 W cm^{-2}). In the dark the absorption recovers mainly back to that of the initial $BlrB_{II,r}$. In the case of 1 min light exposure the absorption first rises steeply (signaling state recovery with $\tau_{s,rec} \approx 2$ s) and then changes over to a recovery with time constant of about 1.5 min (reduced flavin re-oxidation with time constant, τ_{reox}). In the case of 4 min light exposure the flavin cofactor is dominantly reduced. The absorption rise in the dark is first slow and then speeds up to $\tau_{reox} \approx 1.5$ min. The initially slower dark recovery is thought to be due to the time necessary for protein rearrangements which lead to

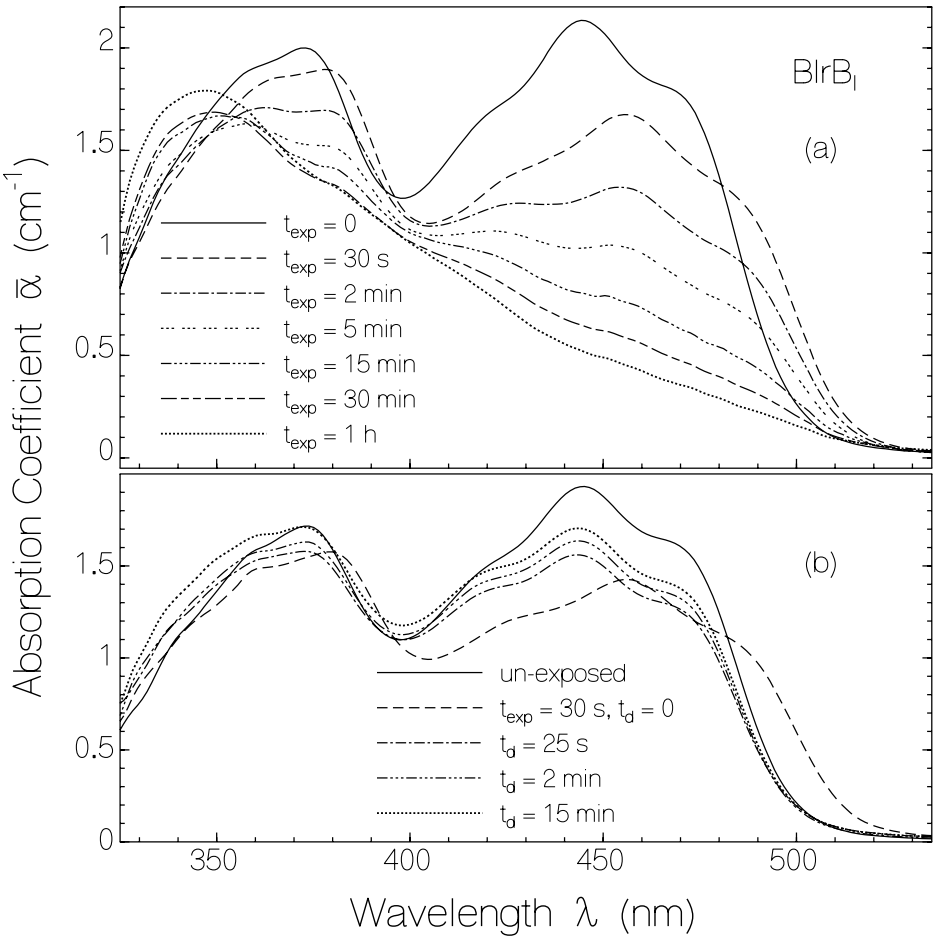

Figure 6-35: Dynamics of photo-degradation for $BlrB_I$ in aqueous solution at pH 8. (a) Length-averaged absorption coefficient spectra, $\overline{\alpha}(\lambda)$, at excitation intensity of I_{exc} = 0.59 W cm^{-2} in wavelength range λ_{exc} = 350-440 nm for several excitation times. (b) Absorption recovery of $BlrB_I$ in the dark after 30 s of light exposures at λ_{exc} = 350-440 nm with I_{exc} = 0.59 W cm^{-2}. Dark time t_d is varied.

the flavin re-oxidation inside binding pocket. The slow start of recovery may alternatively be due to the time required for oxygen to diffuse inside binding pocket to re-oxidize the reduced flavin, if free oxygen is thought to be necessary for re-oxidation.

The initial absorption strength of FAD in $BlrB_{II}$ is not fully reached. This is because of free FAD photo-degradation to lumichrome and lumiflavin derivatives [Hol05]. In keeping the thermodynamic equilibrium, free FAD is replenished from non-covalently bound FAD, and the generated lumichrome and lumiflavin derivatives are non-covalently bound to BlrB.

The absorption dynamics of $BlrB_I$ due to intense long-time light exposure is illustrated in Figs. 6-35 and 6-36. In Fig. 6-35a the change of the absorption spectra due to light exposure is shown.

The spectral absorption shapes are soon dominated by reduced flavin and photoproduct absorption shapes (lumichrome and lumiflavin-derivates [Hol05]). In Fig. 6-35b the absorption recovery after 30 s of light exposure is presented. As is seen, after 30 s of exposure the absorption recovery is moderate. In Fig. 6-36 the temporal development of the absorption coefficient, α_p, at λ_p = 444 nm due to light exposure for different time periods is shown.

After light-switch-off the absorption recovers partly back to the absorption of $BlrB_r$. After 1 min and 2 min of light exposure first a steep absorption rise is observed due to signaling state recovery.

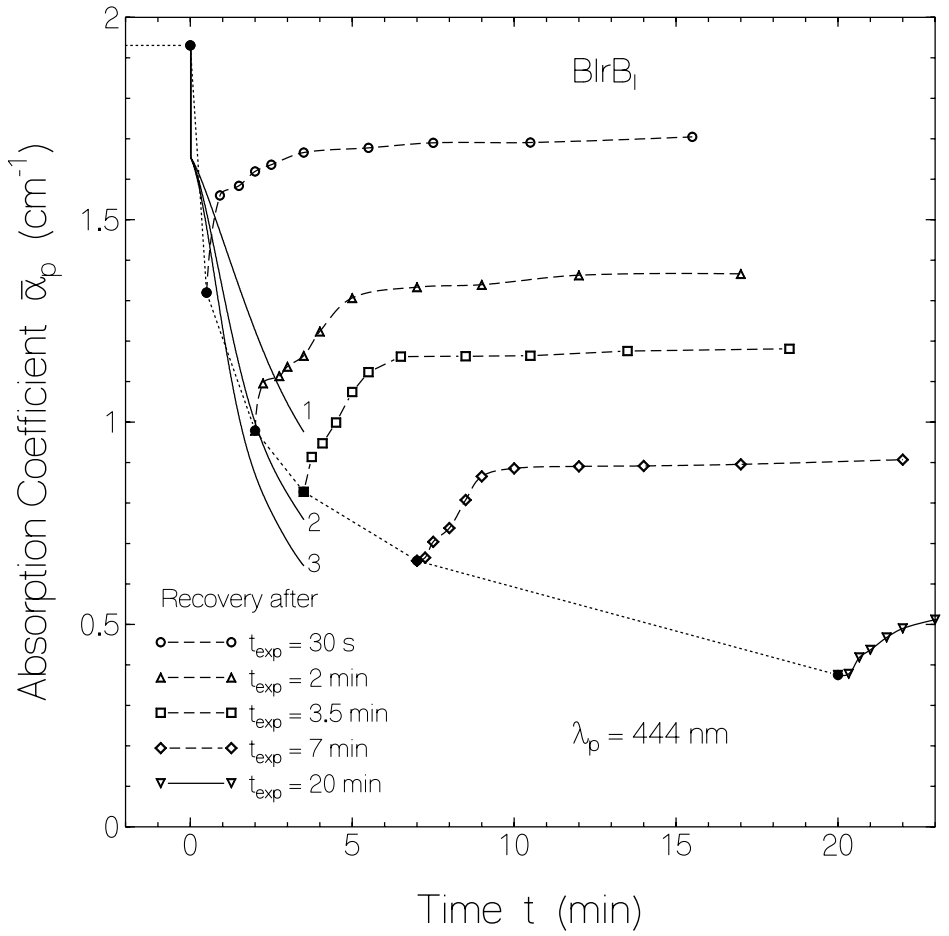

Figure 6-36: Absorption behaviour, $\overline{\alpha}_p(t)$, at λ_p = 444 nm of $BlrB_I$. Light exposure at λ_{exc} = 350-440 nm with I_{exc} = 0.59 W cm^{-2}. Curves are calculated (eqs. 6-19 till 6-26) with parameters in Table 6-3, the cross-sections given in the caption of Fig. 6-34, and (1) $\phi_{sq} = 5\times10^{-4}$, (2) 8×10^{-4}, (3) 1×10^{-3}.

The slowed-down absorption rise is due to reduced flavin re-oxidation. The incomplete absorption recovery is because of the free flavin conversion to lumichrome and lumiflavin-derivatives with lower absorption at $\lambda_p = 444$ nm.

According to Figs. 6-34 and 6-36 effective quantum yields of photoproduct formation for $BlrB_I$ and $BlrB_{II}$ are extracted. They are estimated from the incomplete recovery at wavelength of strong $BlrB_r$ absorption and weak photoproduct absorption after light switch-off and complete $BlrB_s$, $BlrB_{sq}$, and $BlrB_{re}$ recovery. $\phi_{d,eff}$ is approximately given by:

$$\phi_{d,eff} = \frac{N_d}{n_{ph,abs}}. \tag{6-17}$$

where $N_d = \int_0^l N_d dz$ is the length-integrated number density of $BlrB_d$ (FlPr), ℓ is the sample length, and $n_{ph,abs}$ is the density of absorbed photons at the excitation wavelength λ_{exc}. N_d is given by:

$$N_d = \frac{\alpha_{p,0} - \alpha_{p,\infty}}{\sigma_{a,r,p} - \sigma_{a,d,p}} \ell, \tag{6-18}$$

in which $\alpha_{p,0}$ is the initial absorption coefficient, $\alpha_{p,\infty}$ is the final absorption coefficient after light exposure for a period t_{exp} and absorption recovery for a time long compared to τ_{reox}. The number of absorbed photons per cross-sectional area within the time interval t_{exp} is given by eq. 6-5 where t_2-t_1 = t_{exp}.

Exploiting the data of Fig. 6-34 for t_{exp} = 1 min a quantum yield of photoproduct formation of, $\phi_{d,eff}(BlrB_{II}) = 2.3\times10^{-5}$, is obtained for $BlrB_{II}$ and using the data of Fig. 6-36 for t_{exp} = 30 s gives $\phi_{d,eff}(BlrB_I) = 1.1\times10^{-4}$ for $BlrB_I$.

Considering all results from static and dynamic fluorescence and absorption measurements, the photo-cycle dynamics shown in Fig. 6-37 is suggested.

Photo-excitation of the dark-adapted BlrB, $BlrB_r$, causes signaling-state formation, $BlrB_s$ which recovers back to $BlrB_r$ with a time constant $\tau_{s,rec}$ in the dark. Photo-excitation of flavin in $BlrB_s$ state causes reduction to the semiquinone form (called $BlrB_{sq}$) with a quantum efficiency of ϕ_{sq} which further reduces to $BlrB_{re}$. $BlrB_{re}$ re-oxidizes back to the original $BlrB_r$ with a dominant time constant τ_{reox}. To explain the obtained results a thermodynamic equilibrium between BlrB and free flavin is needed. The free flavin photo-degrades to lumichrome and lumiflavin derivatives (abbreviated by FlPr) with a quantum yield of photo-degradation, ϕ_D.

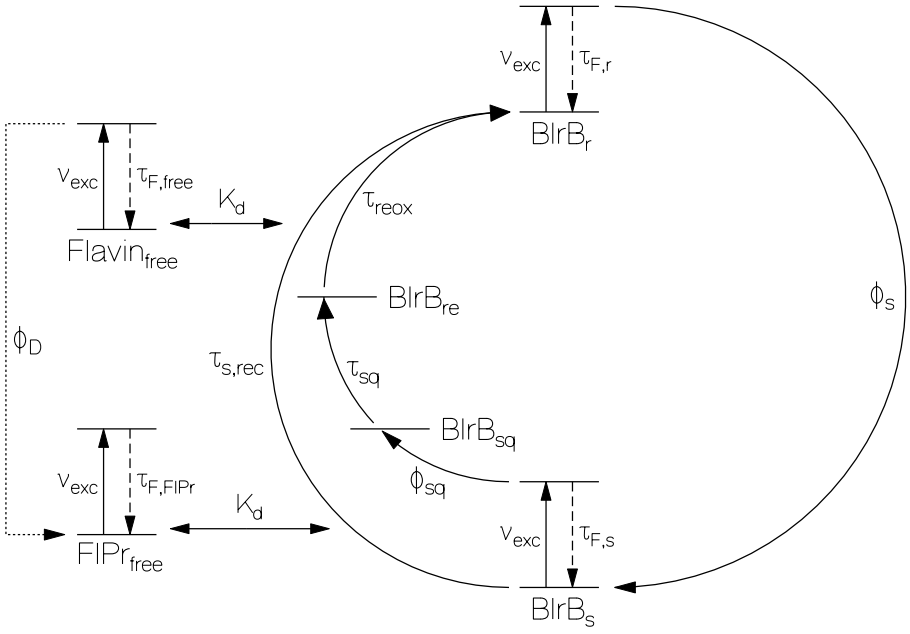

Figure 6-37: Photo-cycle scheme of BlrB and its interaction with the photo-degradation of free flavin

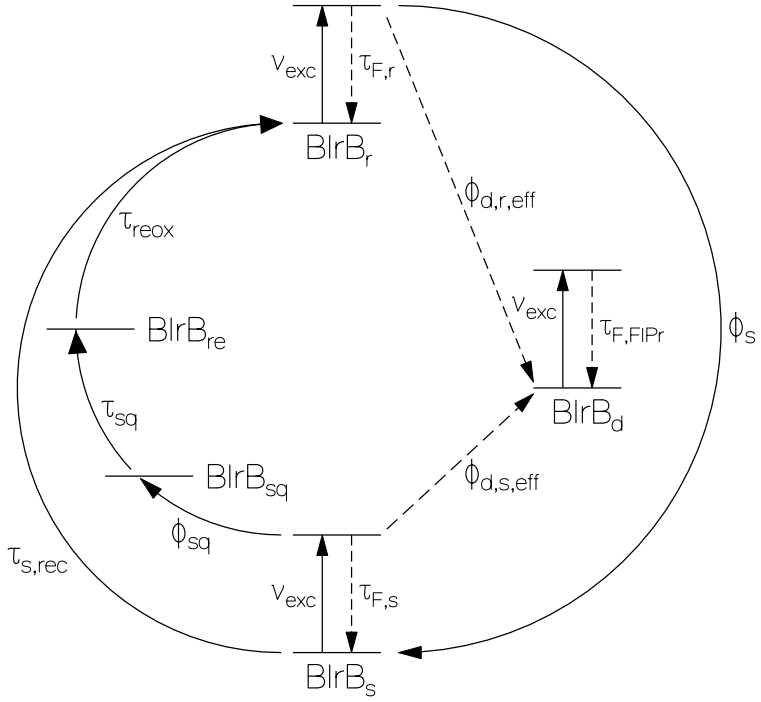

Figure 6-38: Approximate photo-dynamics scheme of BlrB including unbound flavin photo-degradation.

Again a thermodynamic equilibrium between the flavin photoproducts and BlrB is expected (the formed flavin derivatives are thought to be accepted in the BlrB binding pocket). This photo-

cycle scheme applies to both BlrB conformations, $BlrB_f$ and $BlrB_{sl}$, of faster and slower fluorescence lifetime and it applies to both $BlrB_I$ with a mixture of flavin cofactors and to $BlrB_{II}$ with FAD as the only cofactor. For numerical simulations photo-cycle scheme shown in Fig. 6-37 is approximated by the one shown in Fig. 6-38 where it is not distinguished between bound and free cofactor. In other words all original flavin is allowed to degrade with an effective quantum yield of $\phi_{d,eff}$ ($BlrB_d$), and the photoproducts do not take part in a photo-cycle (irreversible photoproducts).

The steady-state dynamics (considered time long compared to excited-state lifetimes of $BlrB_r$, $BlrB_s$, and $BlrB_d$) of the scheme displayed in Fig. 6-38 is given by the following rate equation system for the number densities, N_i of the components $BlrB_{r,j}$, $BlrB_{s,j}$, $BlrB_{sq,j}$, $BlrB_{re,j}$, $BlrB_d$ (j = *f*, *sl*) and the excitation intensity I_{exc}:

$$\frac{\partial N_{r,j}}{\partial t} = -(\phi_s + \phi_{d,r,j,eff})\frac{\sigma_{a,r,exc} I_{exc}}{h\nu_{exc}} N_{r,j} + \frac{N_{s,j}}{\tau_{s,rec}} + \frac{N_{re,j}}{\tau_{reox}}, \tag{6–19}$$

$$\frac{\partial N_{s,j}}{\partial t} = \phi_s \frac{\sigma_{a,r,exc} I_{exc}}{h\nu_{exc}} N_{r,j} - (\phi_{sq} + \phi_{d,s,j,eff})\frac{\sigma_{a,s,exc} I_{exc}}{h\nu_{exc}} N_{s,j} - \frac{N_{s,j}}{\tau_{s,rec}}, \tag{6–20}$$

$$\frac{\partial N_{sq,j}}{\partial t} = \phi_{sq} \frac{\sigma_{a,s,exc} I_{exc}}{h\nu_{exc}} N_{s,j} - \frac{N_{sq,j}}{\tau_{sq,j}}, \tag{6–21}$$

$$\frac{\partial N_{re,j}}{\partial t} = \frac{N_{sq,j}}{\tau_{sq,j}} - \frac{N_{re,j}}{\tau_{reox}}, \tag{6–22}$$

$$\begin{aligned}\frac{\partial N_d}{\partial t} = {} & \phi_{d,r,f,eff} \frac{\sigma_{a,r,exc} I_{exc}}{h\nu_{exc}} N_{r,f} + \phi_{d,s,f,eff} \frac{\sigma_{a,s,exc} I_{exc}}{h\nu_{exc}} N_{s,f} \\ & + \phi_{d,r,sl,eff} \frac{\sigma_{a,r,exc} I_{exc}}{h\nu_{exc}} N_{r,sl} + \phi_{d,s,sl,eff} \frac{\sigma_{a,s,exc} I_{exc}}{h\nu_{exc}} N_{s,sl},\end{aligned} \tag{6–23}$$

$$N_0 = N_{r,f} + N_{s,f} + N_{sq,f} + N_{re,f} + N_{r,sl} + N_{s,sl} + N_{sq,sl} + N_{re,sl} + N_d, \tag{6–24}$$

$$\begin{aligned}\frac{\partial I_{exc}}{\partial z} = {} & -\sigma_{a,r,exc}(N_{r,f} + N_{r,sl}) I_{exc} - \sigma_{a,s,exc}(N_{s,f} + N_{s,sl}) I_{exc} - \sigma_{a,sq,exc}(N_{sq,f} + N_{sq,sl}) I_{exc} \\ & - \sigma_{a,re,exc}(N_{re,f} + N_{re,sl}) I_{exc} - \sigma_{a,d,exc} N_d I_{exc}\end{aligned} \tag{6–25}$$

where z is the coordinate along the propagation direction and $\sigma_{a,r,exc}$, $\sigma_{a,s,exc}$, $\sigma_{a,sq,exc}$, $\sigma_{a,re,exc}$, and $\sigma_{a,d,exc}$ are the absorption cross-sections of the receptor state, signaling state, semiquinone state, reduced state and the photoproducts at the excitation wavelength λ_{exc} respectively. The excitation light transmission is given by $T_{exc} = I_{exc}(\ell)/I_{exc}(0)$. The transmission of a weak probe light at wavelength λ_p is given by $T_p = \exp(-\overline{\alpha}_p \ell)$ with $\overline{\alpha}_p = \int_0^\ell \alpha_p(z)dz/\ell$, where $\alpha_p(z)$ is given by:

$$\begin{aligned}\alpha_p(z) = {} & \sigma_{a,r,p}[N_{r,f}(z) + N_{r,sl}(z)] + \sigma_{a,s,p}[N_{s,f}(z) + N_{s,sl}(z)] + \\ & \sigma_{a,sq,p}[N_{sq,f}(z) + N_{sq,sl}(z)] + \sigma_{a,re,p}[N_{re,f}(z) + N_{re,sl}(z)] \\ & + \sigma_{a,d,p}N_d(z).\end{aligned} \tag{6–26}$$

The dynamics of signaling-state recovery is determined by eq. 6-20 which after light switch-off reduces to:

$$\frac{\partial N_{s,j}}{\partial t} = -\frac{N_{s,j}}{\tau_{s,rec}}, \tag{6–27}$$

giving $N_s(t) = N_s(0)\exp(-t/\tau_{s,rec})$. The absorption coefficient recovery in Fig. 6-31 is given by:

$$\alpha_p(t) = [N_0 - N_s(t)]\sigma_{a,r,p} + N_s(t)\sigma_{a,s,p} = N_0\sigma_{a,r,p} + (\sigma_{a,s,p} - \sigma_{a,r,p})N_s(0)\exp(-t/\tau_{s,rec}), \tag{6-28}$$

where $N_s = N_{s,f} + N_{s,sl}$. A single-exponential fit, eq. 6-6, to the absorption recovery curves of Fig. 6-31 gives the determined signaling-state recovery times. For both $BlrB_I$ and $BlrB_{II}$ a value of $\tau_{s,rec} \approx 2$ s was obtained at room temperature.

For the determination of the quantum yield of photo-induced signaling state formation, ϕ_s, under conditions of short time exposure as applied in Figs. 6-29 and 6-30, the equation system (6-19 till 6-25) reduces to:

$$\frac{\partial N_s}{\partial t} = \phi_s \frac{\sigma_{a,r,exc} I_{exc}}{h\nu_{exc}}(N_0 - N_s) - \frac{N_s}{\tau_{s,rec}}, \tag{6-29}$$

$$\frac{\partial I_{exc}}{\partial z} = -[\sigma_{a,r,exc}(N_0 - N_S) + \sigma_{a,s,exc}N_s]I_{exc}, \tag{6-30}$$

and the length-integrated absorption coefficient, $\overline{\alpha}_p(t)$, at the probe wavelength λ_p is given by:

$$\overline{\alpha}_p(t) = [N_0 - \overline{N}_s(t)]\sigma_{a,r,p} + \overline{N}_s(t)\sigma_{a,s,p}, \tag{6-31}$$

where $\sigma_{a,r,p}$ and $\sigma_{a,s,p}$ are the absorption cross-sections of $BlrB_r$ and $BlrB_s$ at wavelength λ_p, respectively. The length-averaged population number density, $\overline{N}_S$, is defined as $\overline{N}_S = \int_0^\ell N_S(z)dz/\ell$, where ℓ is the sample length.

The solid curves in Fig. 6-30a and 6-30b are calculated for different quantum yields, ϕ_s, by numerical solution of the equation system (6-29, 30) and application of eq. 6-31. The best fit to the experimental data gives $\phi_s(BrlB_{II}) = 0.9\pm0.1$ and $\phi_s(BrlB_I) = 0.4\pm0.1$. This finding shows that the cofactor FAD is high efficient in photo-induced signaling state formation of BlrB. The efficiency of photo-induced signaling state formation of the cofactors FMN and riboflavin is only moderate. Higher efficiency in the signaling state formation by using FAD in the protein binding pocket could be suggested as a reason for FAD, to be the in vivo chromophore.

The lower quantum efficiency of signaling-state formation with FMN and riboflavin cofactors compared to the FAD and higher photo-stability of free FAD compared to free FMN and riboflavin (free FAD is a factor of 20 more stable than free FMN or riboflavin at pH 8 buffer [Hol05]) explains the differences observed between $BlrB_I$ and $BlrB_{II}$ photo-cycle parameters (Figs. 6-34 till 6-36).

To obtain an acceptable fit to $\overline{\alpha}_p(t)$ for $BlrB_I$ and $BlrB_{II}$ in Figs. 6-34 and 6-36 by solving the equation system (6-18 till 6-26) it was necessary to set $\phi_{d,r,sl,eff} \approx \phi_{d,s,sl,eff} \approx 0$ (high photo-stability of flavin in slow BlrB component), $\phi_{d,r,f,eff} = \phi_{d,eff}/x_f$ ($\phi_{d,eff}$ determined experimentally), and $\phi_{d,s,f,eff}(BlrB_{II}) \approx 4\times10^{-6}$, $\phi_{d,s,f,eff}(BlrB_I) \approx 3\times10^{-5}$ (higher photo-stability of BlrB in signaling state because of shorter excited-state lifetime). The best fitting parameters are collected in Table 6-3.
The numerically solved equation system (6-18 till 6-25) with several ϕ_{sq} values for $BlrB_I$ and $BlrB_{II}$ are shown in Figs. 6-34 and 6-36 respectively (thick solid curves). The best agreement with the experimental data is found to be $\phi_{sq} \approx 8\times10^{-4}$ for $BlrB_I$ and $\phi_{sq} = 1.8\times10^{-3}$ for $BlrB_{II}$. In Fig. 6-36 the fit is limited to $t_{exp} \leq 3.5$ min since at longer times already photodegradation takes place at the applied excitation intensity.

The dynamics of flavin-semiquinone ($BlrB_{sq}$) conversion to reduced flavin ($BlrB_{re}$) is determined by eq. 6-21 which after light switch-off reduces to:

$$\frac{\partial N_{sq,j}}{\partial t} = -\frac{N_{sq,j}}{\tau_{sq,j}}. \qquad (6\text{–}32)$$

The absorption coefficient dependence, $\overline{\alpha}_p(t)$, in Fig. 6-33 fits to a two-component single-exponential decay with time constants, $\tau_{sq,1}$ = 9.5 s (fraction 72 %) and $\tau_{sq,2}$ = 6.8 min (fraction 28 %). It is thought that $\tau_{sq,1}$ belongs to the $BlrB_f$ conformation and that $\tau_{sq,2}$ belongs to $BlrB_{sl}$.

The formation of $BlrB_{re}$ from $BlrB_{sq}$ and its re-oxidation to $BlrB_r$ is governed by eq. 6-22. After light switch-off and a time delay of $t > 3\tau_{sq}$, this equation simplifies to:

$$\frac{\partial N_{re}}{\partial t} = -\frac{N_{re}}{\tau_{reox}}, \qquad (6\text{–}33)$$

where $N_{re} = N_{re,f} + N_{re,sl}$ since the formation time, τ_{sq}, is considerably faster than the re-oxidation time. The curves in Figs. 6-34 and 6-36 show that the re-oxidation dynamics is more complex. It may be approximately described with an average single time-constant of $\tau_{reox} \approx 1.5$ min.

Table 6-3. Parameters of BlrB BLUF proteins in aqueous solution at pH 8 and room temperature.

Parameter	$BlrB_I$		$BlrB_{II}$		Comments
Chromophore composition					TLC analysis
x_{FAD}	0.40±0.10		≈1.0		
x_{FMN}	0.30±0.10		≈0		
x_{Rf}	0.25±0.10		≈0		
x_{iso}	0.05±0.03		≈0		
Domain composition					Fluorescence analysis
x_f	0.25±0.05		0.25±0.03		
x_{sl}	0.67±0.05		0.67±0.04		
x_{free}	0.08±0.005		0.08±0.01		
K_d (mol dm^{-3})	6.5×10^{-7}				eq. 6-11
Photo-cycle characterization (temperature ϑ = 22 °C)					
ϕ_s	0.40±0.05		0.90±0.10		Fig. 6-30
$\tau_{s,rec}$ (s)	2.05±0.10		1.95±0.10		Fig. 6-31
$W_b/(hc_0)$ (cm^{-1})			4338		eq. 6-12
ϕ_{sq}	$\approx8\times10^{-4}$		1.8×10^{-3}		Figs. 6-34,36
$\tau_{sq,1}$ (s)			9.5		Fig. 6-33
$\tau_{sq,2}$ (min)			6.8		Fig. 6-33
τ_{reox} (min)	≈1.5		≈1.5		Figs. 6-34,36
$\phi_{d,eff}$	1.1×10^{-4}		2.3×10^{-5}		Figs. 6-34,36 eq. 6-17
State dependent parameters					
	Dark-adapted	Signaling state	Dark-adapted	Signaling state	
ϕ_F	0.024±0.004	0.0125±0.004	0.0161±0.004	0.004±0.001	Fig. 6-26
$\tau_{F,ave}$ (ps)	452±8	238±8	307±8	70±20	eq. 4-19
$\tau_{F,f}$ (ps)	73±30	<40	110±30	< 40	Figs. 6-27,28 eq. 6-16
$\tau_{F,sl}$ (ps)	700±50	<40	700	< 40	Fig. 6-27,28
$\tau_{F,free}$ (ns)	≈5.0	≈5.0	≈0.70	≈0.70	Fig. 6-27,28
$\phi_{d,f,eff}$	1.47×10^{-4}	3×10^{-5}	3.07×10^{-5}	4×10^{-6}	$\phi_{d,eff}/x_f$
$\phi_{d,sl,eff}$	≈0	≈0	≈0	≈0	Fit to eqs. 6-19 till 6-26

Abbreviations: x_{FAD}, x_{FMN}, x_{Rf}, x_{iso}, mole-fractions of FAD, FMN, riboflavin, and non-movable isoalloxazine moiety, respectively. x_f, x_{sl}, x_{free}, mole-fractions of holo-BlrB conformations with fast fluorescence lifetime, slow fluorescence lifetime, and of apo-BlrB, respectively. K_d, dissociation constant. ϕ_s, quantum yield of signaling state formation. $\tau_{s,rec}$, recovery time of BlrB after light exposure from signaling state to receptor state in the dark. $W_b/(hc_0)$, energy barrier from signaling state to receptor state (h is Planck constant, c_0 is vacuum light velocity). ϕ_{sq}, quantum efficiency of photo-induced semiquinone formation from signaling state. $\tau_{sq,1}$, $\tau_{sq,2}$, semiquinone lifetimes of $BlrB_{s,f}$ and $BlrB_{s,sl}$. τ_{reox}, average re-oxidation time of reduced flavin. $\phi_{d,eff}$, effective quantum yield of photo-degradation of BlrB. ϕ_F is fluorescence quantum yield. $\tau_{F,ave}$, average fluorescence lifetime. $\tau_{F,f}$, $\tau_{F,sl}$, $\tau_{F,free}$, fluorescence lifetimes of $BlrB_{r,f}$, $BlrB_{r,s}$, and of free flavin.

6.4 Slr1694

The BLUF protein slr1694 (amino acid residues 1-150, see Fig. 3-4) from the cyanobacterium *Synechocystis* sp. PCC6803 is characterized. Slr1694 expressed in *E. coli* with non-covalently bound FAD, FMN and riboflavin (called $Slr1694_I$) and FAD reconstituted Slr1694 which dominantly contains FAD (called $Slr1694_{II}$) are investigated [Zir06b].

6.4.1 Chromophore composition

The HPLC traces obtained for the extracted chromophore from Slr1694 are shown in Fig. 6-39. they revealed the presence of FAD, FMN and riboflavin in $Slr1694_I$ and in $Slr1694_{II}$. In $Slr1694_{II}$ FAD is the dominant chromophore. The mole fractions of FAD, FMN and riboflavin in $Slr1694_I$ and $Slr1694_{II}$ are listed in Table 6-4.

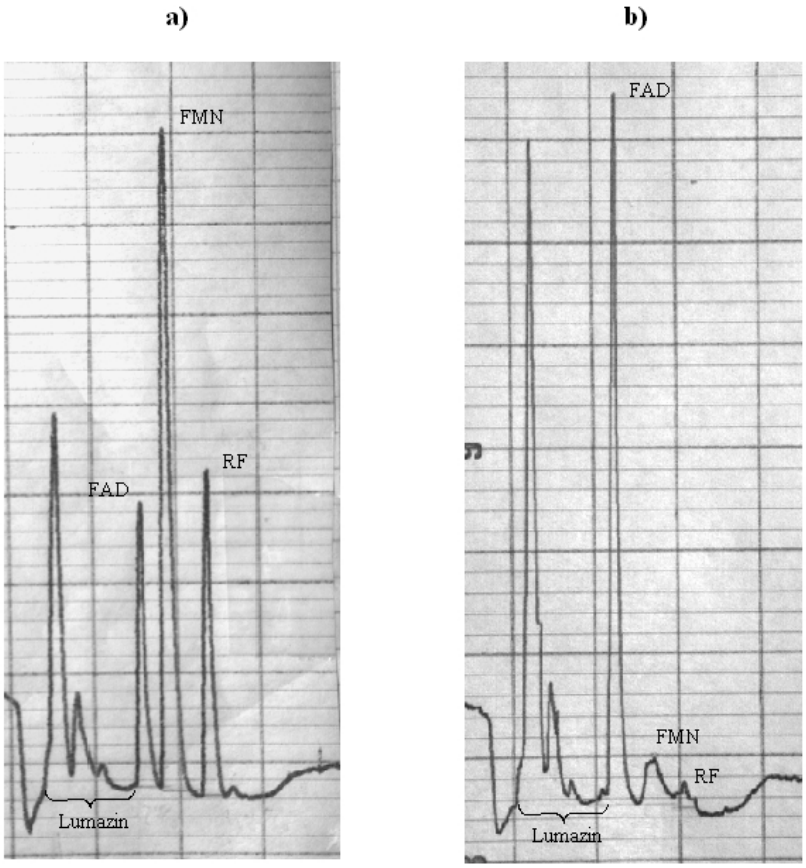

Figure 6-39: HPLC chromatogram for: (a) $Slr1694_I$ and (b) $Slr1694_{II}$.

6.4.2 Absorption studies

The absorption cross-section spectra of fresh dark-adapted Slr1694$_I$ (Slr1694$_{I,r}$) and of saturated light-adapted Slr1694$_I$ (Slr1694$_{I,s}$, produced by exposure at 350-440 nm for 4 s, I_{exc} = 0.265 W cm^{-2}) are displayed in Fig. 6-40. They are calculated from the absorption coefficient spectra and are calibrated with absorption cross-section spectrum of FAD at pH 7 [Isl03] (see chapter 5). Crossing points between absorption spectrum of dark-adapted and light-adapted samples are used to calibrate the absorption cross-section spectra for samples in the signaling-state. The shapes of the absorption cross-section spectra of Slr1694$_{I,r}$ and FAD are quite similar, only the vibronic structure of the S_0-S_1 and S_0-S_2 absorption bands of Slr1694$_{I,r}$ are more pronounced than that of FAD in aqueous solution. The Slr1694$_{I,s}$ absorption spectrum is approximately 15 nm red-shifted compared to the Slr1694$_{I,r}$ spectrum. Within our experimental accuracy the same absorption cross-section spectra were obtained for Slr1694$_I$ and Slr1694$_{II}$ (curves only shown for Slr1694$_I$).

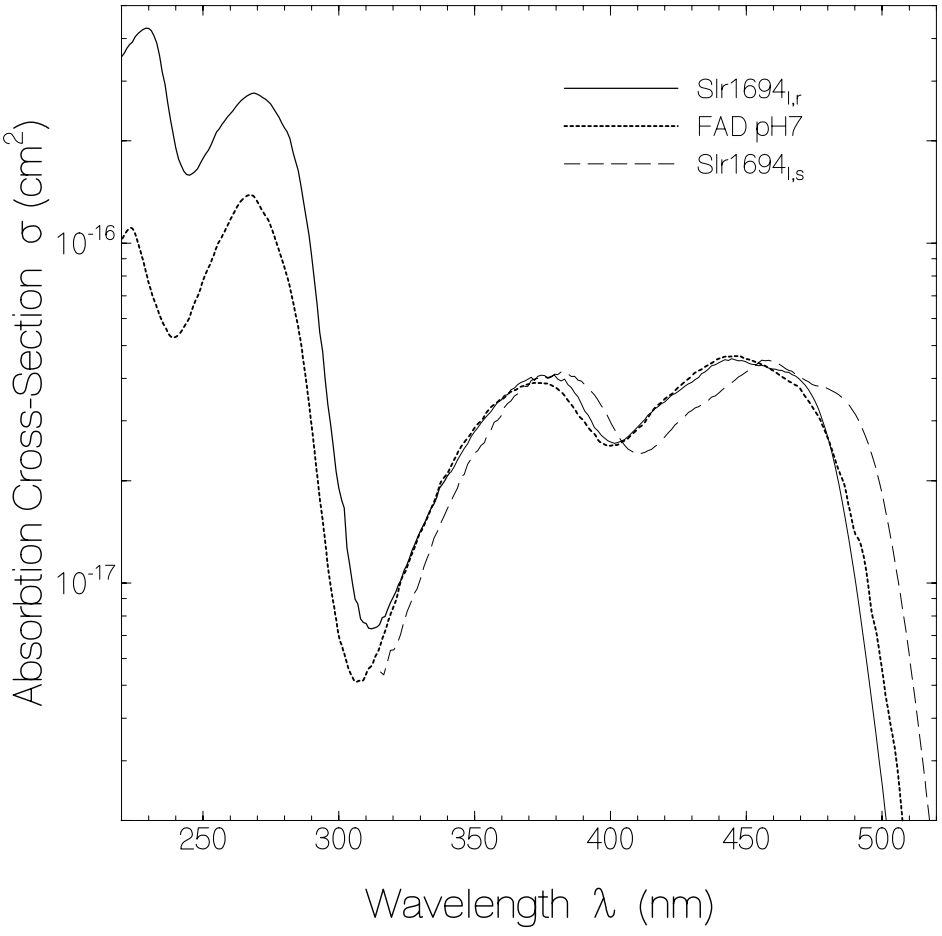

Figure 6-40: Absorption cross-section spectra of Slr1694 in dark-state (Slr1694$_{I,r}$) and Slr1694 in the signaling-state (Slr1694$_{I,s}$) in aqueous solution at pH 8 and of FAD in aqueous solution at pH 7 [Isl03].

6.4.3 Fluorescence studies

The temporal fluorescence traces of $Slr1694_I$ and $Slr1694_{II}$ domains in the dark- and signaling-states are displayed in Figs. 6-41a and 6-41b respectively.

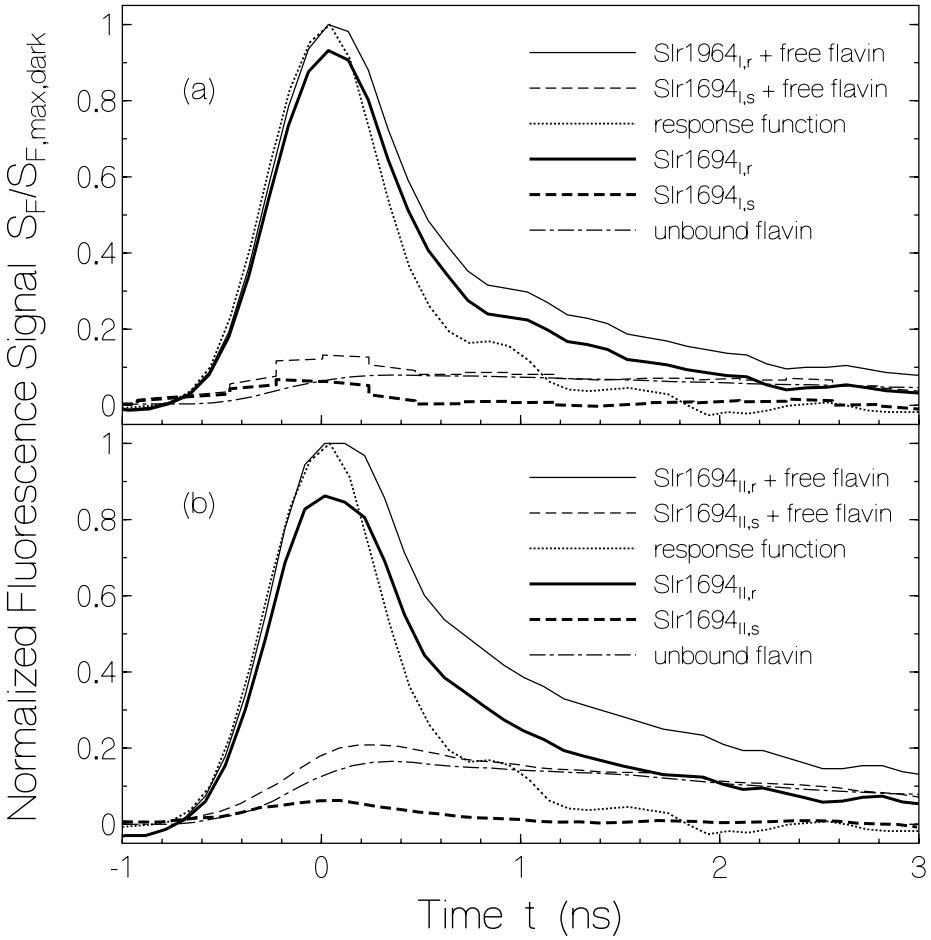

Figure 6-41: Normalized temporal fluorescence signals, $S_F(t)/S_{F,max,dark}$, of $Slr1694_I$ (a) and $Slr1694_{II}$ (b). Dotted curves show response function of the detection system. Thin solid curves belong to dark-adapted state. Thin dashed lines belong to light adapted state with λ_{exc} = 350-440 nm; I_{exc} = 0.3 W cm^{-2}, and duration of light exposure, Δt_{exp} = 15 s. Dash-dotted line shows expected free flavin contribution. Thick lines are expected true Slr1694 fluorescence traces (free flavin contribution is subtracted).

For the dark-state measurements, the samples were kept in dark and excited with a single laser pulses, whereas for the signaling-state fluorescence lifetime measurements, the samples were excited for 15 s with I_{exc} = 0.3 W cm^{-2} at λ_{exc} = 350-440 nm before pico-second laser pulse excitation and the fluorescence detection (real time fluorescence lifetime measurement, see

chapter 5). The thin lines in Fig. 6-41 belong to measured fluorescence traces consisting of fluorescence contributions from the non-covalently bound flavins and of the free flavins. The dotted-line in Figs. 6-41a and 6-41b, show the response function of the detection system (approximately Gausian shape with 1/e-time constant of $\tau_{resp} \approx 370$ ps). The slowly decaying tails are thought to be caused by the free flavin. The expected fluorescence contributions of the free flavins are approximately given by the dash-dotted lines. The shapes of these free flavin fluorescence contributions were obtained by measuring fluorescence traces of a mixture of 37 % FAD, 38 % FMN and 25 % riboflavin for Fig. 6-41a and of a mixture of 91 % FAD, 6 % FMN and 3 % riboflavin in aqueous solution at pH 8 for Fig. 6-41b (the mole fractions were selected to be the same as the mole fractions of FAD, FMN and riboflavin revealed from HPLC analysis for $Slr1694_I$ and $Slr1694_{II}$). The magnitude of the free flavin fluorescence contribution was adjusted to the sample fluorescence tails. The estimated fractions, β_F, of these free flavin signals to the total fluorescence signals are $\beta_{F,I,r} \approx 0.24$ for $Slr1694_{I,r}$ and $\beta_{F,I,s} \approx 0.85$ for the $Slr1694_{I,s}$. These fractions change to $\beta_{F,II,r} \approx 0.36$ of the fluorescence signal in the dark-state and to $\beta_{F,II,s} \approx 0.90$ for the saturated light-adapted state in the $Slr1694_{II}$ case.

For the thick curves, in Fig. 6-41, the fluorescence contribution of the free flavin is subtracted. They are the approximate true fluorescence traces of the non-covalently bound flavins. The fluorescence traces of the bond flavin reveal more than a single exponential fluorescence decay. Using a two-component exponential convolution fit (eqs. 6-1,2,15, see fluorescence lifetime analysis for BlrB) fast component of $\tau_{F,b,fast} = 50\pm 10$ ps with a mole-fraction of about 97±1 % and slow component of $\tau_{F,b,slow} = 800\pm 100$ ps with a mole-fraction of about 3±1 % for both $Slr1694_I$ and $Slr1694_{II}$ are revealed (the mole fractions of the free flavin for $Slr1694_I$ and $Slr1694_{II}$ are calculated by eq. 6-34, see below).

The fluorescence quantum distributions $E_F(\lambda)$, for dark-adapted Slr1694 ($Slr1694_r$) and for Slr1694 in saturated light-adapted state ($Slr1694_s$), in aqueous solution at pH 8 were determined using lumiflavin in water buffered to pH 7 ($\phi_F = 0.235$ [Hol05]) as reference. The results are displayed in Fig. 6-42. The fluorescence quantum yields, ϕ_F, are calculated from the fluorescence quantum distributions, $E_F(\lambda)$, and are listed in Table 6-4. Compared to the fluorescence quantum yields of FAD, FMN and riboflavin the measured fluorescence quantum yields of Slr1694 in the dark-state and in the signaling-state are very low.

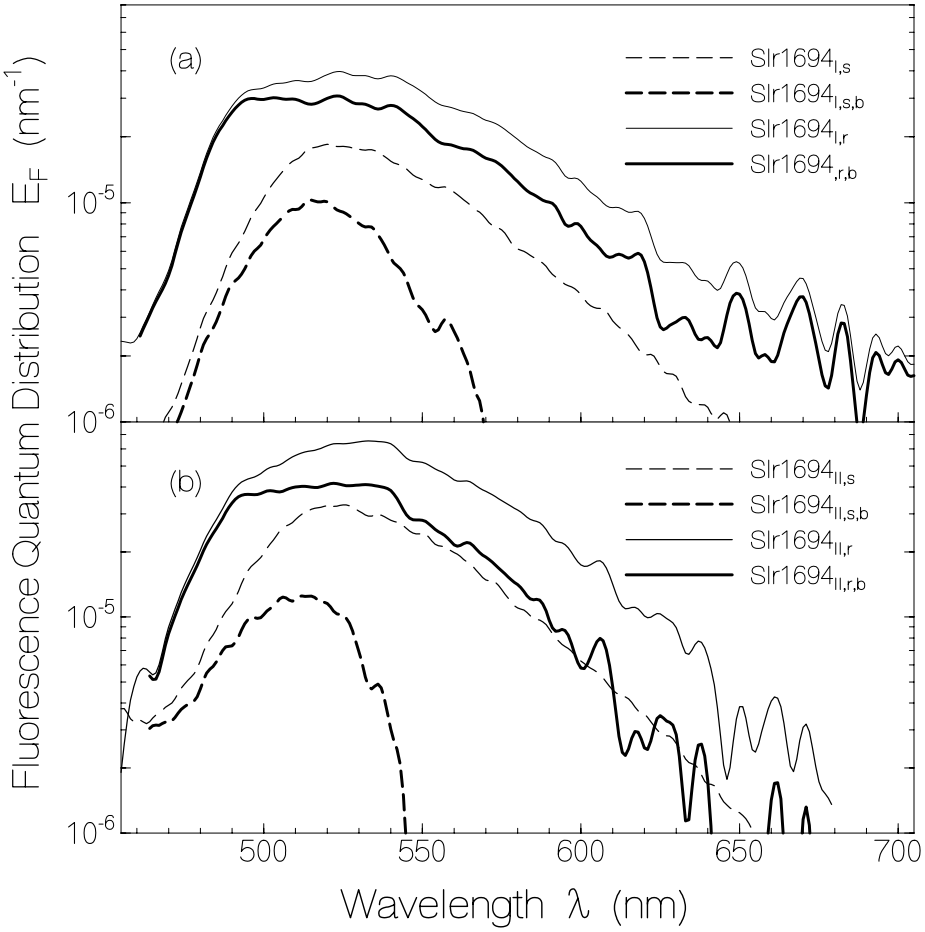

Figure 6-42: Fluorescence quantum distributions of Slr1694 in pH 8 buffer. Excitation at λ_{exc} = 365 nm. (a) $Slr1694_I$ in dark state ($Slr1694_{I,r}$ I_{exc} = 1.3×10^{-4}W cm^{-2}, Δt_{exp} = 1 s, Δt_{acc} = 400 ms) and in signaling state ($Slr1694_{I,s}$, I_{exc} = 7.2×10^{-3}, Δt_{exp} = 15 s, Δt_{acc} = 30 ms).(b) $Slr1694_{II}$ in dark state ($Slr1694_{II,r}$, I_{exc} = 1.3×10^{-4}W cm^{-2} Δt_{exp} = 1 s, Δt_{acc} = 400 ms) and in signaling state ($Slr1694_{II,s}$, I_{exc} = 6.8×10^{-3} W cm^{-2}, Δt_{exp} = 15 s, Δt_{acc} = 30 ms).

They are $\phi_{F,I,r} \approx 0.0042$ and $\phi_{F,I,s} \approx 0.0015$ for $Slr1694_I$. The fluorescence quantum yields change to $\phi_{F,II,r} \approx 0.0064$ in dark-state and $\phi_{F,I,s} \approx 0.0028$ for the signaling-state in the $Slr1694_{II}$ case.

The approximate fluorescence quantum distributions, $E_{F,b}(\lambda)$, belonging to flavin non-covalently bound to Slr1694 are shown in Fig. 6-42 by thick lines. The fluorescence quantum yields of the non-covalently bound flavin in the protein binding pocket, $\phi_{F,b} = (1 - \beta_F)\,\phi_F$, are included in Table 6-4. The fraction of free flavin, x_{free}, is estimated using the free flavin contribution in the total fluorescence signal, β_F, by the relation:

$$x_{free} = \frac{\beta_{F,r}\phi_{F,r}}{x_{FAD}\phi_{FAD} + x_{Ribo}\phi_{Ribo} + x_{FMN}\phi_{FMN}}, \qquad (6\text{-}34)$$

where the mole fractions of FAD, FMN and riboflavin, $x_{FAD}, x_{FMN}, x_{Ribo}$ respectively are substituted from the HPLC analysis. The calculated mole fractions of free flavins for $Slr1694_I$ and $Slr1694_{II}$ are listed in Table 6-4.

Moreover using the relation between radiative lifetime τ_{rad}, average fluorescence lifetime, $\tau_{F,ave}$, and average fluorescence quantum yield $\phi_{F,ave}$ (eq. 4-19), the average fluorescence lifetimes are calculated. The obtained average fluorescence lifetimes, $\tau_{F,ave}$, (calculated from total fluorescence quantum yield, ϕ_F) and the average fluorescence lifetimes for the non-covalently bound flavin, $\tau_{F,b,ave}$, (calculated from the fluorescence quantum yield of non-covalently bound flavin, $\phi_{F,b}$) in Slr1694 are listed in Table 6-4.

6.4.4 Photo-cycle dynamics

The transient absorption development $\overline{\alpha}_p(t)$ at λ_p = 491.5 nm (4.2 nm FWHM) due to light switch-on for a period of 1 min and light switch-off is displayed in Fig. 6-43 for $Slr1694_I$ (a) and $Slr1694_{II}$ (b). The samples are excited at λ_{exc} = 350-440 nm with different intensities in the range from 0.0014 W cm^{-2} to 0.26 W cm^{-2}. The signaling state formation fastens up with excitation intensity and reaches constant levels within the exposure time.

The signaling-state recovery back to the original receptor state in the dark obeys a single-exponential law (eq. 6-6). The extracted recovery time constants, $\tau_{s,rec}$, are listed in Table 6-4 for three different temperatures.

The quantum efficiency of signaling state formation, ϕ_s, is extracted from the absorption rise at 491.5 nm, Fig. 6-43, immediately after light switch-on by calculating the fraction of molecules transformed to the signaling state, ΔN_s, in a time interval, $\delta t = t_2 - t_1$, short compared to the signaling-state recovery time, τ_{rec}, and by calculating the number of absorbed photons in the same time interval, $\Delta n_{ph,abs}$. The following relation is used for calculation:

$$\phi_s = \frac{\Delta N_s}{\Delta n_{ph,abs}}. \tag{6-35}$$

The length-integrated number density of molecules transferred to the signaling state is given by:

$$\Delta N_s = N_0 \ell \frac{\alpha_p(t_2) - \alpha_p(t_1)}{\Delta \alpha_{p,\max}}, \tag{6-36}$$

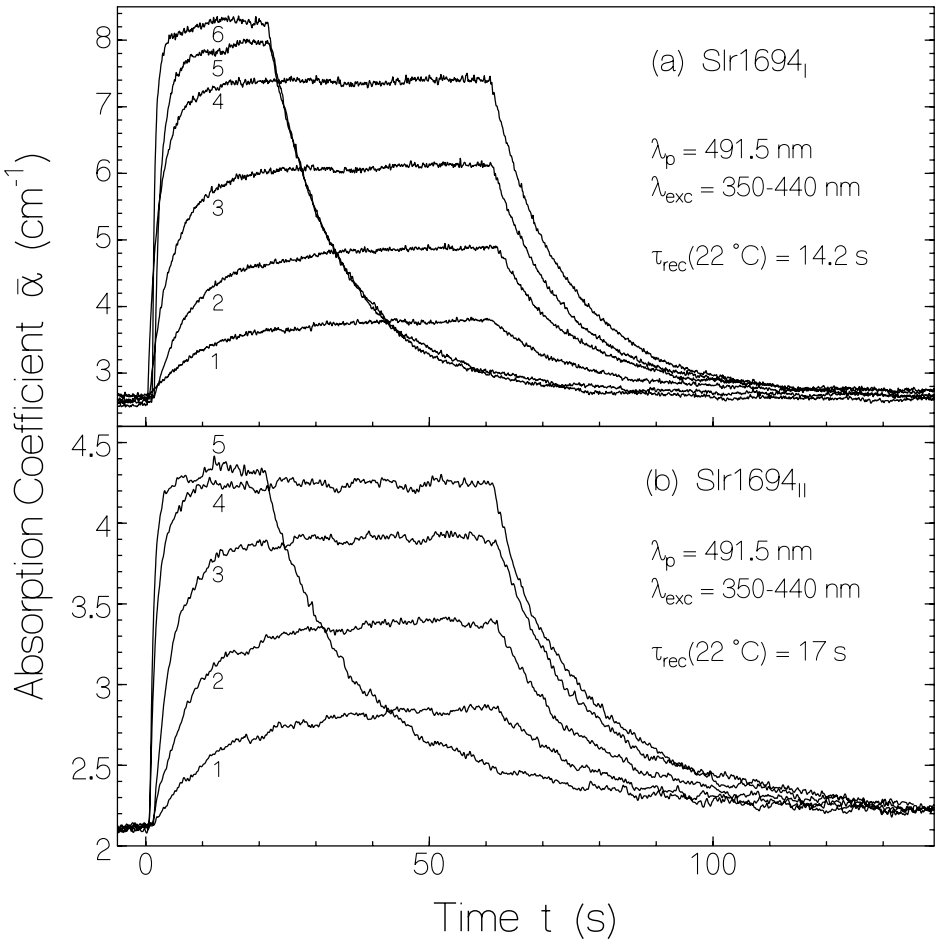

Figure 6-43: Photo-induced signaling-state formation and its recovery to the initial state in dark for $Slr1694_I$ (a) and $Slr1694_{II}$ (b). Samples are excited for 60 s (lower intensities) or 20 s (higher intensities). The curves belong to the following excitation intensities, I_{exc} (in W cm^{-2}): (1) 8×10^{-4}, (2) 0.0024, (3) 0.069, (4) 0.0224, (5) 0.046, (6) 0.142.

where N_0 is the total number density of Slr1694 molecules, $\alpha_p(t_i) = -\ln[T_p(t_i)]/\ell$ is the absorption coefficient at the probe wavelength, λ_p, at time t_i, and $\Delta\alpha_{p,max} = \alpha_{p,max} - \alpha_{p,ini}$ is the maximum absorption coefficient change at λ_p ($\alpha_{p,\max} = \sigma_{a,p,s}N_0$ is the absorption coefficient when the sample is completely converted to the signaling state) and $\alpha_{p,ini}$ is the initial absorption coefficient before exposure. $\sigma_{a,p,s}$ is the absorption cross-section of the signaling state at wavelength λ_p. The number density of absorbed photons is given by eq. 6-5. The quantum yields of signaling state formation are found to be $\phi_s = 0.63\pm0.07$ for both $Slr1694_I$ and $Slr1694_{II}$.

The excitation intensity dependence of the absorption coefficient at a fixed-probe wavelength , 490.3 nm, is displayed with circles in Fig.6-44 for both $Slr1694_I$ (a) and $Slr1694_{II}$ (b). It is used

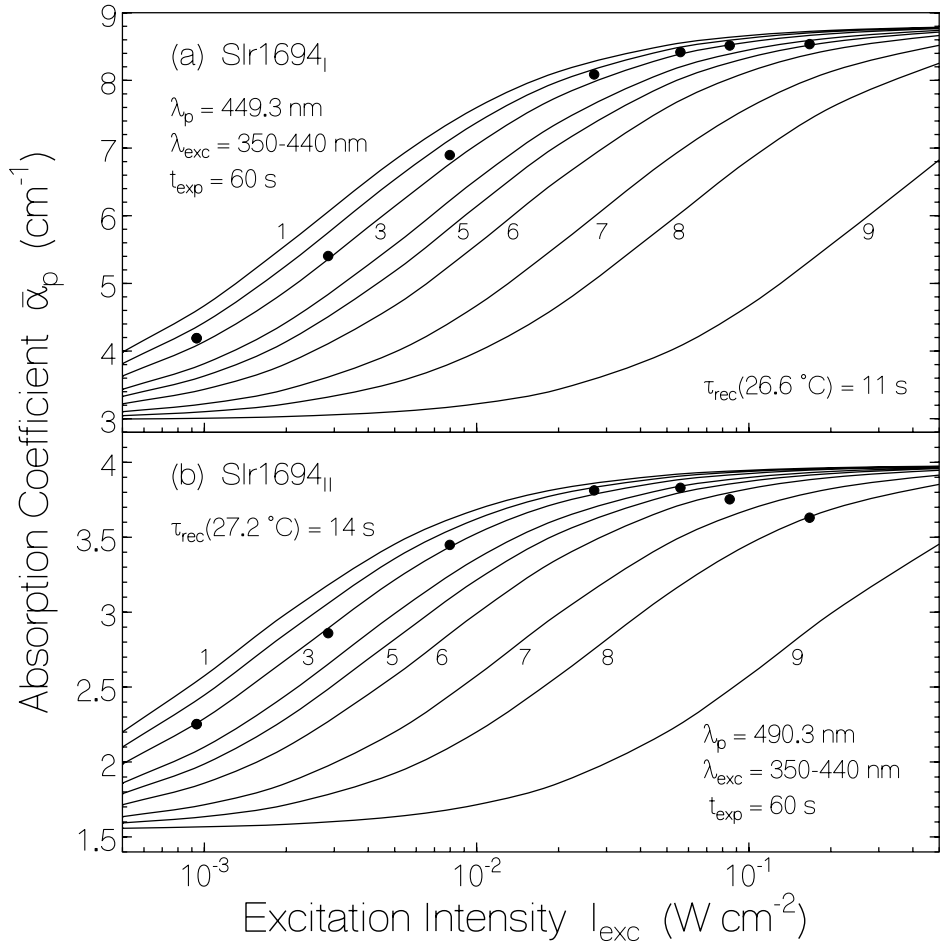

Figure 6-44: Steady-state absorption coefficient, $\overline{\alpha}_p$ at probe wavelength, λ_p, as a function of excitation intensity, I_{exc}, after 60 s light exposure. (a) Slr1694$_I$, and (b) Slr1694$_{II}$. Solid curves are calculated for the quantum yields of signaling state formation, ϕ_s, of: (1) 1, (2) 0.8, (3) 0.6, (4) 0.4, (5) 0.3, (6) 0.2, (7) 0.1, (8) 0.05, (9) 0.01.

alternatively, to calculate the quantum yield of signaling state formation (eqs. 6-8,9,10). The best fits to the measured data points lead to $\phi_s = 0.6\pm0.05$ for both Slr1694$_I$ and Slr1694$_{II}$. The absorption decrease at high intensity in Fig. 6-44b is caused by photo-degradation and photo-reduction at high excitation intensities. Thses processes are more pronounced for Slr1694$_{II}$ than for Slr1694$_I$.

The photo-induced signaling-state formation and back recovery at room temperature were carried out in short-time light exposure measurements in order to avoid photodegradation.

The temporal development of absorption spectra during high-intensity light exposure and back-recovery in dark is shown in Figs. 6-45 and 6-46 for Slr1694$_I$ and Slr1694$_{II}$ respectively.

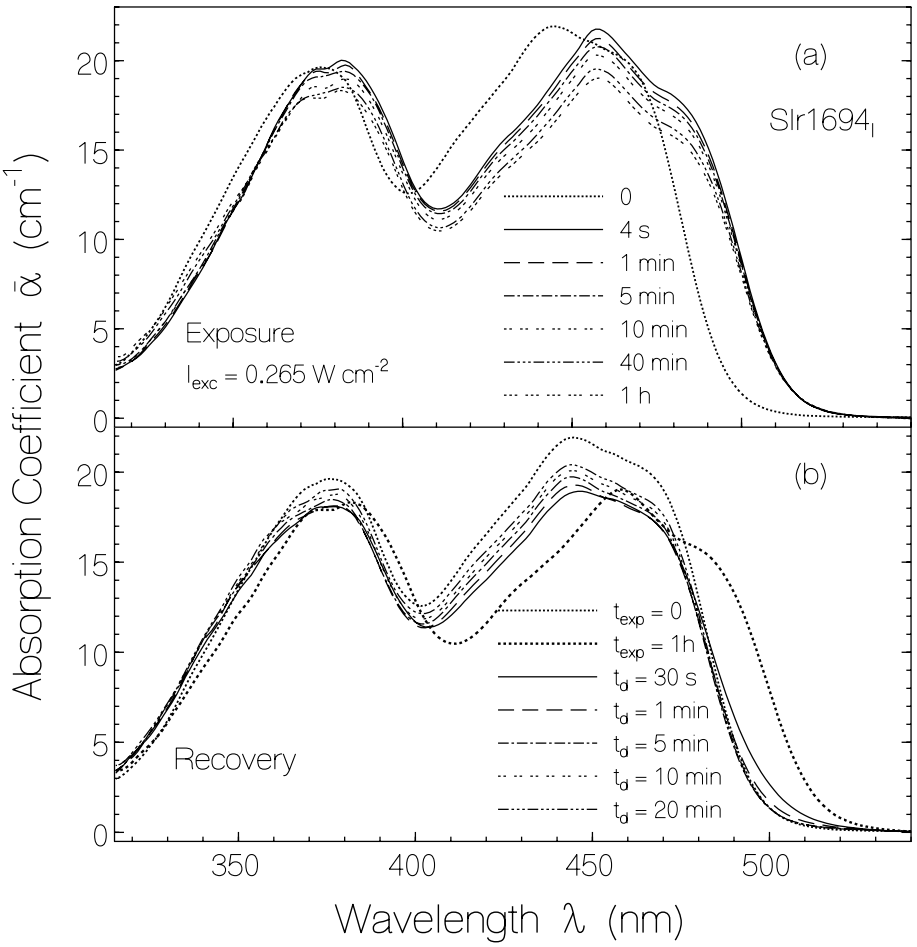

Figure 6-45: (a) Absorption spectra of Slr1694$_I$ at certain times of light exposure. Excitation wavelength λ_{exc} = 350-440 nm; excitation intensity I_{exc} = 0.265 W cm^{-2}. Exposure times are written in the legend. Cell thickness ℓ = 1.5 mm; cell area 1.5 mm × 3.5 mm. Length-averaged absorption coefficient spectra, $\overline{\alpha}(\lambda) = -\ln[T(\lambda)]/\ell$ (T is transmission), are shown. (b) Recovery of absorption spectra of Slr1694$_I$ in the dark at certain times after intense light exposure for 60 min at λ_{exc} = 350-440 nm with I_{exc} = 0.265 W cm^{-2}. Dark times, t_d, are written in the legend.

Samples are excited in a small volume cell, 1.5 mm × 1.5 mm × 3.5 mm, in the wavelength range from 350-440nm with an excitation intensity of $I_{exc} \approx 0.27 Wcm^{-2}$. As shown in Fig. 6-45a for Slr1694$_I$ the transfer from dark-state to the signaling-state is already complete after 4 s light exposure.

Upon prolonged exposure of the signaling-state a gradual decrease at S_0-S_1 absorption band is observed. Fig. 6-45b represents the dark-recovery of Slr1694$_{I,s}$ after 1 hour of exposure with I_{exc} = 0.265 W cm^{-2}. It is worthwhile to note that during the first 30 s, the signaling state already recovers back to the receptor state while a second recovery process continues with a slow

recovery time. Although at least two recovery processes are involved, no complete recovery observed.

Nearly the same temporal behaviour has seen for absorption spectrum of $Slr1694_{II}$ as shown in Fig. 6-46. Again the signaling state is formed within 4 s and at prolonged light exposure the S_0-S_1 absorption band decreases. However the absorption decrease is more pronounced for $Slr1694_{II}$ than for $Slr1694_{I}$. The build-up of the absorption band around 350 nm is also more pronounced for $Slr1694_{II}$.

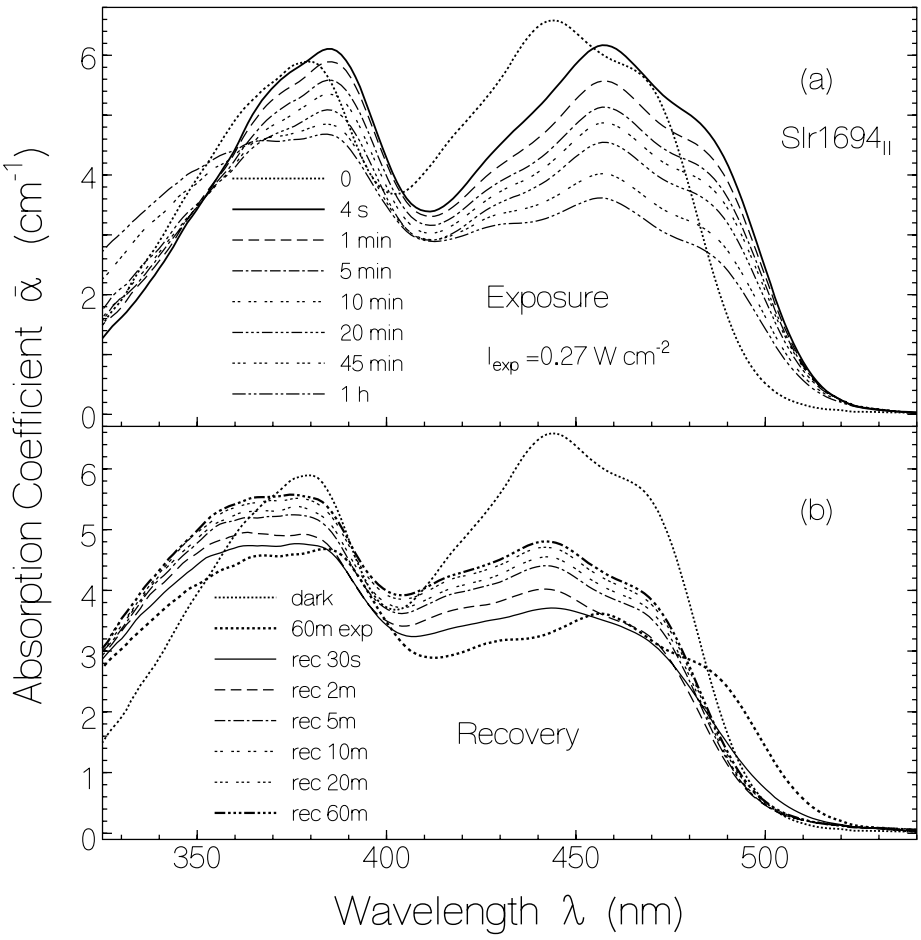

Figure 6-46: (a) Absorption spectra of $Slr1694_{II}$ at certain times of light exposure. Excitation wavelength λ_{exc} = 350-440 nm, excitation intensity I_{exc} = 0.27 W cm^{-2}. Exposure times are written in the legend. (b) Recovery of absorption spectra of $Slr1694_{I}$ in the dark at certain times after intense light exposure for 60 min at λ_{exc} = 350-440 nm with I_{exc} = 0.27 W cm^{-2}. Dark times are written in the legend.

After light-switch-off the signaling-state absorption recovers back to the initial receptor state absorption within 30 s. Similar to $Slr1694_I$ a second recovery process is present and no complete recovery is observed.

These temporal behaviours of the absorption coefficients during light exposure and dark recovery can be followed better by plotting the dynamics for λ_p = 490.3 nm (peak position of the absorption difference between dark and signaling states) and λ_p = 439.7 nm (peak position of the receptor state). These absorption coefficients are displayed in Fig. 6-47a for $Slr1694_I$ and in Fig. 6-47b for $Slr1694_{II}$. For both domains the absorption at 490.3 nm steeply rises and the absorption at 439.7 nm steeply decreases because of signaling state formation. Then the absorption decreases moderately because of free flavin degradation (dominant at the beginning, more pronounced for $Slr1694_{II}$ with larger free flavin content), photo-reduction of $Slr1694_s$ (flavin hydroquinone formation in protein) and photo-degradation of non-covalently bound flavin. Lumichrome is one degradation component in agreement with the absorption spectra in Fig. 6-46 and lumichrome absorption cross-section spectra in Fig. 2-3.

After light switch-off the absorption at 490.3 nm decreases steeply and the absorption at 439.7 nm rises steeply within the first 30 s because of signaling state recovery to the dark state. Then a moderate absorption rise is observed which is because of re-oxidation of the reduced flavins inside the protein. The initial absorption strength is not approached because of photo-degradation of the initially present free flavin and partial photo-degradation of non-covalently bound flavin.
From the slow absorption rise after light switch-off in Fig. 6-47a a re-oxidation time constant of $\tau_{reox} \approx 8.6$ min is determined (dash-dotted fit) for $Slr1694_I$. A re-oxidation time of $\tau_{reox} \approx 5.5$ min is determined from a fit of the absorption recovery in Fig. 6-47b for $Slr1694_{II}$.

The efficiency of flavin cofactor reduction in the signaling-state, ϕ_{red}, is determined from the absorption recovery in the S_0-S_1 absorption region of $Slr1694_r$ due to flavin re-oxidation in the dark after intense light exposure. The quantum yield, ϕ_{red}, of formation of $Slr1694_{red}$ (reduction of flavoquinone form of flavin, Fl_{ox}, to flavohydroquinone form, $Fl_{red}H_2$) is given by:

$$\phi_{red} = \frac{\Delta N_{red}}{\Delta n_{ph,abs}}. \tag{6-37}$$

The length-integrated number density of molecules transferred to the reduced state is given by:

$$\Delta N_{red} = \ell \frac{\alpha_p(t_\infty) - \alpha_p(t_e + 5\tau_{rec})}{\sigma_{a,r,p} - \sigma_{a,red,p}}, \tag{6-38}$$

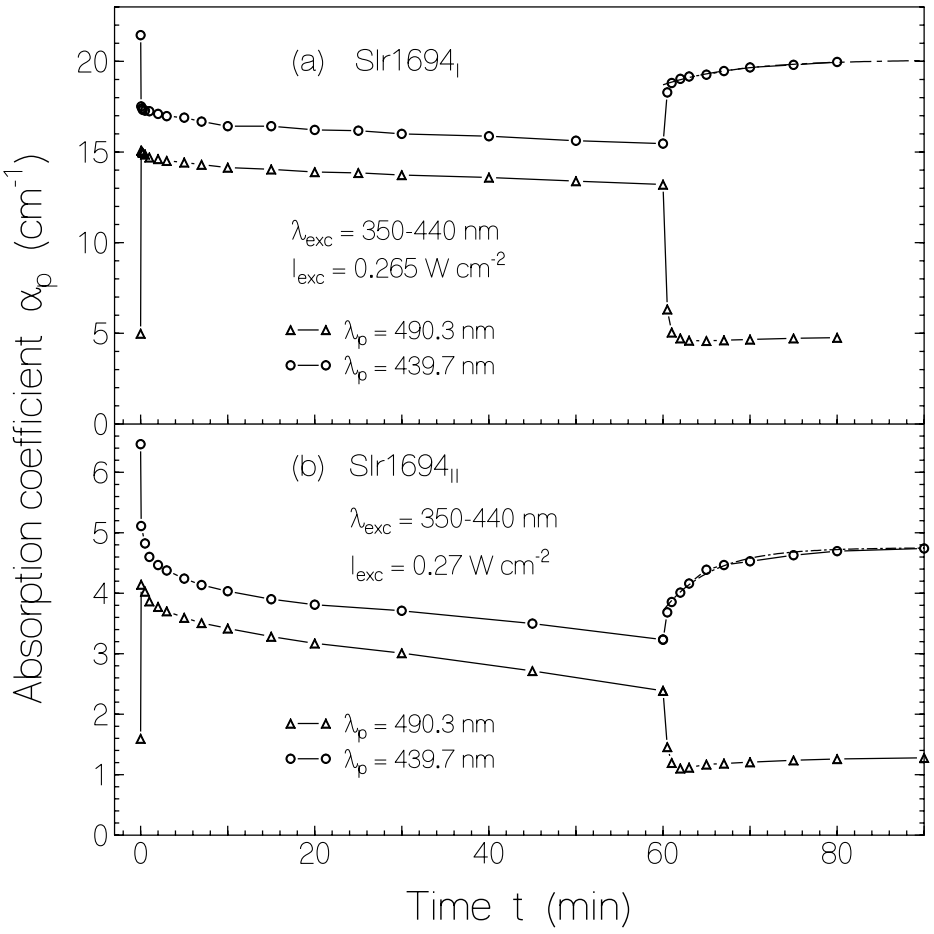

Figure 6-47: Temporal absorption behavior, $\overline{\alpha}_p(t)$, at λ_p = 490.3 nm and at λ_p = 439.7 nm of Slr1694$_I$ (a) and Slr1694$_{II}$ (b) during light exposure and after light exposure in dark (data taken from Figs. 6-45 and 6-46).

where $\sigma_{a,r,p}$ and $\sigma_{a,red,p}$ are the absorption cross-sections of Fl_{ox} in the receptor state and of $Fl_{red}H_2$ at the probe wavelength, λ_p, respectively. t_e is the time position of light switch off. After $t_e + 5\tau_{rec}$ the signaling state has recovered and the further absorption change is due to re-oxidation. The number density of absorbed photons is given by eq. 6-5 (in which $\delta t = \tau_{reox}$, if the exposure time $t_{exp} = t_e - t_0$ is longer than τ_{reox} and $\delta t = t_{exp}$ otherwise).

The incomplete absorption recovery in the S_0-S_1 absorption region of Slr1694$_r$ after intense-light exposure is used to determine the quantum yield of photo-degradation of flavin in the signaling state, $\phi_{s,D}$ (data have taken from Fig. 6-47). These degradation efficiencies are given by:

$$\phi_{s,D} = \frac{\Delta N_r - x_{free} N_0 \ell}{\Delta n_{ph,abs}}, \qquad (6\text{-}39)$$

where ΔN_r is given by:

$$\Delta N_r = \ell \frac{\alpha_p(t_0) - \alpha_p(t_\infty)}{\sigma_{a,r,p}}. \qquad (6\text{-}40)$$

The total number density of flavin molecules, N_0, is given by $N_0 = \alpha_p(t_0)/\sigma_{a,r,p}$. The number density of absorbed photons is given by eq. 6-5 with $\delta t = t_e - t_0$ which is the total exposure time. The higher molar fraction of free flavin found in $Slr1694_{II}$ causes more pronounced photodegradation with respect to $Slr1694_I$ in spite of higher photo-stability of FAD compared to FMN and riboflavin. The free flavin photoproducts or photoproduct intermediates (likely radicals) seem to enhance the Slr1694 photo-degradation [Shi06].

The temporal developments of the fluorescence signal during light exposure for $Slr1694_I$ and $Slr1694_{II}$ are shown in Fig. 6-48. The applied excitation intensity profile is shown in part (a) (λ_{exc} = 350-440 nm, I_{exc} = 0.3 W cm^{-2}). The fluorescence signal was measured by picosecond laser pulse excitation (λ_L = 400 nm, Δt_L = 3 ps) and micro-channel-plate photomultiplier signal detection (real time measurement, see chapter 5). The presented time-integrated fluorescence signal is normalized to the fluorescence signal of not exposed sample. At light switch-on the fluorescence signal steeply decreases because of signaling state formation. Then during light exposure the fluorescence raises gradually since some flavin is converted (degraded) to lumichrome and lumiflavin derivatives [Hol05] which have higher fluorescence quantum yield than free FAD and bound flavin in the signaling state. The fluorescence rise is stronger for $Slr1694_{II}$ (Fig. 6-48c) than for $Slr1694_I$ (Fig. 6-48b) since there is more free FAD in $Slr1694_{II}$ than in $Slr1694_I$ and $Slr1694_{II}$ is less photo-stable. At light switch-off the fluorescence rises step-like because of back recovery of the signaling state to the receptor state (receptor state is stronger fluorescent than signaling state). The performed photo-dynamic studies lead to the photo-cycle scheme shown in Fig. 6-49. There, photo-excitation of dark adapted Slr1694 (called $Slr1694_r$) populates the first excited singlet state (S_1-state), in which flavin may relax to its ground state via radiative or non-radiative processes. The excitation may also lead to flavin-protein restructuring (signaling-state formation). The Slr1694 BLUF protein in the signaling-state ($Slr1694_s$) relaxes back to the initial receptor state, $Slr1694_r$, in the dark at room temperature.

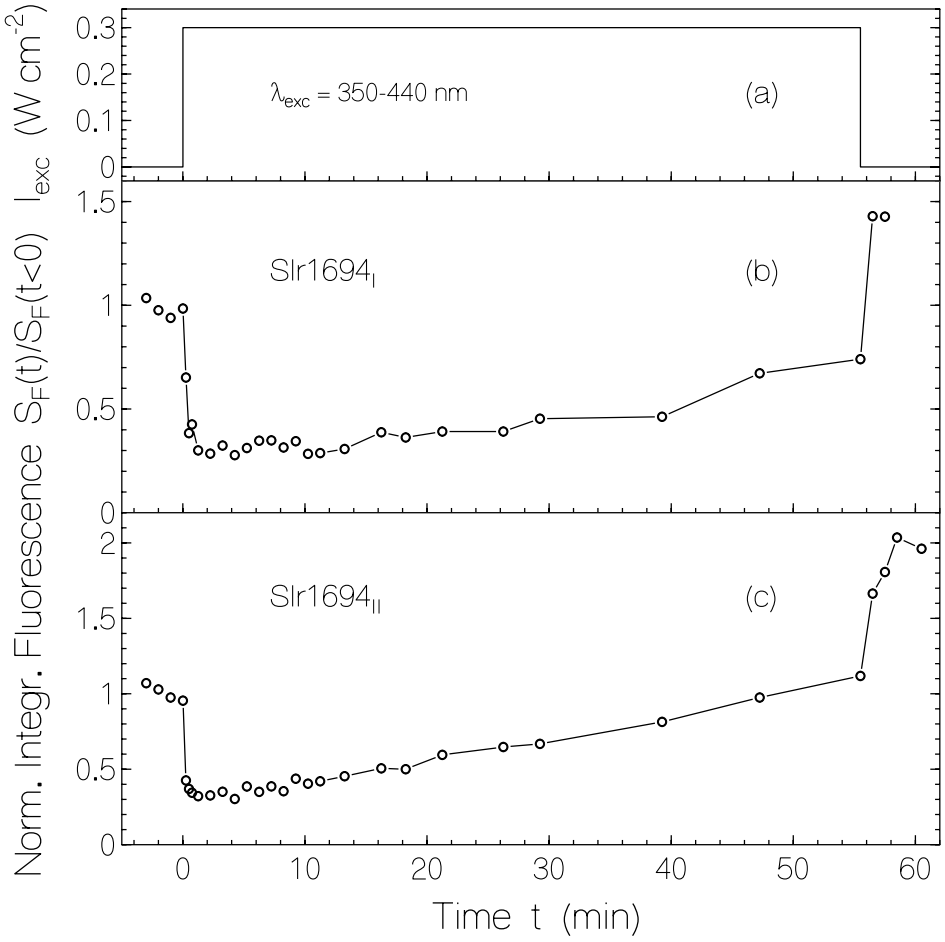

Figure 6-48: Temporal development of time-integrated fluorescence signal of Slr1694$_I$ (b) and Slr1694$_{II}$ (c) due to light exposure. Excitation intensity profile is shown in part (a).

Photo-excitation of the flavin in the signaling-state leads to reduction of Fl_{ox} to $Fl_{red}H_2$ (quantum efficiency $\phi_{s,red}$) and degradation of Fl_{ox} to photoproducts (quantum yield $\phi_{s,D}$). In the dark the formed flavohydroquinone re-oxidizes slowly to the original flavoquinone (time constant τ_{reox}).

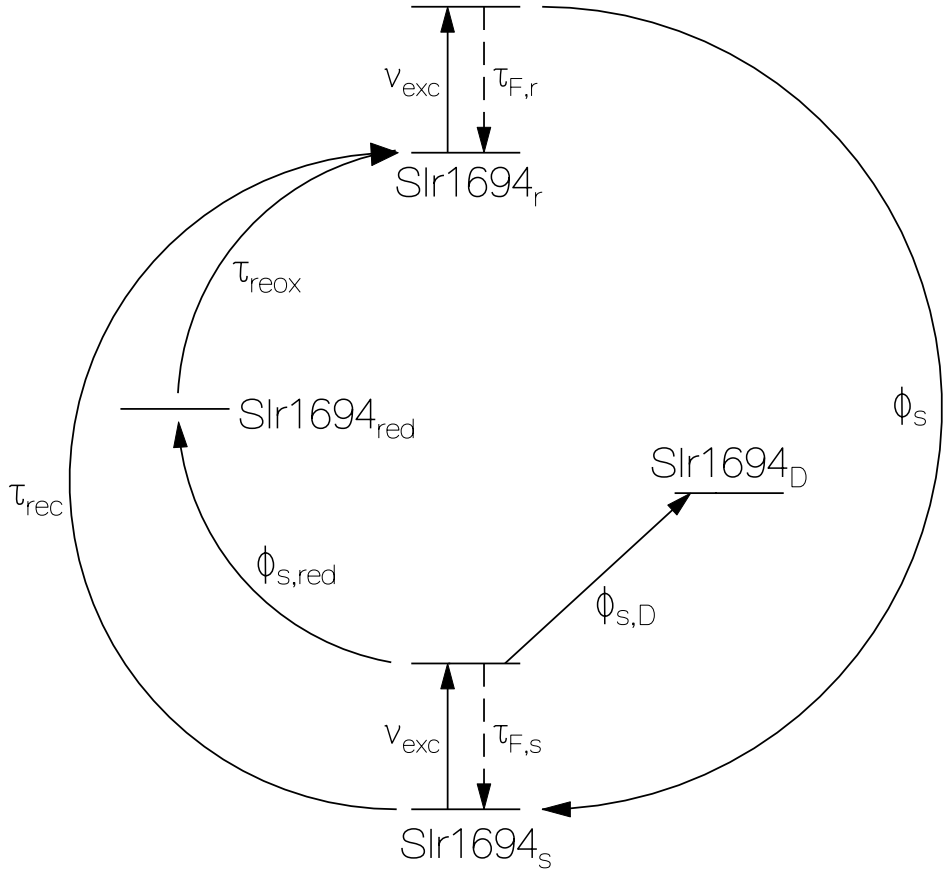

Figure 6-49: Photo-cycle scheme of Slr1694.

Table 6-4. Parameters of Slr1694 BLUF proteins in aqueous solution at pH 8 and room temperature.

Parameter	$Slr1694_I$		$Slr1694_{II}$		Comments
Chromophore composition					HPLC analysis
x_{FAD}	0.37±0.02		0.91±0.01		
x_{FMN}	0.38±0.02		0.06±0.01		
x_{Rf}	0.25±0.02		0.03±0.01		
Domain composition					Fluorescence analysis
x_b	0.994±0.002		0.958±0.005		
x_{free}	0.006±0.001		0.042±0.005		
Photo-cycle characterization					
ϕ_s	0.63±0.07		0.63±0.07		Fig. 6-43,44
τ_{rec} (s)	14.2±0.5		17±0.5		Fig. 6-43, 22 °C
τ_{reox} (min)	8.6±0.3		5.5±0.5		Fig. 6-47
State dependent parameters					
	Dark-adapted	Signaling state	Dark-adapted	Signaling state	
ϕ_F	0.0042±0.002	0.0015±0.001	0.0064±0.002	0.0028±0.001	Fig. 6-42
β_F	≈ 0.24	≈ 0.85	≈ 0.36	≈ 0.90	Fig. 6-41
$\phi_{F,b}$	0.0032±0.0005	$(2.255\pm0.5)\times10^{-4}$	0.0041±0.0005	$(2.7\pm0.5)\times10^{-4}$	Fig. 6-41,42
$\tau_{F,eff}$ (ps)	81.9±5	29.2±2	125±5	54.6±2	eq. 4-19
$\tau_{F,b,eff}$ (ps)	62.5±5	4.4±1	80±10	5.3±1	eq. 4-19
$\phi_{s,red}$		$(1.9\pm0.2)\times10^{-5}$		$(4.8\pm0.4)\times10^{-5}$	Fig. 6-47
$\phi_{s,D}$		$(2.1\pm0.2)\times10^{-6}$		$(5.2\pm0.4)\times10^{-6}$	Fig. 6-47

Abbreviations: x_{FAD}, x_{FMN}, x_{Rf}: mole-fractions of FAD, FMN, and riboflavin, respectively. x_b and x_{free}: mole-fractions of flavin bound to Slr1694 and free flavin, respectively. ϕ_s: quantum yield of signaling state formation. τ_{rec}: recovery time of Slr1694 after light exposure from signaling state to receptor state in the dark. τ_{reox}: average re-oxidation time of reduced flavin. ϕ_F: fluorescence quantum yield. $\phi_{F,b}$: fluorescence quantum yield of non-covalently bound flavin. β_F: fluorescence contribution from free flavin. $\tau_{F,eff}$: effective fluorescence lifetime of flavin in samples. $\tau_{F,b,eff}$: effective fluorescence lifetime of non-covalently bound flavin. $\phi_{s,red}$: quantum efficiency of photo-induced hydroquinone-formation starting from signaling state. $\phi_{s,D}$: quantum yield of photo-degradation of signaling state.

7 Discussion

In this work the application of absorption and emission spectroscopic techniques has allowed the characterization of the photo-cycles of the studied BLUF proteins to the extent accessible to UV-VIS spectroscopy. The obtained photo-cycles have a common feature: It is the spectral red-shift upon blue-light exposure and dark recovery of the red-shifted state (signaling-state) at room temperature. The crystal structures of the studied BLUF proteins show similar folds immediately around the flavin cofactor with highly conserved amino acid residues together with some amino acid residues adjacent to the flavin which are not conserved [Jun05].

In another study, replacing of the AppA blue light sensing domain (amino acid residues 16-107, see Fig. 3-1) by the BLUF domain of PAC from Euglena *gracilis* did not disturb the protein overall function even when they were expressed as separate domains [Han04].

These findings suggest that a similar reaction mechanism very likely holds for all studied BLUF domains, and small differences probably arise from amino acids adjacent to the flavin cofactors which are not conserved and have minor effects on the overall light response.

7.1 Photo induced electron transfer

Our fluorescence lifetime and fluorescence quantum yield measurements revealed low fluorescence quantum yields and short fluorescence lifetimes for the flavin molecules in the BLUF domain binding pocket compared to the free flavin in the buffer.

The most likely mechanism for the observed fluorescence behavior is photo-induced reductive electron transfer possibly from adjacent Tyr, Trp, Phe, His or Cys to the isoalloxazine ring of the flavin cofactors.

Mutation of Tyr21 by Phenylalanine [Kra03] or by Isoleucine [Laa03] in AppA has abolished the photo-cycle. This indicates the involvement of Tyr21 in the AppA photo-cycle. Great efforts have already been undertaken to clarify the light response mechanism of BLUF domains before the crystal structures become available [Laa03,Mas04a,Mas04b,Gau05]. The crystal structures of AppA from *R. sphaeroides* [And05,Jun06], BlrB from *R. sphaeroides* [Jun05], slr1694 from *Synechocyctis sp. PCC6803* [Yua06] and Tll0078 from *Thermosynechococcus elangatus* BP-1 [Kit05] are now available.

The crystal structures for AppA (green), BlrB (blue), Tll0078 (cyan) and Slr1694 (yellow) [Yua06] are compared in Fig. 7-1 together with the hydrogen bond arrangement for AppA and Slr1694 proteins in the flavin binding pocket in dark.

The hydrogen-bond networks in the protein binding pocket of AppA, BlrB and Slr1694 are shown in Figs. 3-3, 3-5 and 3-7 respectively. According to the crystal structures the highly conserved Tyrosine (Tyr21 in AppA, Tyr9 in BlrB and Tyr8 in Slr1694) is a part of the hydrophobic cavity which surrounds the dimethylbenzene portion of the flavin, and its hydroxyl group accepts hydrogen bond from glutamine (Gln63 in AppA, Gln51 in BlrB and Gln50 for Slr1694) which is 100% conserved in the BLUF domains.

As shown in the crystal structure of AppA electron transfer is also possible from Trp104 to isoalloxazine since its distance to N5 is about the same as for Tyr21 (~5Å). However replacing Trp104 with alanine (W104A) [Mas05] or phenylalanine (W104F) [Laa06] kept the photo-cycle intact. This finding shows the dominance of the Tyr21 in the photo-induced electron transfer to the isoalloxazine. However an electron transfer with slower rate from Trp104 to N5 is assumed for the Y21F mutant [Dra05].

Fluorescence quantum yield and fluorescence lifetime analysis revealed the presence of two conformations of the flavin binding pocket (two constituents with different fluorescence lifetimes).

7.2 signaling state formation

The proposed scenario of the signaling-state formation is based on hydrogen bond rearrangement in the flavin binding pocket upon blue light exposure [And05]. The suggested hydrogen bond arrangements in the dark and signaling states are shown in Fig. 3-3 for the AppA protein as a representative of the BLUF family (since the key amino acid residues for photo-cycling are same for all BLUF proteins, a similar light response mechanism is expected for all proteins of the family).

The highly conserved Gln63 makes hydrogen bonds with Tyr21 and N(5) of isoalloxazine and its hydroxyl group makes a hydrogen bond to Trp104 in dark. Upon blue light excitation Gln63 rotates 180 degrees so that the hydroxyl group of Gln63 can make a hydrogen bond to tyrosine while its amino group makes a hydrogen bond with C(4)=O of isoalloxazine [Dra05,Gau05].

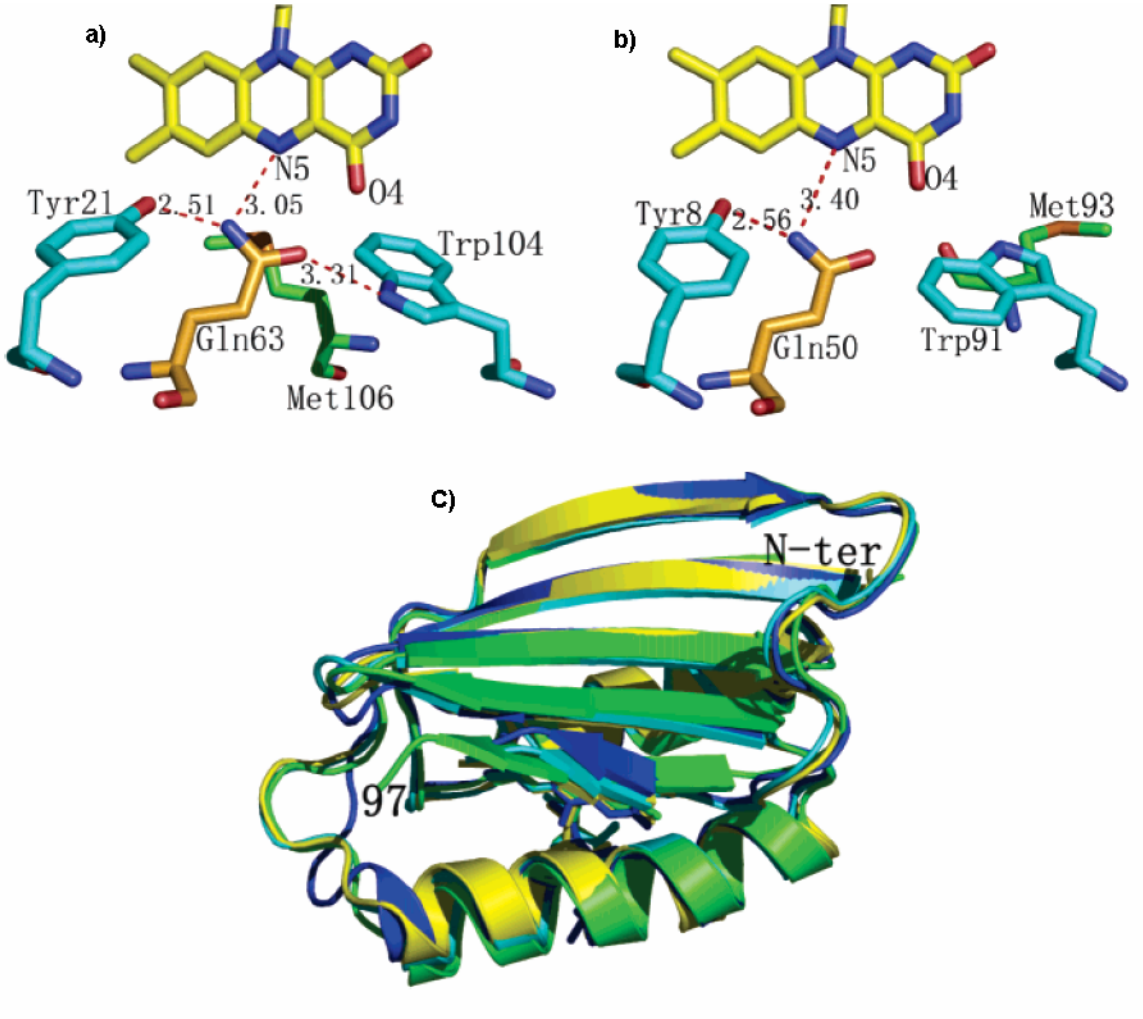

Figure 7-1: Hydrogen bond arrangement for (a) AppA and (b) Slr1694 proteins in dark. (c) Crystal structures for AppA (green), BlrB (blue), Tll0078 (cyan) and Slr1694 (yellow) [Yua06].

This scenario also agrees with the hydrogen bond strengthening observed for C(4)=O locus of isoalloxazine ring in FTIR studies [Mas04a,Mas04b].

The key role of Gln63 is further proved by the finding that signaling-state formation is prevented by mutating Gln63 to alanine in Tll0078 (Q50A) [Kit05] and to leucine in AppA (Q63L) [Unn06]. Also the mutation of Gln63 in AppA with leucine (Q63L) caused a 10nm blue shift observed in the absorption spectrum of AppA-Q63L which indicates the involvement of Gln63 in the hydrogen bonding in the dark-state [Unn06].

7.3 AppA, BlrB and Slr1694 photo-cycles

Although the overall photo-cycle is the same for all BLUF domains (spectral red shift of the absorption band upon blue light exposure and back recovery in the dark at room temperature) there are differences in the photo-cycle dynamics which were found by careful spectroscopic studies. The photo-cycles of the studied samples are compared in Fig. 7-2.

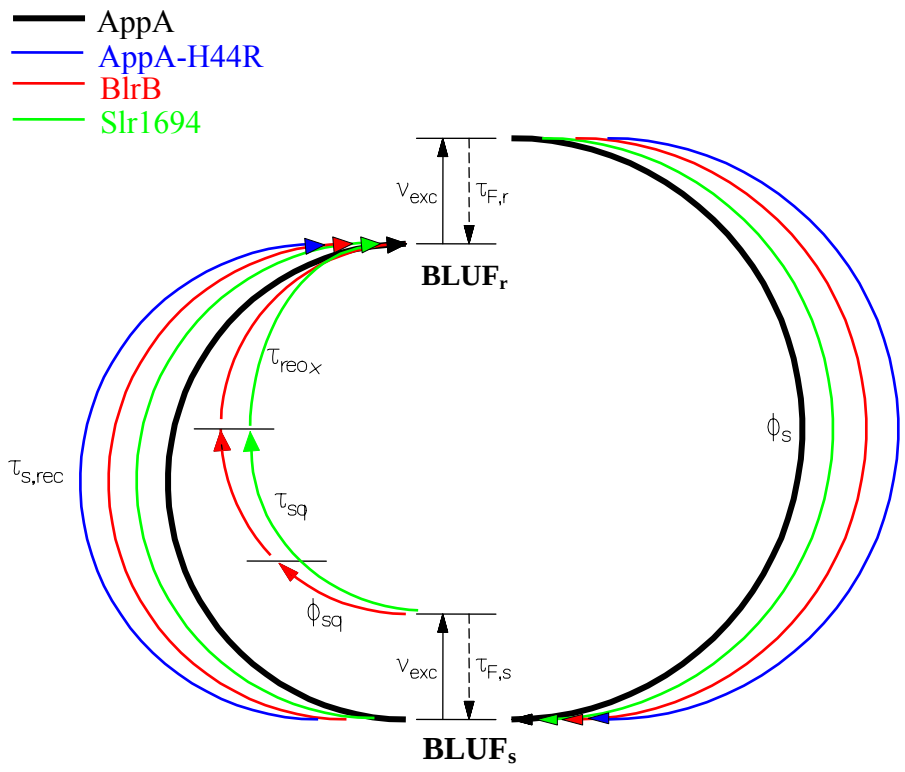

Figure 7-2: Photo-cycles for AppA (black), AppA-H44R (blue), BlrB (red) and Slr1694 (green).

The obtained quantum yields of signaling-state formation are 24% for AppA, 30% for AppA-H44R, 60% for as expressed and FAD reconstituted Slr1694, 40% for BlrB as expressed, and 90% for FAD reconstituted BlrB. The signaling-state recovery to the receptor state in the dark was found to decrease with rising temperature. At room temperature it varies for the measured BLUF proteins from 2 s for BlrB to 17 min for the AppA BLUF domain.

Increasing the quantum yield of signaling-state formation by replacing of Trp104 with phenylalanine in AppA (W104F) [Laa06] and enhancement of dark recovery of signaling state of AppA by replacing Trp104 by alanine (W104A) [Mas05] or by mutation of the Asn32 in Tll0078 [Kit05] (similar to the Asn45 in AppA) indicates that the conserved amino acid residues around the C(4)=O locus of the isoalloxazine ring are important for the relevant photo-cycle parameters.

The photo-cycle parameters also change with a modification of amino acid residues at the N(1)-C(2)=O locus of the isoalloxazine ring. The substitution of His44 by Arg in the AppA (this work), fastens the dark recovery and increases slightly the signaling-state formation efficiency. It also decreases the red-shift of the absorption spectrum by photoexcitation. As seen in Fig. 3-3 in wild-type AppA, His44 makes a hydrogen bond to flavin C(2)=O (see Fig. 3-3). Arg44 in the AppA-H44R mutant can also form a hydrogen bond at this position, although probably with different strength which may explain the observed changes. In wild-type AppA His44 places a positive charge at N(1)-C(2)=O locus of the isoalloxazine ring. A positive charge at the N(1)-C(2)=O position is found in more than 50% of BLUF domains studied so far (e.g. Arg32 in BlrB [Jun05] and Arg65 in Tll0078 [Kit05]) and in nearly all flavoenzymes [Fra00] where it contributes in modulating the reduction potential of the flavin [Ghi89]. It is likely that substitution of His with Arg in AppA-H44R locates the positive charge at a different distance from the N(1)-C(2)=O locus which in turn weakens the hydrogen bond at C(4)=O and consequently causes a smaller red shift and a faster dark recovery. Light-induced increase of hydrogen bonding at the C(2)=O and C(4)=O positions of flavin was found for Slr1694 [Mas04a] by FTIR spectroscopy.

These lines of evidence show that all the conserved residues around the pyrimidine ring of the isoalloxazine in the protein binding pocket are most probably important for the relevant photo-cycle parameters as signaling-state absorption red-shift, signaling-state formation efficiency and signaling-state dark recovery.

Much faster fluorescence signal decays in the signaling state of all investigated BLUF domains indicates a shorter distance between conserved Tyr and flavin.

Fluorescence lifetime measurements showed the presence of some free flavin. The detected amounts of free flavin were about 16% for AppA-H44R, 8% for both $BlrB_I$ (as expressed) and $BlrB_{II}$ (FAD reconstituted), 0.6% for $Slr1694_I$ (as expressed) and 4% for $Slr1694_{II}$ (FAD reconstituted). The observed free flavin in solution for the as expressed BLUF domains ($Slr1694_I$, $BlrB_I$ and AppA-H44R), indicates a thermodynamic equilibrium between the non-covalently

bound flavin and the free flavin. For the FAD reconstituted BLUF domains ($BlrB_{II}$ and $Slr1694_{II}$) the free flavin is left from the reconstitution process (not complete removal of free FAD in dialysis).

Long-time high-intensity exposure experiments revealed flavin photo-degradation and photo-reduction in the signaling-state. The presence of un-bound flavin in solution causes enhanced photodegradation because of low photo-stability of flavin in solution (ϕ_D(FMN) = 7.3×10^{-3}, ϕ_D(FAD) = 3.7×10^{-4} and ϕ_D(riboflavin) = 7.8×10^{-3} [Hol05]). No photodegradation was observed under the applied experimental excitation conditions for wild-type AppA ($\phi_{s,D}<10^{-6}$), whereas no free flavin content was found in solution. The photodegradation efficiency of $\phi_{D,eff}$ = 2×10^{-4} for AppA-H44R, $\phi_{D,eff}$ = $2 \times 10^{-6}$for $Slr1694_I$ and $\phi_{D,eff}$ = 1×10^{-4} for $BlrB_I$ were obtained.

Photo excitation of BlrB and Slr1694 causes photo-reduction which only can occurs inside protein. No reduction mechanism is known [Mas83] for free flavin in the applied buffer conditions. For BlrB a photo-induced reduction of oxidized flavin to flavin semiquinone and fully reduced flavin was observed in the signaling state. The semiquinone formation efficiency of ϕ_{sq} =1.3×10^{-3} has measured for BlrB.

For Slr1694 only photo-reduction to the fully reduced flavin was observed with an efficiency of $\phi_{s,red} = 3.5 \times 10^{-5}$. The reduction step from flavin semiquinone to fully reduced flavin is thought to be faster than the used experimental time resolution of about 1 s (two-step reduction with fast intermediate semiquinone state is likely to occur).

Re-oxidation brings the reduced flavin back to the original oxidized form with time constant of τ_{reox} = 1.5 min for BlrB and τ_{reox} = 7 min for Slr1694. The speed of re-oxidation is determined either by diffusion of dissolved oxygen from the solution into the flavin binding pocket or by self-oxidation in the protein domain.

8 Summary

The BLUF proteins $AppA_{148}$, $AppA_{126}$ and BlrB from R. *sphaeroides* and Slr1694 from *Synechocystis* sp. PCC6803 together with a mutant of the $AppA_{148}$ protein in which His44 is replaced by Arg (H44R) have been studied by continuous absorption spectroscopy, continuous fluorescence spectroscopy, and time-resolved fluorescence spectroscopy.

The chromophore analysis revealed the presence of FMN, FAD and riboflavin in the as expressed BLUF proteins.

Formation of an intermediate state (signaling-state) upon blue-light exposure was observed for all the studied BLUF domains. The signaling-state is distinguished from the receptor state by a slightly red-shifted absorption spectrum, varying between 12 – 16 nm for BlrB and AppA proteins, respectively. The spectral red-shift in the BLUF domains is caused by light induced conformational changes of the protein binding pocket causing modifications of the hydrogen binding upon light absorption [Kra03,And05,Jun05,Yua06].

The efficiency of the signaling-state formation of about 25% for AppA, 30% for AppA-H44R and 60% for as expressed and FAD reconstituted Slr1694 ($Slr1694_I$ and $Slr1694_{II}$) respectively are determined by the analysis of light-intensity dependent absorption changes. For BlrB these values are found to be 40% for as expressed BlrB ($BlrB_I$) and 90% for FAD reconstituted BlrB ($BlrB_{II}$).

The signaling-state recovered back to the receptor state (dark-state) in dark at room temperature within 17 min for AppA, 6.5 min for AppA-H44R, 15 s for Slr1694 and 2 s for BlrB. These differences indicate slightly different barrier heights for ground-state thermal reconstitution from the signaling-state to the receptor state.

Two photo-active conformations with fast and slow fluorescence decay times in the dark- and signaling-states of the BLUF proteins were found by the fluorescence lifetime and fluorescence quantum yield measurements (two conformations with somewhat different flavin-quencher distances).

The short fluorescence lifetimes and small fluorescence quantum yields observed in the dark-state and specially in the signaling-state of the BLUF domains are most likely due to electron transfer from a highly conserved tyrosine (Tyr63 in AppA [And05], Tyr8 in Slr1694 [Yua06] and Tyr9 in BlrB [Jun05]) to the flavin cofactor [Kra03].

Fluorescence lifetime measurements revealed a fraction of flavin about 8% for $BlrB_I$ and $BlrB_{II}$, 0.6% for $Slr1694_I$ and 4% for $Slr1694_{II}$, and 16% for AppA-H44R, not bound to the proteins at room temperature (thermodynamic equilibrium between holoprotein, apoprotein and free flavin in as-expressed domains and incomplete dialysis in FAD reconstituted proteins). Although free flavin was not observed in the case of AppA BLUF, a small fraction of flavins (1-2%) was found not to take part in the photo-cycle (likely adsorbed to the protein surface or misfitted in the protein binding pocket).

The photo-excitation of AppA in the signaling-state caused no more changes in the absorption spectrum, within our experimental accuracy, which shows a high photo-stability of the AppA BLUF domain.

In contrast, prolonged light excitation of BlrB and Slr1694 resulted in the formation of the semiquinone-type flavin ($\phi_{sq} \approx 1\times10^{-3}$) followed by semiquinone reduction (flavin hydroquinone formation) and re-oxidation in the case of BlrB, and the formation of flavin hydroquinone ($\phi_{red} \approx 3.5\times10^{-5}$) followed by re-oxidation of hydroquinone to the quinone form of the flavin in the case of Slr1694.

In BlrB, Slr1694 and AppA-H44R an irreversible photo-degradation of free flavin and the non-covalently bond flavin (with lower efficiency) were also observed.

9 References

[1] www.expasy.org/uniprot/Q3J677

[2] www.expasy.org/uniprot/P74295

[3] www.expasy.org/uniprot/Q3IYE4

[Ahm98] Ahmad, M., Jarillo, J. A., Smirnova, O. and Cashmore, A.R., Nature 392, (1998), 720-723.

[Akh97] Akhmanov, S. A. and Nikitin, S. Yu., physical optics, (1997), Oxford University Press, New York.

[And05] Anderson, S., Dragnea, V., Masuda, Sh., Ybe, J., Moffat, K and Bauer, C. E., Biochemistry 44, (2005), 7998-8005.

[Atk97] Atkins, P. W. and Friedman, R. S., molecular quantum mechanics, third edition, (1997), Oxford University Press, Inc., New York.

[Bar73] Barrio, J. R., Tolman, G. L., Leonard, N. J., Spencer, R. D. and Weber, G., PNAS 70, (1973), 941-943.

[Ber00] Berberan-santos, M. N., PhysChemComm 5, (2000), 18-23.

[Ber02] Van den Berg, P. A. W., Feenstra, K. A., Mark, A. E., Berendsen, H. J. C. and Visser, A. J. W. G., J. Phys. Chem. B 106, (2002), 8858-8869.

[Bir63] Birks, J. B. and Dyson, D. J., the relations between the fluorescence and absorption properties of organic molecules, (1963), Proc. R. Soc. London Ser. A 275.

[Boh83] Bohren, G.F. and Huffman, D. R., absorption and scattering of light by small particles, John Wieley and Sons, New York, (1983).

[Boy92] Boyd, R. W., Nonlinear optics, (1992), Academic Press Inc., USA.

[Bri63].Briggs, W. R., Am. J. Bot. 50, (1963), 196-207.

[Bri99].Briggs W. R. and Huala, E., Annu. Rev. Cell Dev. Biol. 15, (1999), 33-62.

[Bru03] Brudler, R., Hitomi, K., Toh, H., Kucho, K., Ishiura, M., Kanehisa, M., Roberts, V. A., Todo, T., Tainer, J. A. and Getzoff, E. D., Mol. Cell 11, (2003), 59-67.

[Chr01] Christie, J. M. and Briggs, W. R., J. Biol. Chem. 276, (2001), 11457-11460.

[Chr02] Christie, J. M.,Swartz, T. E., Bogomolni, R. A. and Briggs, W. R., Plant J 32, (2002), 205-219.

[Coh57] Cohen-Bazire, G., Sistrom, W. R. and Stanier, R. Y., J. cell. Comp. Physiol. 49, (1957), 25-68.

[Cro01] Crosson, S. and Moffat, K., PNAS 98, (2001), 2995-3000.

[Cro71] Crosby, G. N. and Demas, J. N., J. Phys. Chem. 75, (1971), 991-1024.

[Dam88] Damen, T. C. and Shah, J., appl. phys. lett. 52, (1988), 1291-1293.

[Dem06] Demtröder, W., Atoms, molecules and photons: an introduction to atomic-, molecular- and quantum-physics, (2006), Springer-Verlag, Berlin.

[Dex53] Dexter, D. L., J. Chem. Phys. 21, (1953), 836-850.

[Dra05] Dragnea, V., Waegele, M., Balascuta, S., Bauer, C. E. and Dragnea, B., Biochem. 44, (2005), 15978-15985.

[Drö02] Drössler, P., Holzer, W., Penzkofer, A. and Hegemann, P., chem. Phys. 282,(2002), 429-439.

[Eck82] Eckertova, L., in: physics of thin films, second ed., (1982), Oxford University Press, Oxford.

[Eft91] Eftink, M. R., fluorescence quenching: theory and applications, in: Lackowicz J. R. (Ed), topics in fluorescence spectroscopy, Vol. 2, principles, (1991), Plenum Press, New York.

[Fle86] Fleming, G. R., chemical applications of ultrafast spectroscopy, (1986), Oxford University Press, Oxford.

[För60] Förster, Th., Radiation Res. Supp. 2, (1960), 326-339.

[Fra00] Fraajie, M. W. and Mattevi, A., Trends Biochem. Sci. 25, (2000), 126-132.

[Fri88] Friedrich, W., Vitamins, (1988), Walter de Gruyter, Berlin.

[Gal03] Gallanf, P. and Tolle, N., Planta 217, (2003), 971-982.

[Gal88] Gallanger, S., Short, T. S., Ray, P. M., Pratt, L. H. and Briggs, W. R., PNAS 85, (1988), 8003-8007.

[Gau05] Gauden, M., Yeremenko, S., Laan, W., van Stokkum, I. H. M., Ihalainen, J. A., van Grondelle, R., Hellingwerf, K. J. and Kennis, J. T. M., Biochemistry 44, (2005), 3653-3662.

[Gen98] Genick, U. K., Soltis, S. M., Kuhn, P., Canestrelli, I. L. and Getzoff, E. D., Nature 392, (1998), 206-209.

[Ghi86] Ghisla, S. and Massey, V., Biochem. J. 239,(1986), 1-12.

[Ghi89] Ghisla. S. and Massey, V., Eur. J. Biochem. 181, (1989), 1-17.

[Gil91] Gilbert, A. and Baggott, J., essentials of molecular photochemistry, (1991), Blackwell scientific Publications, GB.

[Gom02] Gomelsky, M. and Klug, G., Tren. Biochem. Sci. 27, (2002), 497-500.

[Gom95] Gomelsky, M. and Kaplan, S., J. Bacteriol. 172, (1995), 4609-4618.

[Gom97] Gomelsky, M. and Kaplan, S., J. Bacteriol. 179, (1997), 128-134.

[Gui90] Guilbault, G. G., practical fluorescence, (1990), Second Edition, Marcel Dekker, Inc., New York.

[Hak00] Haken, H. and Wolf, H. C., the physics of atoms and quanta, introduction to experiments and theory, sixth edition, (2000), Springer-Verlag, Berlin.

[Han04] Han, Y., Braatsch, S., Osterloh, L. and Klug, G., PNAS 101, (2004), 12306-12311.

[Has06] Hasegawa, K., Masuda, S. and Ono, T., Bichemistry 45, (2006), 3785-3793.

[Hol02] Holzer, W., Penzkofer, A., Fruhmann, M and Hegemann, P., photochem. Photobiol. 75, (2002), 479-487.

[Hol04] Holzer, W., Penzkofer, A., Susdorf, T., Alvarez, M., Islam, Sh. D. M. and Hegemann, P., Chem. Phys. 302, (2004), 105-118.

[Hol05] Holzer, W., Shirdel, J., Zirak, P., Penzkofer, A., Hegemann, P., Deutzmann, R. and Hochmuth, E., Chem. Phys. 308, (2005), 69-78.

[Hol99] Holzer, W., Pichlmaier, M., Penzkofer, A., Bradley, D. D. C. and Blau, W. J., Chem. Phys. 246, (1999), 445-462.

[Hor03] Van Der Horst, M. And Hellingwerf, K., Acc. Chem. Res. 37, (2004), 13-20.

[Ihe05] Ihee, H., Rajagopal, S., Srajer, V., Pahl, R., Anderson, S., Schmidt, M., Schotte, F., Anfinrud, P., Wulff, M. and Moffat, K., PNAS 102, (2005), 7145-7150.

[Ise02] Iseki, M., Matsunaga, S., Murakami, A., Ohno, K., Shiga, K., Yoshida, K., Sugai, M., Takahashi, T., Hori, T. and Watanabe, M., Nature 415, (2002), 1047-1051.

[Isl03] Islam, S. D. M., Susdorf, T., Penzkofer, A. and Hegemann, P., chem. Phys. 295, (2003), 137-149.

[Jea93] Jean, J., Volatron, F. and Burdett, J., an introduction to molecular orbitals, (1993), Oxford University press, Inc., Oxford.

[Jun05] Jung, A., Domrotcheva, T., Tarutina, M., Wu, Q., Ko, W. H., Shoeman, R. L., Gomelsky, M., Gardner, K. H. and schlichting, I., (2005), PNAS 102, 12350-12355.

[Jun06] Jung, A., Reinstein, J., Domratcheva, T., Shoeman, R. L. and Schlichting, I., JMB 362, (2006), 717-732.

[Kan96] Kaneko, T., Sato, S., Kotani, H., Tanaka, A., Asamizu, E., Nakamura, Y., Miyajima, N., Hirosawa, M., Sugiura, M., Sasamoto, S., Kimura, T., Hosouchi, T., Matsuno, A., Muraki, A., Nakazaki, N., Naruo, K., Okumura, S., Shimpo, S., Takeuchi, C., Wada, T., Watanabe, A., Yamada, M., Yasuda, M. and Tabata, S., DNA Res. 3, (1996), 109-136.

[Kav93] Kavarnos, G. J., fundamentals of photoinduced electron transfer, (1993), VCH publishers, Inc. New York.

[Ker69] Kerker, M., The scattering of light and other electromagnetic radiation, (1969), Academic Press, New York.

[Kil88] Kiley, P. J., and Kaplan, S., Microbiol. Rev. 52, (1988), 50-69.

[Kit05] Kita, A., Okajima, K., Morimoto, Y., Ikeuchi, M. and Kunio, M., JMB 349, (2005), 1-9.

[Kra03] Kraft, B. J., Masuda, sh., Kikuchi, J., Dragnea, V., Tollin, G., Zaleski, J. M. and Bauer, C. E., Biochemistry, (2003), 42, 6726-6734.

[Laa03] Laan, W., van der Horst, M., Stokkum, I. H. and Hellingwerf, K. J., Photochem. Photobil. 78, (2003), 290-297.

[Laa06] Laan, W, Gauden, M., Yeremenko, S., van Grondelle, R., Kennis, J. T. M. and Hellingwerf, K. J., Biochem. 45, (2006), 51-60.

[Lac83] Lackowics, J. R., principles of fluorescence spectroscopy, (1983), Plenium Press, New York.

[Leh93] Lehninger, A. L., Nelson, D. L. and Cox, M. M., principles of biochemistry, (1993), second ed., Worth Publishers, New York.

[Lin95] Lin, C., Robertson, D. E., Ahmad, M., Raibekas, A. A., Jorns, M. S., Dutton, P. L. and Cashmore, A. R., Science 269, (1995), 968-970.

[Mas00] Massay, V., Biochem. Soc. Trans. 28, (2000), 283-296.

[Mas02] Masuda, Sh. and Bauer, C. E., Cell 110, (2002), 613-623.

[Mas04a] Masuda, Sh., Hasegawa, K., Ishii, A. and Ono, T., Biochemistry 43, (2004), 5304-5313.

[Mas04b] Masuda, Sh., Hasegawa, K. and Ono, T., Biochemistry 44, (2005), 1215-1224.

[Mas05] Masuda, Sh., Hasegawa, K. and Ono, T., Plant Cell Physiol. 46, (2005), 1894-1901.

[Mas83] Massey, V. and Ghisla, S., In biological oxidations, (1983), (Sund, H. & Ullrich, V., eds), Springer, Berlin.

[Mil68] Miles, D. W. and Urry, D. W., Biochemistry 7, (1968), 2791-2799.

[Mil90] Miller, S. M., Massay, V., Ballou, D., Williams, C. H., Diestefano, M. D., Moore, M. J. and Walsh, C. T., Biochem. 29, (1990), 2831-2841.

[Moo63] Moore, W. M., Spence, J. T., Raymond, F. A. and Colson, S. D., 145th national meeting of American chemical society, New York, N. Y., sept. 8-13, (1963).

[Moo69] Moore, W. M. and Charles Baylor, Jr., J. Am. Chem. Soc. 91, (1969), 7170-7179.

[Mül88] Müller, F., Ghisla, S., Bacher, A., Vitamin B2 und natürliche flavine, in: Isler, O., Brubacher, G., Ghisla, S., Kräulter, K., (Eds), Vitamine II, (1988), Thieme Verlag, Stuttgart.

[Mül91] Müller, F., chemistry and biochemistry of flavoenzymes, (1991), (CRC Press, Inc), USA.

[Nak02] Nakamura, Y., Kaneko, T., Sato, S., Ikeuchi, M., Katoh, H., Sasamoto, S., Watanabe, A., Iriguchi, M., Kawashima, K., Kimura, T., Kishida, Y., Kiyokawa, C., Kohara, M., Matsumoto, M., Takeuchi, C., Yamada, M. and Tabata, S., (2002), DNA Res. 9, 123-130.

[Nar04] Narikawa, R., Okamoto, S., Ikeuchi, M. and Ohmori, M., (2004), DNA Res. 11, 69-81

[Ohm01] Ohmario, M., Ikeuchi, M., Sato, N., Wolk, P., Kaneko, T., Ogawa, T., Kanehisa, M., Goto, S., Kavashima, S., Okamoto, S., Yoshimora, S., Narikawa, R. and Tabat, S., (2001), DNA Res. 8, 271-284.

[Oka04] Okajima, K., Narikawa, R., Kondo, K., Ochiai, Y., Katayama, M. and Ikeuchi, M., (2004), plant cell physiol. 45, s124.

[Oka05] Okajima, K., Yoshihara, Sh., Fukushima, Y., Geng, X., Katayama, M., Higashi, Sh., Watanabe, M., Sato, Sh., Tabata, S., Shibata, Y., Itoh, Sh. and Ikeuchi, M., (2005), J. Biochem. 137, 741-750.

[Ovi98] Ovid, M. A. D. and Kenny, E. J., metamorphoses, (1998), Oxford University Press, Oxford.

[Pal97] Palfey, B. A. and Massey, V., Flavin-dependent enzymes, in: Sinnott, M. (Ed.), comprehensive biological catalysis. A mechanistic reference, radical reactions and oxidation/reduction, vol. III, (1997), Academic Press, San Diego, USA.

[Pen87] Penzkofer, A. and Leupacher, W., J. Luminescence 37, (1987), 61-72.

[Pen91] Penfold, R. J. and Pemberton, J. M., Curr. Microbiol. 23, (1991), 259-263.

[Pen94] Penfold, R. J. and Pemberton, J. M.,J. Bacteriol. 176, (1994), 2869-2876.

[Pok05] Pokorny, R., Klar, T., Essen, L.-O. and Batschauer, A., Acta Cryst. F 61, (2005), 935-938.

[Pon95] Ponnampalam, S. N., Buggy, J. J.and Bauer, C. E., J. Bacteriol. 177, (1995), 2990-2997.

[Rey92] Reymond, P., Short, T. W., Briggs, W. R. and Poff, K. L., Plant Physiol. 100,(1992), 655-661.

[Sak02] Sakmar, T. P., Menon, S. T., Marin, E. P. and Awad, E. S., Ann. Rev. 31, (2002), 443-484.

[Sak96] Sakamoto, K. and Nagatani, A., Plant J. 10, (1996), 859-868.

[Sal00] Salomon, M., Christie, J. M., Kneib, E., Lempert, U. and Briggs W. R. and Bogomolni, Biochem. 39, (2000), 9401-9410.

[San00] Sancar, A., Annu. Rev. Biochem. 69, (2000), 31-67.

[Sch00] Schmitz, O., Katayama, M., Williams, S. B., Kondo, T., Golden, S. and Cika, S., Science 289, (2000), 765-768.

[Sch01] Schanz, R., Kovalenko, S. A., Kharlanov, V. and Ernsting, N. P., appl. Phys.lett. 79, (2001), 566-568.

[Sch75] Schuman Jorns, M., Schöllnhammer, G. and Hemmerich, P., Eur. J. Biochem. 57, (1975), 35-48.

[Sch77] Schulman, G., fluorescence and fluorescence spectroscopy: physicochemical principles and practice, (1977), Pergamon Press Ltd, Edington, Hill Hall, Oxford, Uk.

[Sch87] Schmidt, J., Penzkofer, A., J. Chem. Phys. 91, (1989), 1403-1409.

[Shi06] Shirdel, J., Penzkofer, A., Prochazka, R., Daub, J., Hochmuth, E and Deutzmann, R., Chem. Phys. 326, (2006), 489-499.

[Shi92] Shimada, H., Iba, K.and Takamiya, K., plant cell physiol. 33, (1992), 471-475.

[Son06] Song, S. H., Dick, B., Penzkofer, A., Pokorny, R., Batschauer, A. and Esses, L. O., Annu. Photochem. Photobiol. B 85, (2006), 1-16.

[Spr93] Sprenger, W. W., Hoff, W. D., Armitage, J. P. and Hellingwerf, K. J., J. Bacteriol. 175, (1993), 3096-3104.

[Spu00] Spudich, J. L., Yan, C., Jung, K. H. and Spudich, E. N., Annu. Rev. Cell. Dev. Biol. 16, (2000), 365-392.

[Str62] Strickler, S. J.and Berg, R. A., J. chem. Phys. 37, (1962), 814-822.

[Swa01] Swartz, T. E., Corchnoy, S. B., Christie, J. M., Lewis, J. W., Szundi, I., Briggs, R. A. and Bogomolni, R. A., J. Biol. Chem. 276, (2001), 36493-36500.

[Unn06] Unno, M., Masuda, Sh., Ono, T. and Yamauchi, S., JACS 128, (2006), 5638-5639.

[Val02] Valeur, B., Molecular fluorescence ,principles and applications, (2002), Wiley-VCH Verlag GmbH, Weinheim.

[Web66a] Weber, G, in: E. C. Slater (Ed), flavins and flavoproteins, (1966), B. B. A. Library, vol. 8, Elsevier, Amsterdam, The Netherlands.

[Web66b] Wester, C., Isis. 57, (1966), 5-23.

[Whi06] Whippo, C. W. and Hangarter, R. P., The Plant Cell 18, (2006), 1110-1119.

[Whi53] Whitby, L. G., Biochem. J. 54, (1953), 437-442.

[Xia00] Xiao, W., Brown, L. S., Needlman, R., Lanyi, J. K. and Shin, Y. K., J. Mol. Biol. 304, (2000), 715-721.

[Yeh98] Yeh, K. C. and Lagarias, J. C., PNAS 95, (1998), 13976-13981.

[Yua06] Yuan, H., Anderson, S., Masuda, Sh., Dragnea, V., Moffat, K. and Bauer, C. E., Biochemistry 45, (2006), 12687-12694.

[Zir05]. Zirak, P., Penzkofer, A., Shiereis, T., Hegemann, P., Jung, A. and Schlichting, I., Chem. Phys. 315, (2005), 142-154.

[Zir06a]. Zirak, P., Penzkofer, A., Schiereis, T., Hegemann, P., Jung, A. and Schlichting, I., J. Photochem. Photobiol. B 83, (2006), 180-194.

[Zir06b]. Zirak, P., Penzkofer, A., Lehmpfuhl, C., Mathes, T. and Hegemann, P., J. Photochem. Photobiol. B 86, (2006), 22-34.

[Zir07]. Zirak, P., Penzkofer, A., Hegemann, P. and Mathes, T., Chem. Phys. (2007), in press
Photo-dynamics of BLUF mutant H44R of AppA from *Rhodobacter sphaeroides.*

10 Appendix

Protein amino acids and their fundamental (**R-**) groups with their 3-letter and (1-letter) abbriviations

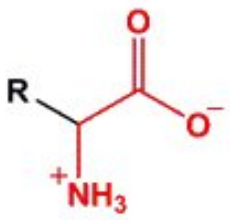

Neutral amino acids

Glycine Gly (G) — H—

Alanine Ala (A) — H_3C—

Valine Val (V) — H_3C—CH(—CH_3)—

Leucine Leu (L) — H_3C—CH(—CH_3)—CH_2—

Isoleucine Ile (I) — H_3C—CH_2—CH(—CH_3)—

Serine Ser (S) — HO—CH_2—

Threonine Thr (T) — H_3C—CH(—OH)—

Sulfur amino acids

Cysteine Cys (C) — HS—CH_2—

Methionine Met (M) — H_3C—S—CH_2—CH_2—

Cyclic amino acids

Proline Pro (P)

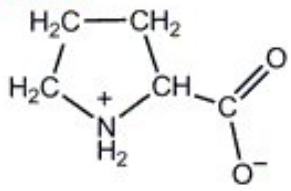

Aromatic amino acids

Phenylalanine Phe (F) — —CH_2—

Tyrosine Tyr (Y) — HO— —CH_2—

Tryptophan Trp (W)

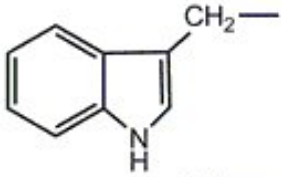

Histidine His (H)

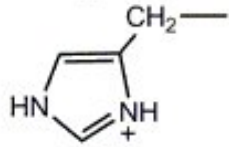

Basic amino acids

Lysine Lys (K)

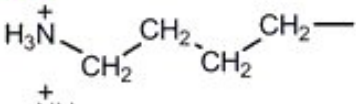

Arginine Arg (R)

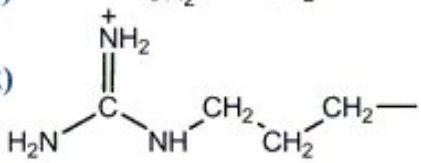

Acidic amino acids & their amides

Aspartic acid Asp (D)

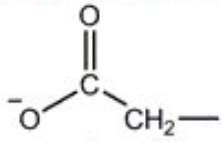

Asparagine Asn (N)

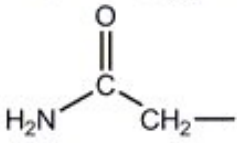

Glutamic acid Glu (E)

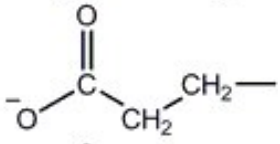

Glutamine Gln (Q)

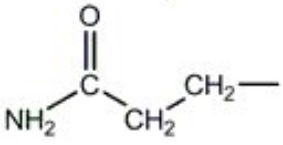

11 Acknowledgement

A journey is easier when you travel together

This thesis is the result of three years work where I have been accompanied and supported by many people. My last remaining task is to acknowledge these people.

Foremost, I would like to thank my advisor, Professor Alfons Penzkofer for providing me the opportunity to study in University Regensburg and to complete my Phd thesis. I am very grateful for his patience, motivation, enthusiasm, and immense knowledge which made him a great mentor. I will be obliged to him in my whole life.

I also appreciate Professor Ilme Schlichting and especially Professor Peter Hegemann for supplying the biological samples and their very helpful advices.

Special thanks for my great colleagues: Dr. Thomas Susdorf and Ludwig Endres who were always there to help. Dr. Sang-Hun Song for his friendship. Amit Tyagi and Ashu Kumar Bansal for their kindness. David del Agua from CISC, Spain, who was always helpful, especially after my operation. Javid Shirdel from my home town with whom I had a lot to share during these three years and who was always willing to help.

Special thanks to our secretaries Mrs. König and Mrs. Schäfer who in spite of their busy schedule helped me whenever needed.

Thanks to Mrs. Merkel, Mr. Ascherl and their colleagues in mechanical work shop for their technical support. I am grateful to Mr. Riedl and his colleagues in the electronic workshop who were always there to help.

I owe gratitude to all my friends in graduate college ”Sensory photoreceptors in natural and artificial systems” and DFG forschergruppe “Blue light sensory photoreceptors, FOR 526”, namely Tilo Mathes, Catrin Lehmpfuhl, Christian Vogel, Astrid Jung and Keyarash Sadeghian. I should also acknowledge for all great talks in graduate college and FOR 526 which were very informative.

I thank all my friends in Iran who supported me during whole my stay here in Germany.

I am grateful to Professor Habib Tajalli from whom I have learned a lot as a student and during my career in Iran. He means a lot to me than just a teacher.

At last, but not the least, I owe special gratitude to my family for continuous and unconditional support: To my mother and my father for the interest they showed in my studies and the

motivation they gave me during those tiring times when I had doubts about my studies. I dedicate this work to my mother and late father.

Finally, special thanks to my very kind brother, who took all my duties at home making it possible for me to take this chance to come to the Germany and continue my studies.

Regensburg, March 2007